THE JOURNAL
OF
CHEMICAL PHYSICS

VOLUME 16, NUMBER 1 JANUARY, 1948

Dielectric Properties of Aqueous Ionic Solutions. Parts I and II.

J. B. HASTED, D. M. RITSON, AND C. H. COLLIE
The Clarendon Laboratory, Oxford, England

(Received June 20, 1947)

The dielectric constants and loss angles of a series of concentrated aqueous ionic solutions have been measured at wave-lengths of 10 cm, 3 cm, and 1.25 cm. From these results the values of the static dielectric constant and relaxation time for these solutions have been calculated on the basis of the Debye formula, which appears to hold accurately. All salts show a lowering of the dielectric constant and a shift in the relaxation time of water. It is found that the dielectric constant ϵ can be represented by a formula $\epsilon=\epsilon_\omega+2\bar{\delta}c$, where ϵ_ω is the dielectric constant of water, c is the concentration in moles per liter, and $\bar{\delta}$ has values between -7 and -15 for various salts in concentrations of up to 2 *M*.

In Part I the measurements are described and the results discussed in relation to the structure of ionic solutions. In Part II the validity of the Debye-Sack saturation theory of the dielectric constant and the effects of the fall of dielectric constant on the electrolytic properties of concentrated solutions are discussed.

PART I

Introduction

A LARGE variety of methods have been used to determine the dielectric properties of salt solutions. The difficulty of the determination lies in the high value of the loss angle δ which is given by the relation, $\tan\delta=2\sigma/f\epsilon$ where σ is the conductivity, in e.s.u., f the frequency, and, ϵ the dielectric constant.

At the frequencies available when the early measurements were carried out, it was necessary either to work with extremely dilute solutions, the deviations of which from the dielectric properties of water are correspondingly small, or to work with very high values of $\tan\delta$, which greatly limits the accuracy of measurement. It is even difficult from a study of the literature to decide whether the dielectric constant of an ionic solution increases or decreases with increasing concentration.[1] It was shown by Hückel[2] that a variation of dielectric constant would have a significant, if not dominating, effect on the properties of concentrated salt solutions. Further, Sack made a theoretical estimate of the lowering of dielectric constant that would be expected because of the saturation of the dielectric in the neighborhood of an ion. Both these studies are of great theoretical interest. It is therefore important to study the dielectric properties of ionic solutions in a region where $\tan\delta$ is comparatively low, i.e., at frequencies of the order of 10^{10} cycles a second. We have previously described methods used to determine the dielectric properties of water in the range $\lambda=1$ to 10 cm. The methods used depended only on the validity of Maxwell's equations, and the use

[1] See for summary C. H. Douglas Clark, *The Fine Structure of Matter* (Chapman and Hall, Ltd., London, 1941), p. 232.
[2] E. Hückel, Phys. Zeits. **26**, 93 (1925).

of standard attenuator technique.[3] The limits to the accuracy of measurement were entirely technical and did not arise from any uncertainty in the theory. It was found possible to work with reasonable accuracy with values of $\tan\delta$ of the order of 1.5.

In the present paper these methods are applied to ionic solutions. There are two disadvantages of measurements at these frequencies:

(1) Correction must be made for anomalous dispersion so that measurements at a number of frequencies are necessary. It can be shown that the results obtained may be interpreted on the basis of a single time of relaxation, slightly different from that of water. This enables accurate calculation of the static dielectric constant to be made, and further conclusions to be drawn from the behavior of the relaxation time. An apparent disadvantage may thus be turned to good account.

(2) With the 2–4 percent accuracy in ϵ, obtainable in solutions of $\tan\delta=1.5$, deviations from the static dielectric constant of water are only noticeable in solutions of 0.5- to 2-M concentration; dilute solutions can therefore not be studied by these methods.

Methods of Measurement

Of the methods developed for the measurement of the dielectric properties of water and heavy water, which are fully described by the authors,[4] the three most suitable have been selected for study of ionic solutions. These are: (1) the direct measurement of the absorption coefficient κ in a rectangular wave guide; (2) the measurement of absorption coefficient in two cylindrical wave guides full of solution, the two diameters being selected to be just above and just below cut-off for the wave guide used. By this method both n, the refractive index, and κ, the absorption coefficient, are determined; (3) measurement of the change in Q of an H_{01} resonator on the introduction of an axial capillary containing liquid.

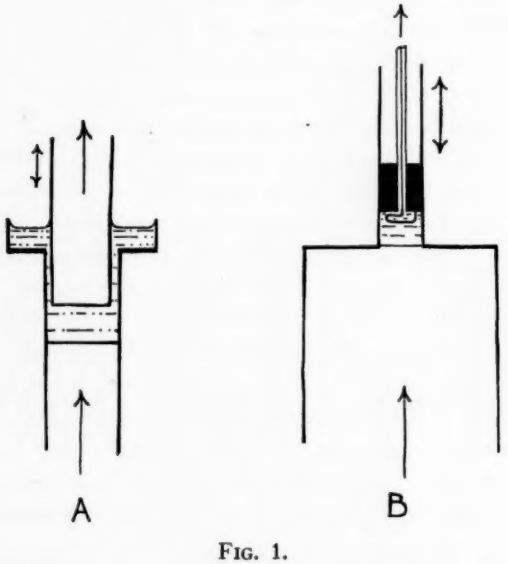

FIG. 1.

(1) The rectangular wave-guide cell used for measurements of κ at 3 cm and 1.25 cm is shown diagrammatically in Fig. 1*A*. A pure H_{01} mode is propagated in the liquid-filled guide, and a smaller guide picks up the wave after a known distance. The variation of response as the smaller guide is moved through the liquid is compared with the response variation of a standard piston attenuator. Since the attenuation is exponential, a plot of absolute attenuation, as determined by the distance moved through the liquid against the piston attenuator, should be a straight line, from the slope of which κ may be calculated. The achievement of a straight-line plot confirms that a single pure mode is being propagated in the liquid. With a movement through 30 db of attenuation, with a dead space at the beginning of 15 db, which is possible if a superheterodyne method of response measurement is used, an accuracy of 1 percent in κ is obtained. The method was found to give results at 3 cm in agreement with those obtained by the second method described here.

(2) Absorption coefficients were measured at both 3 cms and 10 cm by similar technique using the H_{11} mode in filled cylindrical wave guides near the cut-off diameter, fed from a rectangular guide as shown in Fig. 1*B*. A loop on the end of concentric line is used to pick up the response. The propagation constants p_1 and p_2 in the cylindrical guides are given by the relations:

$$p_1^2=(n_1-j\kappa_1)^2=\epsilon'-j\epsilon''-k_1c^2/\omega^2,$$
$$p_2^2=(n_2-j\kappa_2)^2=\epsilon'-j\epsilon''-k_2c^2/\omega^2,$$

where $k_1=1.831/r_1$ and $k_2=1.831/r_2$, r_1 and r_2

[3] R. J. Clayton, J. E. Houldin, H. R. L. Lamont, and W. E. Willshaw, J. Inst. Elec. Eng. **93**, 97 (1946).

[4] C. H. Collie, J. B. Hasted and D. M. Ritson, Proc. Phys. Soc. **73** (1948).

TABLE I. Dielectric properties of NaCl solutions. Observed values of ϵ' and ϵ'', the latter corrected for conductivity, are compared with values calculated from the corresponding values of ϵ_s and λ_s.

Temperature	Normalcy	Equivalent conductivity (I.C.T.)	10 cm $\epsilon'_{obs.}$ ±3	10 cm $\epsilon''_{obs.}$ corr. ±3	10 cm $\epsilon'_{calc.}$	10 cm $\epsilon''_{calc.}$	3 cm $\epsilon'_{obs.}$ ±1.3	3 cm $\epsilon''_{obs.}$ corr. ±1	3 cm $\epsilon'_{calc.}$	3 cm $\epsilon''_{calc.}$	1.27 cm $\epsilon'_{obs.}$ ±1	1.27 cm $\epsilon''_{obs.}$ corr. ±1	1.27 cm $\epsilon'_{calc.}$	1.27 cm $\epsilon''_{calc.}$	ϵ_s ±2	λ_s in cm ±.04
21°C	0.5	85.6	72.8	12.6	71.9	11.3	58.6	28.3	58.9	28.4	—	—	—	—	73.9	1.71
	1.0	78.7	67.4	13.1	67.5	10.1	56.2	25.0	56.0	25.7	30.1	30.4	29.6	30.8	69.1	1.63
	1.5	73.0	61.5	12.7	63.1	8.9	52.5	22.3	53.3	23.1	—	—	—	—	64.3	1.55
	2.0	68.6	56.2	11.8	58.0	7.9	49.6	20.7	49.4	20.6	27.8	26.0	27.6	26.3	59.0	1.51
	3.0	59.7	—	—	—	—	45.8	18.5	45.5	18.4	—	—	—	—	54.0	1.47
	5.0	42.4	—	—	—	—	41.8	15.7	41.9	15.8	—	—	—	—	48.4	1.39
1.5°	0.5	54.3	—	—	—	—	44.7	36.1	44.5	35.9	—	—	—	—	77.6	2.95
	1.0	49.7	—	—	—	—	43.0	32.8	42.7	32.4	—	—	—	—	71.0	2.80
	2.0	43.3	—	—	—	—	39.4	26.4	39.6	26.5	—	—	—	—	60.0	2.49
	3.0	38.0	—	—	—	—	35.9	21.4	35.9	21.3	—	—	—	—	51.0	2.26
	5.0	32.3	—	—	—	—	28.8	15.1	28.6	14.9	—	—	—	—	38.3	2.07
0°	.66	50.1	70.7	22.9	71.2	19.4	45.5	36.5	45.3	36.7	—	—	—	—	79.1	2.96
10°	.66	63.2	70.4	19.1	72.2	14.5	51.9	32.1	53.4	32.4	—	—	—	—	75.5	2.17
20°	.66	81.2	69.1	15.1	70.1	11.0	56.3	27.2	57.5	27.6	—	—	—	—	72.0	1.70
30°	.66	98.8	67.7	12.0	65.8	8.1	55.7	21.8	56.8	21.6	—	—	—	—	66.6	1.35
40°	.66	117.4	62.8	10.0	62.4	6.3	54.3	16.9	54.4	16.8	—	—	—	—	63.0	1.10

being the radii of the guides. We thus have the equations:

$$\epsilon' = \frac{(c^2/\omega^2)(k_1^2\kappa_1^2 - k_2^2\kappa_2^2)}{\kappa_1^2 - \kappa_2^2} - (\kappa_1^2 + \kappa_2^2),$$

$$\epsilon'' = 2\kappa_1[\epsilon_1' - (k_1^2c^2/\omega^2) + \kappa_1^2]^{\frac{1}{2}},$$

representing both dielectric constants ϵ' and ϵ'' in terms of the two absorption coefficients κ_1 and κ_2. The latitude in the choice of r_1 and r_2 is sufficient to allow the two measurements of the attenuation in the guide to be approximately independent measurements of n and κ, the optical constants in free space.

This method is used for the real dielectric constant at 3 cm and for both dielectric constants at 10 cm. It was found to give results for water at 10 cm in agreement with those obtained by a similar method in rectangular guide, and also using an E_{010} resonator with axial capillary.

In both methods constancy of power during the experiments was insured by checking back to the initial position of liquid cell or attenuator movement and noting the (unchanged) value of the response. Detailed descriptions of the experimental methods are given in the earlier papers.

(3) The H_{01} resonator method for the determination of n at 1.25 cm is described in an earlier paper.[4]

In all methods the circulation of water pumped from a thermostat through jackets on the apparatus provided temperatures constant to ±0.2°C.

Conductivity Measurements

It is necessary to make a correction for the conductivity before the correct value of ϵ'' can be found. On solutions of which the low frequency conductivity was not available in the literature, rough measurements were made in a cell with platinum electrodes of area 0.2 sq cm, 8 cm apart, using standard a.c. bridge technique. The accuracy was about 2 percent. The values obtained are given in the same table as the dielectric constant results.

Results

The experimental values of ϵ' and ϵ'' at 10 cm and 3 cm for sodium chloride solutions are given in Table I and those of other solutions in Table II. The measurements in Table II are all at 25°±0.2°C, but those on NaCl in Table I were taken at various temperatures in order to study the effects more fully. For the same reason some readings at 1.25 cm were taken on the NaCl solutions. Corrections for conductivity are made according to the equation:

$$\epsilon''_{\text{correct}} = \epsilon'_{\text{observed}} + (2\sigma/f),$$

where σ is the specific conductivity in e.s.u. and

f the frequency. For the purpose of these corrections there is assumed to be no change in this conductivity with frequency, an assumption which is discussed later. It is possible to analyse the corrected results in terms of a static dielectric constant ϵ_s, falling to an atomic dielectric constant ϵ_0. If there is a single relaxation time the relations below are generally true, and not dependent on the dielectric model.

$$\epsilon' = n^2 - \kappa^2 = (\epsilon_s - \epsilon_0)/(1+\omega^2\tau^2) + \epsilon_0$$
$$= (\epsilon_s - \epsilon_0)/(1+[\lambda_s/\lambda]^2) + \epsilon_0,$$

$$\epsilon'' = 2n\kappa = \frac{(\epsilon_s - \epsilon_0)\omega\tau}{1+\omega^2\tau^2} = \frac{(\epsilon_s - \epsilon_0)[\lambda_s/\lambda]}{1+[\lambda_s/\lambda]^2},$$

$$\lambda_s = 2\pi c\tau,$$

where τ is a single time of relaxation, corresponding to a wave-length λ_s ("*Sprungwellenlange*") and λ, ω, and c have their usual significance. In the tables the experimental values of ϵ' and ϵ'' at each frequency are compared with the values calculated from the corresponding values of ϵ_s and λ_s. These values of ϵ_s and λ_s are chosen so as to give the best fit to the experimental data when the above equations are used.

It is clear that the accuracy of measurement depends on the value of $\tan\delta$, being greatest where $\tan\delta$ is smallest, that is, for solutions of lowest conductivity. The estimated accuracies given below are those for a typical case, a normal solution of KCl, NaCl, or RbCl.

Accuracy in	ϵ' at 10 cm	±3
	ϵ'' 10 cm	±3
	ϵ' 3 cm	±1.3
	ϵ'' 3 cm	±1
	ϵ' 1.25 cm	±1
	ϵ'' 1.25 cm	±1
	ϵ_s	±2
	λ_s	±0.04

TABLE II. Dielectric properties of solutions at 3 and 10 cm, at 25°C. Observed values of ϵ' and ϵ'', the latter corrected for conductivity, are compared with values calculated from the corresponding values of ϵ_s and λ_s. Conductivity values are denoted "*T*" when taken from the International Critical Tables, "*E*" when found experimentally.

			3 cm					10 cm						
Salt	Normalcy	Equivalent conductivity	$\epsilon'_{obs.}$ ±1.3	$\epsilon'_{calc.}$	$\epsilon''_{obs.}$	$\epsilon''_{obs.}$ corr. ±1.0	$\epsilon''_{calc.}$	$\epsilon'_{obs.}$ ±3.0	$\epsilon'_{calc.}$	$\epsilon''_{obs.}$	$\epsilon''_{obs.}$ corr. ±3.0	$\epsilon''_{calc.}$	ϵ_s ±2	λ_s in cm ±.04
LiCl	0.5	81.0*T*	58.3	58.9	33.6	26.0	25.7	69.0	70.6	34.6	10.7	10.0	71.2	1.55
	1.0	72.9*T*	53.9	53.6	37.4	23.3	22.5	60.6	63.0	51.9	8.0	8.6	64.2	1.52
	1.5	67.0*T*	49.0	48.1	39.6	20.2	19.7	52.5	55.5	64.8	5.0	7.4	57.0	1.49
	2.0	62.0*T*	44.2	44.1	41.1	17.0	17.5						51.0	1.45
RbCl	0.5	125.5*E*	59.5	60.8	37.0	25.0	26.5	72.1	72.0	46.2	8.9	10.2	73.5	1.54
	1.0	114.7*E*	56.1	57.1	45.1	23.2	24.1	71.0	67.0	77.5	9.4	9.2	68.5	1.50
	1.5	107.5*E*	52.5	53.4	52.8	22.0	21.9						63.5	1.47
	2.0	104.5*E*	49.2	49.7	59.9	20.2	19.7						58.5	1.43
KCl	0.5	117.2*T*	60.0	60.8	37.2	25.9	26.5	70.3	72.0	45.7	10.5	10.2	73.5	1.54
	1.0	111.9*T*	57.4	57.1	45.2	23.6	24.1	64.3	67.0	73.9	6.8	9.8	68.5	1.50
	1.5	107.6*T*	54.4	53.4	53.0	21.8	21.9						63.5	1.47
	2.0	104.2*T*	49.0	49.7	58.4	18.4	19.7						58.5	1.43
$BaCl_2$	1.0	80.5*T*	52.3	53.4	37.7	22.2	22.4	64.1	62.8	57.1	8.8	8.6	64.0	1.50
	2.0	68.5*T*	44.1	43.6	43.3	16.9	16.8						51.0	1.42
HCl	0.25	377.0*T*	58.3	59.3	44.2	26.0	26.6	75.9	71.0	64.4	7.8	10.2	72.5	1.59
	0.5	360.0*T*	55.7	56.5	63.6	26.3	25.3						69.0	1.59
NaOH	0.25	206.0*T*	58.9	60.0	36.5	26.6	26.8	75.7	71.0	42.6	11.7	10.3	73.0	1.58
	0.5	196.0*T*	57.0	55.7	43.6	24.7	24.4	66.5	67.0	56.4	4.9	9.5	68.0	1.56
KI	0.198	126.4*T*	61.0	61.5	32.0	27.2	27.2	73.1	74.0	25.5	10.4	10.7	75.0	1.56
	0.396	122.0*T*	58.7	59.8	34.4	25.1	25.7	73.3	71.0	40.1	11.1	10.0	72.0	1.52
NaF	0.415	83.7*E*	58.3	60.4	31.7	25.0	26.6	71.3	72.0	28.2	7.4	10.3	73.0	1.55
	0.830	70.2*E*	56.2	57.3	35.2	24.0	24.5	72.4	68.0	43.4	8.4	9.5	69.0	1.52
$LaCl_3$	0.52	77.5*E*	57.3	58.4	33.0	25.2	25.6	70.9	70.0	33.1	8.9	9.9	71.0	1.54
	1.04	69.2*E*	52.6	53.3	35.9	22.0	22.4	66.1	63.0	51.0	7.8	8.8	64.0	1.50
KF	0.242	108.9*E*	61.5	61.5	32.0	27.9	27.5	73.5	73.5	24.6	8.8	10.7	75.0	1.58
	0.484	98.4*E*	58.9	59.3	34.9	25.7	26.1	72.1	70.5	35.9	7.3	10.1	72.0	1.56
NaI	0.428	100.8*T*	59.4	59.3	33.4	25.1	25.3	71.5	70.0	34.2	8.3	9.5	71.0	1.50
	0.856	94.4*E*	54.5	54.2	36.4	20.8	21.5						64.0	1.42
$MgCl_2$	0.468	84.9*T*	57.4	58.5	32.9	25.2	25.7	70.0	70.0	36.9	13.0	10.1	71.0	1.56
	0.935	74.3*E*	53.8	53.5	36.3	23.0	22.9	64.9	63.5	49.8	8.1	8.6	64.5	1.53
Na_2SO_4	0.5	70.0*T*	57.3	57.9	33.2	26.4	25.0						73.0	1.54
	1.0	59.0*T*	55.0	55.9	36.5	25.1	23.4						67.0	1.49
	2.0	45.5*T*	51.2	51.7	38.4	20.8	20.1						60.5	1.40

The accuracy of the calculated values of ϵ_s and λ_s depends on the correct choice of ϵ_0. This has been taken as 5.5, the value which has been found most suitable in the interpretation of our previous results on water. Additional weight is lent to this value for water by the infra-red measurements of Rubens[5] and Hawley Cartwright.[6] It is found that n, which is not much greater than 2 at 152μ, rises as the wave-length increases. It is unlikely that a very large depression or elevation of ϵ_0 for water occurs when ions are added, but a variation of ± 1 would only alter the values of ϵ_s by ± 1 percent.

The possibility of fitting the data to the above equations employing a single time of relaxation adds additional weight to the results; but the accuracy of some measurements at 10 cm is unsatisfactory when compared with our similar measurements on water, even when allowing for the higher loss angle. The experimental method was not pushed to its limit of accuracy, there being three principal defects:

(1) Selection of too large a diameter of smaller wave guide for the absorption measurement of ϵ'.

(2) Unevenness in the cylindrical wave-guide walls in absorption measurements.

(3) Mechanical defects of the pick-up probe movement.

The first two defects arose owing to the difficulty of drilling 5-mm diameter holes through distances greater than about 7 cm if commercial drills are used. Therefore the wave guides were made of extruded copper tube, which is only available in certain diameters, and which shows defects when it is strained by the soldering of water jackets. The movement of the pick-up probe was designed for measurements on water, through which greater distances are traveled; it was therefore not so accurate for the small movements required in measurements on ionic solutions.

At 3 cm the cylindrical wave guides of diameters of a few millimeters were machined, and a standard micrometer used for the movement. There is every prospect of being able to increase the accuracy of these methods beyond even that at 3 cm, since the errors are not theoretical but technical in origin.

[5] H. Rubens, V. D. Physik. Ges. **17**, 315 (1915).
[6] C. Hawley Cartwright, J. Chem. Phys. **4**, 413 (1936).

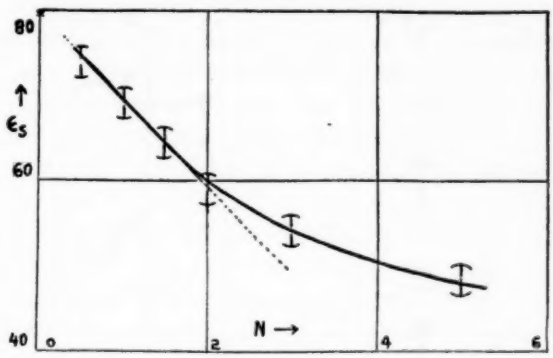

FIG. 2. Static dielectric constant of NaCl solution plotted against normality N. Temperature 21.0°C.

Previous Measurements

Previous measurements on ionic solutions at low frequencies suffer from the drawback of a high loss angle mentioned above.

The small increase in the dielectric constant of dilute solutions observed by Wien is not in conflict with the present results, since the variations in question are not of great magnitude, and might very well take place before the fall in the dielectric constant of concentrated solutions comes into play. This can be seen from Fig. 2 in which the static dielectric constant of NaCl solution is plotted against the concentration. It is clear, however, that the considerable fall of dielectric constant observed by Sack is in disagreement with the present results. Some of the most reliable work, that of Wyman,[7] and Drake, Pierce and Dow[8] on dilute solutions at 60 cm and 4 meters, shows that the lowering of dielectric constant is of such small magnitude as would be in keeping with our results on concentrated solutions. The only available results on concentrated solutions at centimetric wave-lengths are those of Elle[9] at 4 cm using a free-wave method with damped waves from a Herzian oscillator, and those of Cooper[10] on NaCl solutions at wave-lengths down to 7 cm using a transmission-line reflection method. The latter are in rough agreement with the results of the present authors, though not interpreted as such. (In his Fig. 4 much better agreement would be obtained by employing our values of the dielectric constant.)

[7] J. Wyman, Phys. Rev. **35**, 623 (1930).
[8] F. H. Drake, G. W. Pierce, and M. T. Dow, Phys. Rev. **35**, 613 (1930).
[9] D. Elle, Ann. d. Physik **30**, 355 (1937).
[10] R. Cooper, J. Inst. Elec. Eng. **93**, 69 (1946).

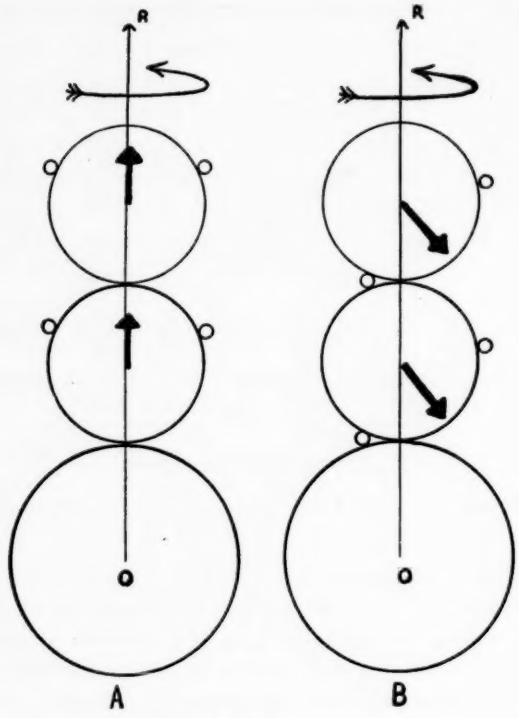

FIG. 3. Methods of hydration round an ion—*A*, cation; *B*, anion.

Discussion

(a) *Conductivity*

The consistency of the results with the above equations, assuming the conductivity to be the same as the d.c. value, is in confirmation not only of the accuracy of the results but also of the correctness of choice of value for the conductivity. It is interesting to note that the increase of conductivity of a dilute solution at a sufficiently high frequency predicted on the Debye-Falkenhagen theory[11] cannot be of significant size in these concentrated solutions. It can be seen from the experimental results that an increase in conductivity of more than 3 percent at 10 cm or 10 percent at 3 cm is not likely. The Debye-Falkenhagen theory does not apply quantitatively to solutions of these concentrations, but for a weaker solution, N/2 NaCl, the increase would be of the order of 20 percent at 3 cm and 5 percent at 10 cm. It is therefore probable that the effect is smaller, or occurs at a higher frequency, than would be predicted for these concentrations by use of the theory in its present form.

There is also the possibility of a fall of conductivity in solutions containing ions of abnormal mobilities such as H^+. The abnormal mobility of the hydrogen is believed to be due to its passage through water by an exchange mechanism which is written as follows:

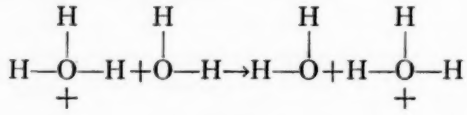

It was predicted by Hückel[12] that at wave-lengths of the order of 8 cm the conductivity of hydrogen ions should fall to the normal value for monovalent ions. Hückel's treatment, like that of other authors, assumes a Lorentz field

$$E+[(\epsilon+2)E/3]$$

acting on the ions, but this should perhaps be replaced by an Onsager field $3E/2$. With this modification we should not expect the fall of conductivity to occur until about 5 mm.

TABLE III. Values of $\bar{\delta}$ and $\bar{\delta}\lambda_s$.

	$\bar{\delta}\pm1$	$\bar{\delta}\lambda_s\pm2$
HCl	−10	0
LiCl	− 7	− 3.5
NaCl	− 5.5	− 4
KCl	− 5	− 4
RbCl	− 5	− 4.5
NaF	− 6	− 4
KF	− 6.5	− 3.5
NaI	− 7.5	− 9.5
KI	− 8	− 9.5
$MgCl_2$	−15	− 6
$BaCl_2$	−14	− 8.5
$LaCl_3$	−22	−13.5
NaOH	−10.5	− 3
Na_2SO_4	−11	− 9.5
	Values of δ^+, δ^-, $\delta\lambda_s^+$, $\delta\lambda_s^-$	
	δ^+, $\delta^-\pm1$	$\delta\lambda_s^+$, $\delta\lambda_s^-\pm2$
H^+	−17	+ 4
Li^+	−11	− 3
Na^+	− 8	− 4
K^+	− 8	− 4
Rb^+	− 7	− 5
Mg^{++}	−24	− 4
Ba^{++}	−22	− 9
La^{+++}	−35	−15
F^-	− 5	− 4
Cl^-	− 3	− 4
I^-	− 7	−15
OH^-	−13	− 2
SO_4^-	− 7	−11

[11] H. Falkenhagen, *Electrolytes* (Oxford University Press, London, 1934), p. 73.

[12] E. Hückel, Zeits. f. Elektrochemie **34**, 546 (1928).

TABLE IV. Minimum hydration of positive ions.

H^+	10
Li^+	6
Na^+	4
K^+	4
Rb^+	4
Mg^{++}	14
Ba^{++}	14
La^{+++}	22

Now the maximum decrease of conductivity is estimated as above from the experimental results on HCl in Table II to be 3 percent at 10 cm and 10 percent at 3 cm. This would indicate either that the replacement of the Lorentz field by the Onsager field in Hückel's treatment is justified, or that the exchange process occurs at a still greater rate. Measurements were also made of the absorption coefficient of $2N$ and $5N$ HCl at 1.25 cm, and the experimental values are sufficiently large ($2N$, $\kappa=4.74$, $5N$, $\kappa=5.04$) to indicate that at this wave-length there is no considerable decrease in conductivity.

(b) *Dielectric Constant*

We shall now consider qualitatively the experimentally measured depression of the dielectric constant of water brought about by the addition of ions. The most acceptable model is one of each ion attracting a sheath of several layers of water molecules around it; the dielectric properties of these molecules are naturally different from those of the molecules not in the neighborhood of an ion, and the effects fall off as we go further from the ion itself. The types of hydration believed to exist round a positive and a negative ion are shown in Fig. 3, *A* and *B*.

In solutions of concentrations less than $2M$, a linear relationship between the dielectric constant and the concentration is found:

$$\epsilon=\epsilon_\omega+2\bar{\delta}c,$$

where ϵ_ω is the static dielectric constant of water, c is the concentration in moles per liter, and $\bar{\delta}=(\delta^+ + \delta^-)/2$, δ^+ and δ^- being the (negative) contributions from the two ions, assumed univalent in this case. Values of $\bar{\delta}$, δ^+ and δ^- are given in Table III, it being necessary to assume the relative contributions of the two ions in a single case. We choose the case of sodium chloride, and $\delta^+_{Na^+}$ is taken as -8 and $\delta^-_{Cl^-}$ as -3 on the following basis; a negative ion, attracting water molecules as in Fig. 3*B*, still leaves them partially free to rotate, and so saturates them less than would a cation which attracts them as in Fig. 3*A*.[13] Therefore, the depression of dielectric constant is much larger for cations than anions; quantitative treatment in Part II of this paper gives $\delta^+=-10$, $\delta^-=-1$; on the other hand, the differences between the saturation are probably not so sharply defined as this; we have therefore estimated that

$$\delta^+_{Na^+}=-8\pm1 \quad \text{and} \quad \delta^-_{Cl^-}=-3\pm1.$$

It is possible to estimate the minimum hydration possible round a cation from the values of δ^+, on the following basis: the model adopted in Part II of this paper is one in which short-range order dominates the orientation of the inner hydration sheath, effectively removing a fraction of the water molecules from playing any part in the dielectric process; outside this there is a region in which a small amount of saturation takes place, so that these molecules make a small contribution to the fall of dielectric constant; it is reasonable to assume that this accounts for about a quarter of $\delta^+_{Na^+}$, that is, -2. Subtracting this contribution, we have for the minimum number of water molecules in the inner sheath, N,

$$(-\delta^+-2)/\epsilon_\omega=NM/1000,$$

where M is the molecular weight of water. Values of this minimum hydration number N are given in Table IV.

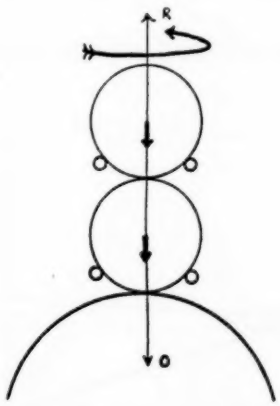

FIG. 4. Possible hydration round a large anion.

[13] D. H. Everett and C. H. Coulson, Trans. Faraday Soc. **36**, 633 (1940).

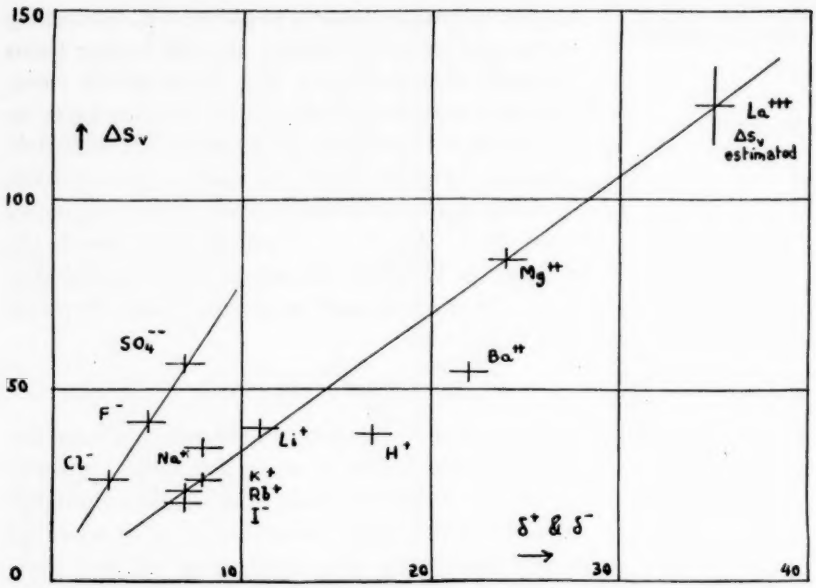

FIG. 5. Plot of ΔS_v against δ^+ and δ^- various ions.

These results, in particular the value of $N=4$ for ions such as Na^+ are of the correct order so far as the inner sheath is concerned, but it should be emphasized that this method can only give a lower limit to the hydration number; molecules in the first sheath are only incompletely prevented form taking part in the dielectric process, and therefore the hydration number will be correspondingly greater. The freedom of rotation of the water molecules in the sheath round an anion makes it impossible to treat these ions in the same way.

A quantitative treatment of the dielectric constant depression is given in Part II of this paper, but the following points may be noted here.

1. The cation contribution is dependent on its charge.

2. Cations of small radius make a larger contribution than those of large radius. Both these facts are in accordance with the present ideas on the hydration of cations.

3. A number of effects operate in determining the anion contribution, which is on the whole smaller than that of the cation. It is possible that large anions such as I^- bind the water molecules by both hydrogen atoms, as in Fig. 4, and so have a greater saturating effect than the small anions, which leave their hydration molecules free to rotate as in Fig. 3b. The large contribution of OH^- is explained on the basis that it can attract and saturate water molecules very easily, in a pattern similar to that of the water itself, without undue disturbance of the water lattice.

4. As will be recalled later, values of δ^+ and

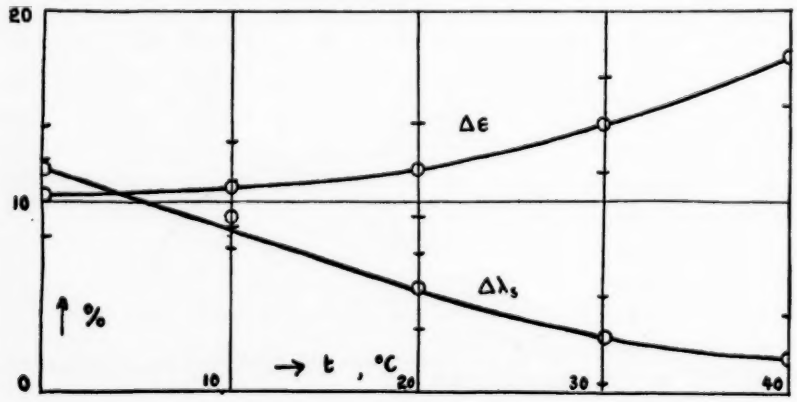

FIG. 6. Plot of percentage depressions of dielectric constant ($\Delta\epsilon$) and relaxation wave-length ($\Delta\lambda_s$) against temperature for 0.66N NaA.

δ^- are of the same order as those assumed by Hückel in his theory of concentrated solutions; but the relative values for different ions are not quantitatively the same.

It is of interest to compare our values of δ^+ and δ^- with ionic entropy data. In a recent paper,[14] Frank and Evans give the molal entropy of vaporization of ions at 25°, on changing from a molar solution to a gas at one-atmosphere pressure. This entropy change ΔS_v is to be regarded as being a measure of the ordering of water molecules in the vicinity of an ion (compare with Latimer[15]) comparable to the lining up of the water molecules. According to Frank and Evans part may be due to the restriction of an ion into a free volume box of water molecules. Since the solutions are of molar concentration in each case, there should be a certain correlation between ΔS_v and δ^+, and probably a different correlation with δ^-. These are shown in Fig. 5. It is significant that δ_I^--lies on the cation correlation line, indicating the rigid dipole type of hydration.

The "structure-breaking entropy" of Frank and Evans is considered under the heading of relaxation-time depression.

As can be seen from Fig. 2, the linear dependence of dielectric-constant depression on concentration no longer holds at concentrations above $2M$. It is possible to regard solutions in this region as ionic lattices with interspersed water molecules. At least we may be certain that the saturation effects of adjacent ions overlap. On this type of model the prediction of dielectric constant behavior is much more difficult.

It may be seen from Table I that the dielectric-constant depression is greater at high temperatures than at low. This is more clearly shown in Fig. 6, in which the percentage depression of the dielectric constant of water by $0.66N$ NaCl is plotted against temperature. This effect could be explained on the assumption that the short-range order round an ion increases with the temperature, as the competing order of the water decreases. This would imply that the hydration increases with the temperature, a problem which requires further experimental elucidation.

(c) *Relaxation Time*

The linear depression of the relaxation wavelengths of water by the addition of ions at concentrations of less than $1.5M$, which is shown in Fig. 7, may be discussed on the same basis as the dielectric constant depression. The authors[4] discuss the mechanism of re-orientation in water and heavy water in the light of experimental results. Comparison with the viscosity data of water and heavy water over a temperature range leads us to believe that re-orientation takes place by molecules undergoing the same process as that of viscous flow, or self-diffusion, that is, a

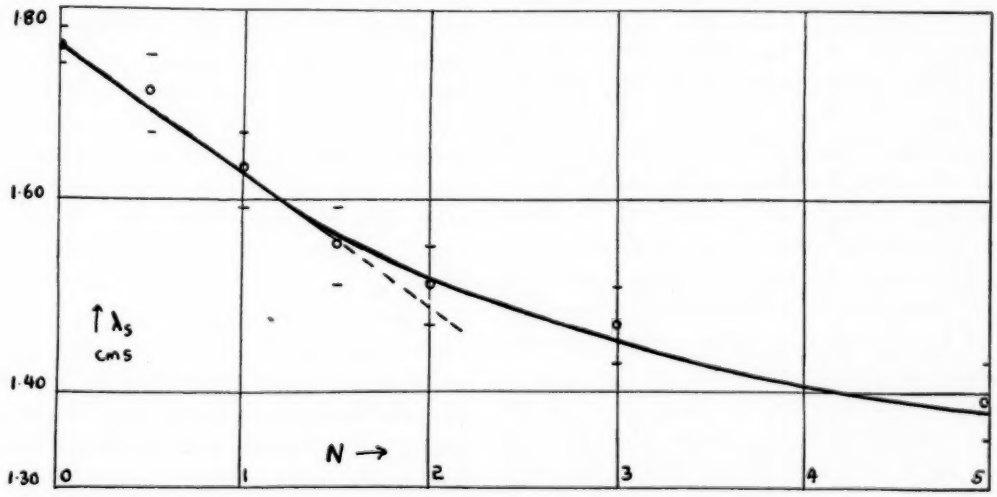

FIG. 7. Plot of relaxation wave-length of NaCl solution against normality N.

[14] H. S. Frank and M. Evans, J. Chem. Phys. **13**, 479 (1945).
[15] W. M. Latimer, Chem. Rev. **18**, 349 (1935).

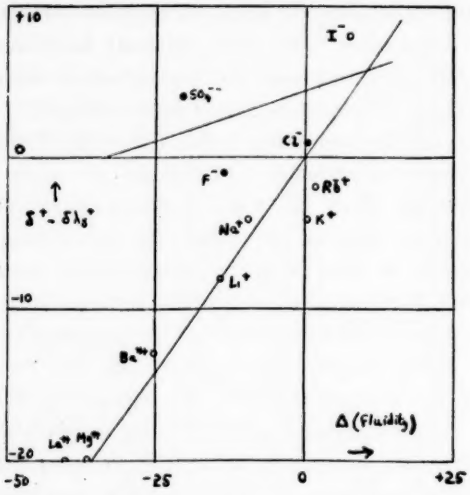

FIG. 8. Speculative correlation of fluidity elevation with sum of short-range and long-range effects. Anions, represented as blackened circles, lie on shorter line. Errors of ± 6 in $\delta^+ - \delta\lambda_s^+$ not marked in.

replacement of empty lattice spaces by molecules which themselves leave further spaces for replacement. Thus re-orientation takes place at the moving boundaries of the broken pieces of "lattice."

Most ions when added to water rupture the lattice, creating more boundaries at which re-orientation can take place; they have a so-called "structure-breaking" effect, of which the depression of relaxation time or wave-length is a reasonable index.

Using a similar notation to that of dielectric-constant depression, we have at concentration lower than $1.5M$; $\lambda_s = \lambda_{s\omega} + 2\bar{\delta}\lambda_s c$, where $\lambda_{s\omega}$ is the relaxation wave-length of water, and $\bar{\delta}\lambda_s = (\delta\lambda_s^+ + \delta\lambda_s^-)/2$, $\delta\lambda_s^+$ and $\delta\lambda_s^-$ being the (negative) contributions from the two ions, both taken as univalent in this case. In Table III are given values of $\delta\lambda_s^+$, $\delta\lambda_s^-$, and $\bar{\delta}\lambda_s$, it being assumed that in a solution of ions of equal radius, such as KF, there are equal contributions from K and F (compare with Bingham[16]). The error of ± 2 in $\bar{\delta}\lambda_s$ is such that these values can only be regarded as semiquantitative.

It is apparent that $\delta\lambda_s^+$ is dependent on the charge of the cation, and is greater for large ions than for small, much-hydrated ions of the type of Li^+, Mg^{++}, and H^+. The concept of a large ion breaking the structure more than a small ion, because it is difficult to fit into the structure without splintering, is reasonable. Moreover these qualitative differences are in agreement with the generally accepted views on the interpretation of x-ray diffraction, Raman and infra-red absorption spectra, and on the depression of the temperature of maximum density.

It is usual to correlate relaxation-time data with macroscopic viscosity data, as was done by the authors in the case of water and heavy water. In dilute solution the increase of viscosity is satisfactorily explained on the theory of Falkenhagen and Dole,[17] which employs the concept of the ionic atmosphere, but at high concentrations there is a negative viscosity effect which requires a different explanation. Finkelstein[18] developed a theory of the re-orientation of solvent molecules, giving a positive viscosity effect varying with the concentration; but we must be able to explain the effects of various ions in concentrated solution in both elevating and depressing the viscosity. In this connection the "ionic elevation of fluidity" of Bingham[16] is of value. Let us first examine the relaxation-time data purely from the point of view of "structure-breaking" effect. Frank and Evans[14] tabulate values of a quantity ΔS_{st} which can be regarded as the entropy change due to the disturbing effect of the ion and hydration sheath on the surrounding water; but it contains other factors also. We should expect this to be correlated with $\delta\lambda_s^+$ and with Bingham's elevation of fluidity. The values of $\delta\lambda_s^+$ are not sufficiently accurate to correlate with ΔS_{st}, but for monovalent ions there is no violent disagreement. For polyvalent ions, however, ΔS_{st} is not calculated, and large negative values of fluidity elevation appear. Now polyvalent ions are shown on the basis of relaxation time to have a strong structure-breaking effect and they should therefore give large positive elevations of fluidity. There is, therefore, a second factor operating in the cases of viscosity or fluid flow. This is the short-range order effect, by which water molecules in the inner hydration sheath, by reason of their strong orientation, are made more viscous and depress the fluidity. This effect, analogous to the depression of dielectric constant, will be greater for polyvalent ions, and

[16] E. C. Bingham, J. Phys. Chem. **45**, 885 (1941).

[17] See H. Falkenhagen, reference 11, p. 245 for summary.

[18] B. N. Finkelstein, Phys. Zeits. **31**, 130, 165 (1930).

will be correlated to δ^+. A speculative treatment involving both effects, that is, correlating fluidity elevation, with values of $\delta^+ - \delta\lambda_s^+$, is shown in Fig. 8, but the present level of accuracy is such that further measurements of relaxation wave-length are necessary before this picture of viscosity can be regarded as fully justified by relaxation-time measurements.

The variation of depression of relaxation wave-length with temperature is shown in Fig. 6, in which the percentage depression by $0.66M$ NaCl is plotted against temperature. The effect of the ions is greater at low temperatures than at high, as can be seen from the following picture; the low values of the relaxation wave-length of water at low temperatures indicate that the boundaries at which re-orientation takes place are much more rare; yet the effect of the ions in introducing new boundaries is of the same order as at higher temperatures, since the size and number of the hydration sheaths is of the same order; therefore, the introduction of the ions into the water will have a proportionately greater effect on the frequency of occurrence of the boundary, and so on the relaxation wave-length.

Conclusion

We therefore find that it is possible to give a reasonable qualitative explanation of our results on depression of dielectric constant and relaxation time on the basis of the model outlined above. In Part II of this paper we shall consider the depression of dielectric constant from the standpoint of dielectric theory, and the bearing of these results on electrolyte theory.

PART II

D. M. Ritson and J. B. Hasted

In Part II of this paper the theory of dielectric saturation in the neighborhood of an ion is shown to give values for the depression of dielectric constant of concentrated ionic solutions of the same order as those found experimentally in Part I. Modern theories explaining the deviations of concentrated solutions from the Debye-Hückel theory are considered, and semi-quantitative estimations made of the various contributing factors—*viz.*: Dielectric constant variation, Bjerrum-type association, co-volume correction, and structure-breaking effect.

Theoretical Treatment of the Dielectric Constant Depression

It was predicted by Sack[1] that the dielectric constant of an aqueous ionic solution would be considerably lower than that of water. On the basis of the Debye theory of dielectrics he calculated a depression which was about a hundred times greater than the experimental values recorded in Table III, Part I of this paper.

In general we should expect that any theory based on the assumption that an ion is surrounded by a continuous dielectric medium of macroscopic dielectric constant, should give a lower limit to the actual dielectric saturation in the neighborhood of an ion; short-range order round the ion, which is ignored when we treat the surrounding medium as continuous, must further increase the saturation.

The apparent discrepancy between calculation and experiment arises from the use of a Debye model for the dielectric constant, which assumes an improbably small value for the dipole moment in water. We have attempted in this paper to bring Sack's original conception of the electric field of an ion effectively saturating the surrounding dielectric into line with more recent views on the structure of water.

There are two fundamental difficulties encountered in any such treatment. There is still considerable uncertainty as to the correct model for the dielectric constant of water, and there is no method of treating the short-range order round the ion. One is therefore limited to obtaining a qualitative estimate of the effect, and showing that this estimate is in agreement with experiment.

We consider first a point charge placed in a continuous dielectric medium. For this dielectric medium we take two models.

[1] H. Sack, Phys. Zeits. **27**, 206 (1926); *ibid.* **28**, 199 (1927).

Model 1 is a dielectric obeying Onsager's equation exactly. At 25°C we can approximate to water by taking values for the dipole moment μ_0 of 1.88 Debye units and refractive index $n^2=4.13$, leading to a dielectric constant of 78.7. There is one grave drawback to this model, namely, that it gives an effective moment (the dipole moment plus the dipole moment induced by the reaction field) of 3.77 Debye units, which is rather improbable.

We obtain for the dielectric constant ϵ

$$\epsilon E=\frac{4\pi}{V}\frac{(n^2+2)(2\epsilon+1)}{3(2\epsilon+n^2)}L\left[\frac{\epsilon(n^2+2)}{(2\epsilon+n^2)}\frac{\mu_0^2}{kT}E\right]+\frac{3\epsilon(n^2-1)E}{2\epsilon+n^2},$$

where L is the Langevin function, and all the other symbols have their usual significance.

We can make the approximation

$$\epsilon E=\frac{4\pi}{V}\frac{(n^2+2)}{3}L\left(\frac{(n^2+2)}{2}\frac{\mu_0^2}{kT}E\right)+\frac{3}{2}(n^2-1)E,$$

and on substituting the values given above we find at 25°C that

$$\epsilon E=5.69E+1.58\cdot10^6L(1.39\cdot10^{-4}E).$$

In addition to this treatment, which is open to the criticism given above, we have taken a second model. This is an empirical modification of Kirkwood's[2] formula for small fields, so that it applies to large fields. Kirkwood's formula gives

$$\epsilon E=(4\pi/V)[\alpha E+(u\bar{u}/3kT)E],$$

where u is the effective dipole moment, and $\bar{u}$ is the moment plus the moment induced in the surroundings.

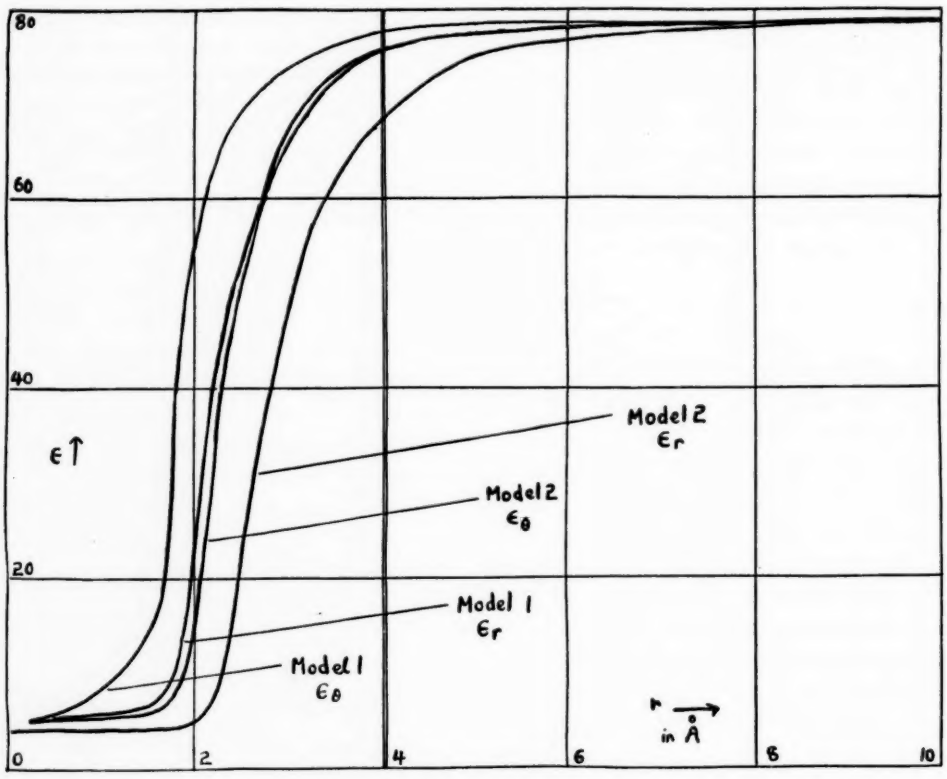

FIG. 1. Plot of dielectric constants ϵ_r, ϵ_θ against distance r in angstroms from an ion.

[2] J. Kirkwood, J. Chem. Phys. 4, 592 (1936).

We have made the empirical modification

$$\epsilon E=(4\pi/V)\alpha E+uL(u/kT)E.$$

Putting $u=2.45$ Debye units, which is Verwey's[3] estimate of its magnitude, we obtain

$$\epsilon E=4E+1.03\cdot 10^{6}L(2.18\cdot 10^{-4}E).$$

Although this second formula is certainly not entirely correct, our main interest is to show that our value for the saturation effect is not markedly dependent on the model we adopt.

Now consider the point charge as the center of coordinates r_1 and θ. We know that the field E_r round the ion must obey the equation

$$\text{div}(E+4\pi P)=0,$$

or

$$E+4\pi P=e/r^2. \tag{1}$$

We shall write this equation in the form

$$AE_r+BL(CE_r)=e^2/r^2, \tag{1a}$$

where for, model 1,

$$A=5.69,\quad B=1.58\times 10^{6},\quad C=2.18\times 10^{-4},$$

and for model 2,

$$A=4,\quad B=1.03\times 10^{6},\quad C=2.18\times 10^{-4}.$$

We now define two dielectric constants

$$\epsilon_r=\partial P/\partial E_r,\quad \epsilon_\theta=\partial P/\partial E_\theta.$$

The significance of these quantities lies in the fact that they represent the effective dielectric constants when a small additional field is applied.

From Eq. 1(a) we see that

$$\epsilon_r=A+BC[dL(CE_r)/d(CE_r)], \tag{3(a)}$$

and

$$\epsilon_\theta=A+B[L(CE_r)/E_r]. \tag{3(b)}$$

These are the effective dielectric constants when a small additional field is applied either along or perpendicularly to the radius vector.

We have plotted in Fig. 1 values of ϵ_r and ϵ_θ against those calculated from Eqs. 3(a), 3(b), and (1).

When $r>4$A, the values of ϵ do not differ appreciably from ϵ_s and can be expressed accurately by the approximations

$$\epsilon_r=\epsilon_s[1-(3b/r^4)], \tag{4a}$$

$$\epsilon_\theta=\epsilon_s[1-(b/r^4)], \tag{4b}$$

where in model 1, $b=57.8\times 10^{-32}$, and in 2, $b=163\times 10^{-32}$. These results are obtained by expanding $L(x)$ as $(x/3)-(x^3/45)+\cdots$, and neglecting terms above the second.

Returning now to the original problem of the effect of an ion of finite size on the surrounding dielectric, it is apparent that in the region below 4A, which is of the order of the radius of the first hydration sheath, the representation of the dielectric as continuous will not be a valid approximation. Therefore, for simplicity, we have made the following assumptions:

(a) That we can represent a positive ion as surrounded by a completely saturated first shell, and beyond that by continuous dielectric of dielectric constant given by (4a) and (4b). We assume that a saturated shell has a radius $r_+ + 2r_\omega$ where r_+ is the radius of the ion, r_ω that of the water.

(b) That the negative ion can be represented by a completely unsaturated first shell of dielectric constant ϵ_s, surrounded outside a radius of $r_- + 2r_\omega$ by continuous dielectric.

We shall now consider the application of a small field to the region round a point charge. We can represent the applied field E by a potential ψ. We shall only briefly indicate the argument which can be found in full in Debye's *Polar Molecules*, Chapter VI. As $r\to\infty$ we know that ψ must be of the form

$$\psi=-[E_r+(\mu/r^2)]\cos\theta. \tag{5}$$

We assume that

$$\psi=-[Ef(r)+(\mu/r^2)g(r)]\cos\theta$$
$$=E\cdot R(r)\cos\theta,$$

for

$$r>r_\pm+2r_\omega.$$

Now it is a fundamental equation of electromagnetic theory that

$$\text{div}\epsilon\cdot\text{grad}\psi=0.$$

This gives, on rearrangement,

$$\frac{d}{dr}\left[\epsilon_r r^2\frac{dR(r)}{dr}\right]-2\epsilon_\theta R(r)=0. \tag{6}$$

The solution of this equation is

$$f(r)=-r[1-(2b/r^4)], \tag{6a}$$

$$g(r)=(1/r^2)[1+(b/r^4)], \tag{6b}$$

[3] E. J. W. Verwey, Rec. Trav. Chim. 60, 127 (1941).

if

$$r<r_{\pm}+2r_{\omega}.$$

The solution must be of the form $\psi=Ar\cos\theta$, where A is a constant, as the dielectric constant is now independent of r and θ.

Putting in the boundary condition that ψ is everywhere continuous and that $\epsilon_r(d\psi/dr)$ is also continuous, we obtain

$$\mu=(\epsilon_\theta-1)/(2\epsilon_\theta+1)(r_{\pm}+2r_{\omega})^3.$$

The total polarization P_r outside $r=r_{\pm}+2r_{\omega}$ is given by

$$P_r=\frac{1}{4\pi}\int\left(\epsilon_r\frac{d\psi}{dr}+\epsilon_\theta\frac{d\psi}{d\theta}\right)dT,$$

where dr is any volume element. Therefore,

$$P_r=\tfrac{1}{2}\int_{r_{\pm}+2r_{\omega}}^{\infty}\int_0^{\pi}r^2\left(\epsilon_r\frac{d\psi}{dr}+\epsilon_\theta\frac{d\psi}{d\theta}\right)\sin\theta\cdot drd\theta. \quad (7)$$

We require to obtain the decrease in polarization ΔP of the medium caused by the presence of the central ion. If we write P_0 for the polarization of the medium if no ion were present, P_s for the polarization in the first sheath round the ion, we obtain

$$\Delta P_+=P_0-P_{r+}-P_{s+}. \quad (8)$$

The dielectric constant ϵ_s for a normal solution is, therefore, $\epsilon_s=\epsilon_\omega+2\bar{\delta}c$, where $\bar{\delta}=(\delta^+-\delta^-/2)$ and

$$\delta^+=N\Delta P_+\cdot 4\pi\cdot 10^{-3}. \quad (9)$$

Substituting the values we have obtained for ϵ_r, ϵ_θ, and ψ, and ignoring terms of the order of $(b/r^4)^2$, we find

$$\Delta P=[-Db/4(r+2r_{\omega})^4]-P_s. \quad (10)$$

It also follows from our initial assumptions that for negative ions $P_s=0$, for positive ions $P_s=r^3\epsilon_\omega/3$. This leads directly to the following values for δ^+ and δ^- for ions of radii $r_+=r_-=1$A, and r_ω equal to 1.36A:

Model 1, $\delta^+=-11.5$, $\delta^-=-1.5$, and $\bar{\delta}=-6.5$.
Model 2, $\delta^+=-13$, $\delta^-=-3$, and $\bar{\delta}=-8$.

The calculated values of $\bar{\delta}$ are thus of the right order of magnitude. The main contribution to the dielectric lowering comes almost entirely from the first sheath. The large increases for Li^+, H^+, and OH^- ions are undoubtedly due to the extent of short-range order round the ions. For divalent and trivalent ions the above calculation is unsatisfactory, as the short-range order probably extends further than the first shell.

Theory of Concentrated Solutions of Strong Electrolytes

In 1926 Hückel[4] suggested that the deviations from the Debye-Hückel theory of strong electrolytes at moderate concentrations could be explained by supposing that the dielectric constant was a function of the concentration. He suggested the law for the dielectric constant D of a solution of molecular concentration c, $D=D_0-2\bar{\delta}c$ where D_0 is the dielectric constant of the solvent; he showed that this led to a formula for the activity of an electrolyte of the following type:

$$\log_{10}f=\mathbf{D}+Bc, \quad (11)$$

where $\mathbf{D}$ is the usual Debye-Hückel term of the type $[0.4343z_+z_-e^2\kappa/2D_0kT(1+\kappa a)]$, where

$$\kappa=\left[\frac{4\pi ne^2(\nu_+z_+^2+\nu_-z_-^2)}{D_0kT}\right]^{\frac{1}{2}}, \quad (11a)$$

n is the number of molecules of salt per cc, ν_+ and ν_- the numbers of positive and negative ions of valencies z_+ and z_-, corresponding to one molecule of salt, e the electronic charge in e.s.u., k the Boltzmann constant, and a the ionic radius measured in angstrom units.

Hückel's term Bc, due to the variation of the dielectric constant, is given by the relation:

$$Bc=\frac{0.4343e^2}{nD_0^2kT}\left(\frac{\nu_+\delta^+}{a^+}+\frac{\nu_-\delta^-}{a^-}\right). \quad (11b)$$

Now the type of relation $\log_{10}f=\mathbf{D}+Bc$ is a well-known explanation of the variation of activity with concentration, found experimentally. Values of $B_{\text{experimental}}$ for a large number of salts are given by Harned and Owen.[5] Using $\bar{\delta}$ and a as adjustable parameters, Hückel obtained remarkedly good agreement with these values of $B_{\text{experimental}}$. We were interested to find

[4] E. Hückel, Phys. Zeits. 26, 93 (1925).
[5] Harned and Owen, *The Physical Chemistry of Electrolytic Solutions* (Reinhold Publishing Corporation, New York, 1943).

that our experimental values of δ^+ and δ^-, given in Part I of this paper, were of the same order of magnitude and showed the same qualitative trends as those used by Hückel, although quantitatively the agreement is not good.

Later authors rejected the view that the deviations were due to changing dielectric constant, and attributed them to other causes. It is likely that a number of different factors contribute, each one involving a term Bc; we shall consider each in turn and attempt to assess semiquantitatively its contribution to B. They are as follows:

1. Van der Waals co-volume correction.
2. Correction due to the breaking up of the water structure by the ions.
3. Correction due to the type of ionic association envisaged by Bjerrum.
4. Varying dielectric constant correction, outlined above.

Co-Volume Effect

Since the distance of closest approach of two ions is fairly large, it would seem likely that a van der Waals co-volume correction must be made to the activity. Van Rysselberghe and Eisenberg[6] have calculated values of B on this basis, using Ursell's treatment. We have investigated whether it is legitimate to apply such a correction by assuming a highly simplified lattice model.

If we consider the distribution of n molecules on N lattice points, such that around each molecule the neighboring positions must be unoccupied, we find that the number of distinguishable configurations Ω is given by

$$\Omega=\left(\frac{(N-n)!\cdot(N-n)!}{(N-2n)!N!}\right)^x\cdot\frac{N!}{(N-n)!n!},\qquad \text{for } N\gg n. \quad (12)$$

This result is obtained by using a very general method of enumerating lattice configurations, which we shall describe elsewhere. The equation for Ω follows from the fact that we have x axes along which each center must be separated by at least two lattice points. The probability that any random configuration satisfies this condition along any axis is given by the expression in the brackets. The power x gives the simultaneous probability that we can satisfy the condition along the axes simultaneously. $N!/(N-n)!n!$ represents the total number of random distinguishable configurations.

We now consider a model approximating to a number of solvated molecules B in a solvent A. A two-dimensional model is shown diagrammatically in Fig. 2. The B molecules and their solvation sheath occupy one unit cell of the lattice. This type of model is chosen as being similar to water, where the coordinated sheath of water molecules fits into the general lattice structure. For simplicity we consider a cubic lattice.

Let there be N_A solvent molecules A, and N_B solute molecules B. $8N_B$ of the solvent molecules A are held by the N_B solute molecules. There are 13 axes along which the B's must be separated by at least one cell. Four axes are shown in the two-dimensional figure. The number of positions that it is possible for B molecules to occupy is N_A. Making the assumption that the solution is "regular," i.e., that the potential and molecular energies are not altered for the different configurations, we can write down the configurational partition function with the aid of Eq. (12) as

$$\Omega=\left(\frac{(N_A-N_B)!(N_A-N_B)!}{(N_A-2N_B)!N_A!}\right)^{13}\cdot\frac{N_A}{(N_A-N_B)!N_B!}. \quad (13)$$

The "partial potentials" are given by

$$\mu_A=\mu_{0A}-kT(\partial\ln\Omega/\partial N_A), \quad (14a)$$

$$\mu_B=\mu_{0B}-kT(\partial\ln\Omega/\partial N_B). \quad (14b)$$

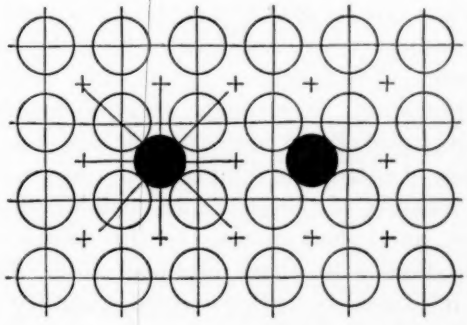

FIG. 2. Two-dimensional cubic lattice of (unfilled) solvent molecules A, showing closest position of approach of two (blackened) solute molecules B.

[6] P. van Rysselberghe and S. Eisenberg, J. Am. Chem. Soc. **61**, 3030 (1939).

If we consider the case for $N_A \gg N_B$ so that we can ignore term in $(N_B/N_A)^2$ we find that

$$\mu_A \simeq \mu_{0A} + kT \ln(N_A/N_A+N_B), \quad (15a)$$

$$\mu_B \simeq \mu_{0B} + kT \ln(N_B/N_A+N_B) \times[1+28(N_B/N_A)]. \quad (15b)$$

If we had assumed van der Waal's law we should have written the equation as

$$\mu_A \simeq \mu_{0A} + kT \ln(N_A/N_A+N_B), \quad (16a)$$

$$\mu_B \simeq \mu_{0B} + kT \ln(N_B/N_A+N_B) \times[1+32(N_B/N_A)]. \quad (16b)$$

We see, therefore, that in the particular case we have considered above, the expressions reduce to a form very near to that of van der Waals law; it follows that the treatment of ions in solution may be made along similar lines to that of molecules in a gas, and it is likely that the application of Ursell's method may be made with success. Harned and Owen's[5] revision of van Rysselberghe and Eisenberg's[6] treatment gives a value of $B=2.2063\times10^{-3}\times a^3$ for a single 1:1 electrolyte, or $\frac{3}{2}\times2.2063\times10^{-3}\times a^3$ for a single 2:2 electrolyte, where a represents the distance of closest approach of two ions measured in angstrom units. For consistency we have used the empirical values of a which are obtained by fitting the experimental activity coefficients to Eq. (11). These values are given by Harned and Owen[5] and are greater than the crystallographic radii.

Structure-Breaking Effect

The interactions of the ion with the water lattice is also an important contributing factor; it has been brought out clearly in a recent paper of Frank and Evans.[7] The authors point out that for "structure-breaking" salts the water lattice becomes increasingly random with increasing concentration. Accordingly, dilution should be accompanied by a decrease of entropy. The change of entropy of dilution with concentration is a measure of the structure-breaking effect of an ion, and values obtained by this method show correlation with those obtained from Raman and infra-red absorption spectra, viscosity data, etc. There is, in addition, some sort of correlation with the shift of relaxation time of the water by the ion, experimental values of which were given in Part I of the present paper. When the relaxation-time measurements are considered in conjunction with the previous study by the authors of the re-orientation process in water and heavy water, it appears likely that relaxation-time shift can be regarded as a fairly reliable measure of structure-breaking effect. As was demonstrated by Falkenhagen,[8] it is impossible to obtain the correct heats of dilution from Hückel's theory, and it would seem equally difficult for modern theories to account fully for the activity coefficient deviations without taking lattice effects into account. It is, however, the free energy and not the entropy change with which we are concerned, and this is, of course, smaller. We found in the first part of this paper that the effect was much greater at low temperatures than at high, and this will lead us to predict that activity deviations are likely to be much greater near the freezing point than at high temperatures.

However, it is not yet possible to calculate even approximately the contribution made by this effect to the value of B, and we have, therefore, made an estimate simply by subtracting the other contributions from the experimental value.

It will be seen from Table III where the contributions to B are tabulated, that the structure-breaking contributions so obtained are in accordance with the usual comparisons between various ions, i.e.,

$$Ba^{++} > Rb^{+} + > K^{+} > Na^{+} > H^{+},$$

and are, moreover, fairly small.

Bjerrum-Type of Ionic Association

Bjerrum[9] attempted to account for anomalies at high concentrations by assuming that ionic association occurs. He calculates the electrostatic and other forces acting between two ions, and equates the resulting potential energy with mean kinetic energy at various inter-ionic distances. Within a certain distance the ions will "associate." The association constant $(1-\alpha)$ depends on concentration in a complicated, but

[7] H. S. Frank and M. Evans, J. Chem. Phys. **13**, 479 (1945).

[8] H. Falkenhagen, *Electrolytes* (Clarendon Press, Oxford, England, 1934), p. 282.

[9] N. Bjerrum, D. Kgl. Dansk. Vid. Selsk. Medd. **7**, No. 9 (1926); Ergeb. der exakt. Naturwiss. **6**, 125 (1926).

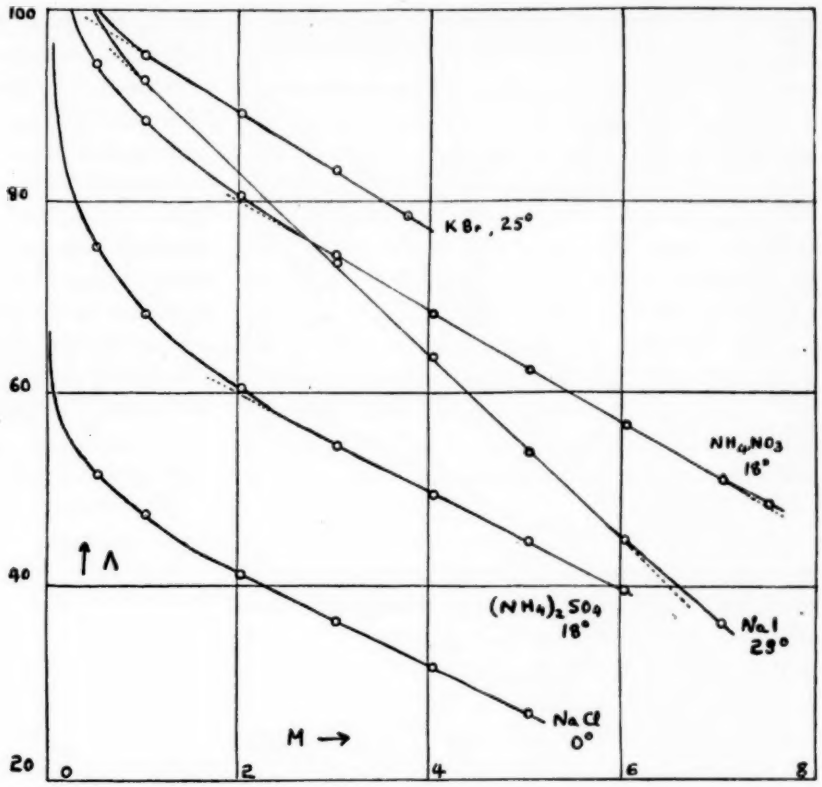

FIG. 3. Typical equivalent conductivities $\Lambda \times 10^{-6}$ mho/10^{-3} gmole plotted against concentration M. Data from I.C.T. Values of Λ for KBr at 25°, depressed by 20 divisions for reasons of space.

approximately linear, manner, but may be shown to be of the order of 0.14 in molar solution of 1:1 electrolyte of ionic radii sum equal to 2.82A. For higher concentrations, smaller ions, ions of higher valency, and solvents of low dielectric constant the association will be higher.

It is unfortunately impossible to accept the calculated values of $(1-\alpha)$ on Bjerrum's theory, or to calculate back from the heats of dilution, since a number of approximations are made which are not permissible in more concentrated solutions; moreover, at distances of less than 4A from an ion the dieclectric constant is a rapidly varying quantity, as is shown above. However, it appears very likely that some sort of association of this type occurs in concentrated solutions because there certainly are strong forces acting between ions at very short distances.

The only method of estimating Bjerrum's association that remains is by treatment of the conductivity data. Let us consider in detail the simplest case, a 1:1 strong electrolyte at 25°C, in which there can be little question of incomplete dissociation in the usual sense of the term, but for which accurate conductivity data over a wide concentration range exist. Such a case is potassium bromide, for which there are the measurements of Jones and Bickford.[10] Between concentrations of $1.5-6N$ many such salts, including the present case, show a linear dependence of equivalent conductivity on concentration. This is illustrated for a number of cases in Fig. 3, for which the data have been taken from the International Critical Tables. It is true that many salts show a non-linear dependence in such concentrated solution, for instance, salts of lithium. But, nevertheless, the dependence in a large number of the simplest cases is linear, and this fact must be explained. Now it is with solutions of these concentrations that we are concerned when investigating Bjerrum association, because the effect is more significant in this range. It is well known that for the conductivity of dilute solutions, many equations with satisfactory theoretical basis have been proposed (Onsager[11]), but all explain the dependence on the square root of the concentration which is found

[10] G. Jones and C. F. Bickford, J. Am. Chem. Soc. 56, 602 (1934).
[11] L. Onsager, Phys. Zeits. 28, 277 (1927).

TABLE I. Approximate percentage Bjerrum association $100(1-\alpha)$ calculated from conductivities of concentrated solutions.

Electrolyte	Approximate percentage association estimated for normal solution	Temperature °C	Data
HCl	11	18	I.C.T.
NaCl	10	0	I.C.T.
NaCl	10	18	I.C.T.
KCl	5	18	I.C.T.
NaI	9	25	I.C.T.
KBr	5	25	Jones and Bickford*
KI	5	18	I.C.T.
RbCl	4	18	I.C.T.
CsCl	4	18	I.C.T.
$BaCl_2$	12	25	Jones and Dole**

* See reference 10.
** See reference 12.

in dilute solution; modifications are made to Onsager's equation to explain deviations from this. It is very unlikely that such modifications will transform the dependence into a linear one in concentrated solution, by the addition of a term which counter-balances the non-linear dependence, nor is it likely that a viscosity correction will transform the relationship into a linear one; in other words, a single equation of the accepted type will not hold over the entire concentration range unless the Onsager term reduces to a constant value and a linear term, $-K_c$, is introduced at high concentrations only. The empirical equation of Jones and Dole[12] is an example of this type of behavior:

$$\Lambda=\Lambda_\infty-A\sqrt{c}/(1+G\sqrt{c})-Kc, \qquad (17)$$

but in order to fit the dilute solution data, the constants of this equation are so chosen that it does not reduce to a linear equation until very high concentrations ($\sim 10N$) are reached. Although this equation is capable of explaining the experimental data over the widest concentration range, and is of a theoretically satisfactory form, the parameters are chosen entirely empirically, and a single equation of this type would not be capable of explaining both the dilute solution data and the linear dependence in concentrated solution. In particular, the values of K are such that it is difficult to find a theoretical explanation of them. It is necessary to find a theoretical equation which holds in dilute solution and reduces to a constant term by the time a concentration of about $2N$ is reached; at greater concentrations, a new effect comes into play to explain the linear dependence. We shall assume that this effect is the Bjerrum association. Its linear dependence on concentration cannot be predicted theoretically, in fact, as we have seen above, the dependence on concentration is believed to be complicated, but only approximately linear. But in view of the criticisms of the theory given above, the original treatment is not unsatisfactory.

We have thus two equations involving the concentration on which the conducivity depends:

(1) An equation which we will call C, tending to a constant conductivity value at concentrations greater than $1.5M$. The form of this equation will be discussed later.

(2) A simple equation D, holding over the linear range; $\Lambda=\alpha\Lambda'$ where $1-\alpha$ is the degree of association and Λ' is the constant value to which equation C has tended. We can estimate the association approximately from the slope of the conductivity-concentration curve. The accuracy is limited by the following facts:

(1) It is not possible to obtain a good value for Λ'; we have used what seems the most reasonable value, namely, that obtained by producing the linear section back to zero concentration.

(2) It is doubtful whether a viscosity correction should be applied and if so what form it should take. There seems to be insufficient justification for simply multiplying the conductivity by the macroscopic viscosity, as, for instance, Jones and Dole have done. We have omitted the viscosity correction entirely.

The approximate values of percentage association in normal solution estimated in this way for a number of electrolytes are given in Table I, to the nearest whole number. The qualitative dependence on ionic radius and valency are according to theory.

It remains to discuss the form of equation C. It is possible to explain the data below $0.02N$ on a theoretical basis, and at the same time obtain a relation which is capable of tending to a constant value. The equation

$$\Lambda=\Lambda_\infty-A\sqrt{c}/(1+G\sqrt{c})$$

[12] G. Jones and M. Dole, J. Am. Chem. Soc. **52**, 2245 (1930).

which was first suggested by Lattey[13] as an empirical relationship, and was used with the addition of a Kc term by Jones and Dole, has actually a theoretical basis provided the constants are chosen correctly. Kaneko[14] suggested that the introduction of a factor of $1+\kappa a$ in the denominator would correct the Onsager theory for the finite size of the ion. Although this suggestion has not been given much consideration, and although the treatment has been criticized, it is apparent that this factor corresponds to the $1+\kappa a$ which appears in the denominator of the Debye-Hückel expression for the logarithm of the activity coefficient of a concentrated solution; it seems perhaps a plausible correction. For dilute solutions we have the equation (C′):

$$\Lambda=\Lambda_\infty-O\sqrt{c}/(1+\kappa a), \qquad (C')$$

where $O\sqrt{c}$ is the theoretical Onsager term, a modification of the original Debye-Hückel expression.

This type of treatment is supported by our experimental results on Debye-Falkenhagen conductivity increase at high frequency. We found the increase in concentrated solutions to be much smaller than would be expected on the original theory. If the Debye-Hückel conductivity term is diminished by the factor $1+\kappa a$, this becomes intelligible, since it is only this term which is annulled at high frequencies. An independent term reducing the equivalent conducivity of concentrated solutions below its value at infinite dilution, the type of term we introduce as being due to Bjerrum association, would not be affected: so that the high frequency conductivity would not show such a large increase above the d.c. conductivity.

In the above equation for dilute solutions there are no empirical factors, but the equation will not hold except in dilute solutions, although its range is greater than that of the Onsager equation. The exact position for potassium

TABLE II. Experimental data of Jones and Bickford for KBr equivalent conductivity at 25°C compared with various equations.

c	$\Lambda_{obs.}$	Λ_0(Onsager) calculated back from obs.	ΔShedlovsky	ΔΔShedlovsky	ΔJones and Dole	ΔΔJones and Dole	ΔPresent equation	ΔΔPresent equation
0.00025	150.16	151.65	150.16	0.00	150.24	−0.08	150.16	0.00
.00036	149.87	151.66	149.88	− .01	149.93	− .06	149.89	− .02
.0005	149.55	151.66	149.57	− .02	149.61	− .06	149.57	− .02
.00075	149.12	151.70	149.12	.00	149.13	− .01	149.12	.00
.001	148.78	151.76	148.75	.03	148.74	.04	148.75	.03
.0016	148.02	151.79	148.02	.00	147.98	.04	148.02	.00
.002	147.64	151.86	147.62	.02	147.56	.08	147.61	.03
.005	145.47	152.14	145.46	.01	145.36	.11	145.44	.03
.01	143.15		143.19	− .04	143.11	.04	143.12	.03
.02	140.26		140.25	.01	140.25	.01	140.07	.15
.05	135.44		135.36	.08	135.51	− .07	134.74	.70
.1	131.19		131.19	.00	131.27	− .08		
.2	126.59		127.61	−1.02	126.62	− .03		
.5	120.35		127.33	−6.98	120.23	.12		
1.0	115.46				115.50	− .04		
2.0	109.37				110.98	−1.61		
3.0	103.55				108.39	−4.84		
3.75	98.70				106.98	−8.26		

Onsager	$\Lambda_0=(\Lambda+59.790\sqrt{c})/(1-0.2274\sqrt{c})$
Shedlovsky	$\Lambda=151.63-94.27\sqrt{c}+100.96c(1-0.2274)\sqrt{c}$
Jones and Dole	$\Lambda=151.84-103.77\sqrt{c}/(1+1.8953\sqrt{c})-0.492c$
Present equation	$\Lambda=151.63-94.27\sqrt{c}/(1+1.08\sqrt{c})$

Horizontal lines indicate limits beyond which equations do not fit the observed data.

[13] R. T. Lattey, Phil. Mag. **4**, 831 (1927).
[14] S. Kaneko, J. Chem. Soc. Japan **56**, 793, 1320 (1935); *ibid.* **58**, 985 (1937).

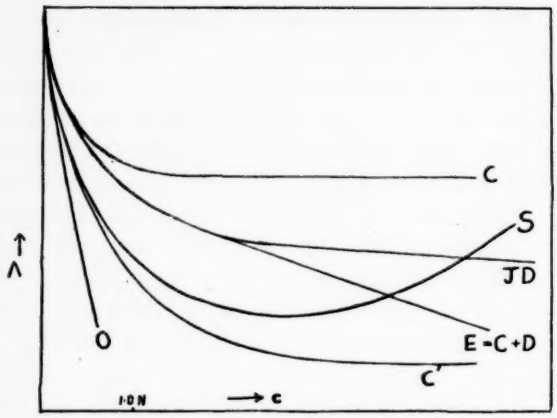

FIG. 4. Qualitative variation of equivalent conductivity with concentration according to various equations. *E*, experimental; *C*, *C'*, *D*, equations as in text; O, Onsager; S, Shedlovsky; JD, Jones and Dole.

bromide at 25° is given in Table II,* and the type of behavior of the Onsager, Shedlovsky,[15] and present equations is shown qualitatively in Fig. 4. Our values of a are from the ionic radius in the crystal.

There is no doubt that the equation of Jones and Dole fits the data over the widest concentration range, but it fails at high concentration and is moreover entirely empirical. The viscosity correction which the authors apply widens the range, but will not reduce the equation to a linear variation; moreover, it is of doubtful theoretical validity. The Onsager equation deviates steadily at concentrations greater than $0.001N$, but when modified, as suggested here, will hold to $0.02N$, whereas the Shedlovsky equation with one empirical factor deviates from $0.1N$. We have tried our modification of the Onsager equation on Shedlovsky's data for HCl, LiCl, NaCl, KCl,[16] for which the agreement is satisfactory up to about $0.01N$.

The form of the equation is therefore promising, but it cannot be regarded as even approximately correct in concentrated solution, since the assumptions underlying the Onsager term do not apply. We cannot therefore offer any detailed explanation of how the equation of type *C* is made up, and must be content simply to offer this as a possible method of treatment of the linear variation of conductivity with concentration in concentrated solution.

It will be seen that this method of estimating association is somewhat similar to that used by Davies and his collaborators[17] in more dilute solutions of incompletely dissociated salts. The cases considered here, would, however, be regarded as completely dissociated on Davies' treatment.

Our estimated values of $1-\alpha$, given in Table I, are a direct contribution to the value of B in the activity equation. Although the contributions to B are estimated in other cases at 25°, there are no sufficient experimental data available at this temperature. In these cases, estimations of $(1-\alpha)$ at 18°C have been used. As will be seen by comparing the values of NaCl at 0° and 18°, there is very small temperature dependence. But it appears that the amount of Bjerrum association is an extremely difficult term to estimate.

Variable Dielectric-Constant Correction

If we accept the fact that this correction is only a contribution to the value of B and need not be equated to the experimentally determined values of this constant, it is no longer necessary to treat a or $\delta^{\pm}$ as adjustable parameters in Hückel's theory. We have, therefore, calculated contributions to B on the basis of Eq. (11b), using Harned and Owen's[5] experimental values of a and our experimental values of $\delta^{\pm}$. The justification for using these values of a is that the dielectric constant will only vary outside the distance of closest approach of the ions.

Conclusions

In Table III are given the contributions to B from the various effects considered above; the contribution from the structure-breaking effect

TABLE III. Valves of contribution to activity coefficient correction factor *B*.

Electrolyte	B Experimental	B Bjerrum	B Hückel	B Co-volume	B Structure
HCl	+0.13	−0.11	+0.09	+0.18	−0.03
NaCl	+0.04	−0.10	+0.05	+0.16	−0.07
KCl	+0.02	−0.05	+0.05	+0.09	−0.07
RbCl	+0.02	−0.04	+0.06	+0.07	−0.08
$BaCl_2$	+0.03	−0.12	+0.11	+0.18	−0.14

$B_{experimental} = B_{Bjerrum} + B_{Hückel} + B_{co\text{-}volume} + B_{structure}$.

* The calculations are taken from the paper of Jones and Bickford.

[15] T. Shedlovsky, J. Am. Chem. Soc. **54**, 1405 (1932).

[16] T. Shedlovsky, J. Am. Chem. Soc. **54**, 1411 (1932).

[17] C. W. Davies, Trans. Faraday Soc. **23**, 351 (1927).

is not calculated theoretically, but estimated by subtracting the other contributions from the experimental value of B. It should be possible eventually to correlate the values estimated in this way with data obtained by other methods, although only entropies, and not free energy data are at present available. As has been mentioned above, the structure-breaking contributions are qualitatively correct for different ions, i.e.,

$$Ba^{++} > Rb^{+} > K^{+} > Na^{+} > H^{+}.$$

This order would be more strongly accentuated if the crystallographic radii, with an allowance for the first hydration sheath, had been used instead of Harned and Owen's empirical values in calculating the various contributions.

Unfortunately the Bjerrum association for lithium cannot be easily estimated, as the conductivity curve is not linear with concentration over a wide range. It is clear that considerable progress must be made in study of the various effects before a quantitative verification of the behavior of activity coefficients of concentrated solutions can be made. Our table is extremely tentative and little weight should be attached to the numerical values.

Many of the effects described would be capable of direct experimental verification.

Accurate measurements of the Falkenhagen effect over a concentration range $0-1N$ and over a frequency range would be capable of showing whether the high frequency conductivity is a linear function of concentration, and, hence, whether Bjerrum association can be evaluated from conductivity data, as has been done in this paper. Further experimental work on this problem is in the course of preparation.

The importance of structure-breaking effects of the ions could be evaluated by measuring activities and heats of dilution at low temperatures where this effect should be very marked, and at high temperatures when it should be of much less importance. Further comparison of the dilution of salts with those of rare gases, to explain the anomalies mentioned by Frank, are also indicated.

Significant data could be obtained by carefully selected experiments and analyses of the existing data on mixtures of electrolytes where the covolume effect and dielectric effect of the salts present would probably be the determining factors.

It appears that future progress in electrolyte theory of concentrated solutions must be in an experimental evaluation of the various factors involved and by a vigorous theoretical attack on the basic problems of solute-solvent interaction.

Acknowledgments

The work described in this paper has been carried out on behalf of the Director of Physical Research, Admiralty, and the authors wish to record their thanks for permission to publish. The authors are grateful to Lord Cherwell for kindly extending to them the facilities of the Clarendon Laboratory, and to Dr. R. P. Bell, F.R.S., and to Mr. T. L. Cottrell for helpful suggestions.

THE JOURNAL OF CHEMICAL PHYSICS VOLUME 16, NUMBER 1 JANUARY, 1948

Discussion of the Absolute Reaction Rate of Unimolecular Decompositions

JOSEPH O. HIRSCHFELDER
Department of Chemistry, University of Wisconsin, Madison, Wisconsin
(Received June 19, 1947)

In the usual theory of absolute reaction rates it is assumed that the molecules in the activated complex are in statistical equilibrium with the molecules in the initial state. This assumption is not justified in the case of unimolecular decompositions because the molecules in the initial state must gain the energy of activation by a stepwise process, usually by the transfer of quanta of vibrational energy from one normal mode to another. The size of these energy jumps and their frequency inevitably affect the over-all reaction rate. The problem is considered in considerable detail for a rough idealized mode. In this case, the actual reaction rate should be smaller by a factor of 0.5 to 0.387 than the value computed from the usual theory of absolute rates. A rigorous development would require further development of the original Ramsperger-Rice-Kassel treatment.

IN the usual theory of absolute reaction rates it is assumed that the molecules in the activated complex are in statistical equilibrium with the molecules in the initial state. This assumption is not justified in the case of unimolecular decompositions because the molecules in the initial state must gain an energy of activation by a stepwise process, usually by the transfer of quanta of vibrational energy from one normal mode to another. The size of these energy jumps and their frequency inevitably affect the over-all reaction rate. The treatment given here is a generalization of the recent work of Zwolinski and Eyring.[1]

In the case of normal chemical reactions where neither the initial nor the final state is unimolecular, the assumption of statistical equilibrium is probably valid. However, the equilibrium assumption may require modification if the activation energy is not large compared to kT, as in the case of some problems of viscous flow.

Unimolecular reactions involve a special consideration which is not important in other cases. The way in which the systems obtain their energy of activation may determine the rate at which the decomposition takes place. The usual theory of absolute reaction rates must be modified to take this into account, otherwise it would lead to erroneous conclusions. For example, the usual theory of absolute reaction rates leads to absurd results under the following conditions. Consider the possibility of a diatomic molecule AB dissociating unimolecularly without transfer of energy by radiation. The potential energy is shown in Fig. 1 as a function of the separation between A and B. Physically it is clear that the atoms A and B cannot unite nor can AB dissociate without either a collision with another molecule or the transfer of energy by radiation. However, we can examine the problem from the standpoint of the theory of absolute reaction rates. According to all of the rules, it is permissible to consider the top of the energy hump as the activated state. Expressions for the rate of dissociation and the rate of association can be written down in the usual manner. The impossibility of a collision between A and B resulting in a stable molecule AB is expressed by setting the transmission coefficient equal to zero for the association reaction. This is altogether reasonable and does not require any further comment. However, the transmission coefficient for the dissociation reaction is certainly unity since the potential energy curve of Fig. 1 indicates that A and B repel each other for separations greater than that of the activated state. Furthermore, all of the other factors in the expression for the rate of decomposition of AB are finite and non-vanishing. Thus the theory of absolute reaction rates leads to a non-vanishing rate of dissociation of a diatomic molecule where it should have given zero. This paradox disappears when we examine the way in which the molecule AB gains its energy of activation, i.e., only by collision with other molecules. Since the system cannot get from the initial to the activated states under the

[1] Zwolinski and Henry Eyring, J. Am. Chem. Soc. (in process of publication).

hypothetical conditions which we imposed, the normal theory of absolute reaction rates does not apply. Or in the language of statistical mechanics, that part of phase space corresponding to the activated state is inaccessible to the molecules in the initial state so that no unimolecular decomposition is possible. The accessibility of the activated state is therefore an important factor in reaction kinetics.

Polyatomic molecules, in contrast to diatomic molecules, can decompose unimolecularly without requiring energy transfer by radiation. The energy surges from one degree of freedom to another within the molecule until the energy of activation is accumulated in the degree of freedom along which the molecule decomposes. The original Ramsperger-Rice-Kassel[2] treatment is still, after twenty years, the most fundamental approach to this problem. Ramsperger, Rice, and Kassel developed equations for the rate of decompositions in terms of the specific transition probability for the transfer of vibrational energy. These transition probabilities depend on the exact shape of the potential energy surface (or the anharmonicity of the vibrations). The lower vibrational states of the normal modes are almost harmonic, and energy transfers are infrequent. The higher vibrational states are no longer independent, energy transfers are frequent, and the system behaves classically. Unfortunately, no one has ever developed a satisfactory theory for the specific transition probabilities, so that it is not possible to use the Ramsperger-Rice-Kassel equations for the solution of practical rate problems. Instead, the Eyring theory of absolute reaction rates is usually applied.

The use of the theory of absolute reaction rates for the unimolecular decomposition of a polyatomic molecule implies two assumptions: First, the molecule is sufficiently large that it may be considered as a heat reservoir possessing a characteristic temperature independent of the other molecules in the vessel. For any given molecule this approximation becomes better the higher the pressure. Thus the experimental variation of the unimolecular rate constant with pressure is the best test for the validity of this assumption. The assumption is justified at pressures sufficiently high so that the unimolecular rate constant is no longer dependent on pressure. The second assumption is that the molecules in the activated state are in equilibrium with the molecules in the initial state. This is the condition which we wish to examine in this present paper. For this purpose we fix our attention on the vibrational quantum state of the degree of freedom along which the molecule decomposes. In going from the initial to the activated state the molecule passes successively through each of the vibrational states. Sometimes energy is lost to other degrees of freedom within the molecule and this quantum number decreases; at other times, energy is gained from the other degrees of freedom and this quantum number increases. Thus the process of gaining the energy of activation is quite devious in contrast to bimolecular reactions where the activation energy is attained in a single violent collision. The following calculation shows that the number of molecules in the activated state is somewhat less than would be expected from statistical equilibrium with the initial state if this energy of activation is accumulated in a number of steps.

Consider a hypothetical polyatomic molecule in which the vibrational quantum number in the degree of freedom along which the decomposition procedes is indicated by J. Let the initial state be called "O" and the activated state "N." The successive reactions by which the molecule goes from the initial to the activated state are indicated by

$$0 \underset{k_{r1}}{\overset{k_{f0}}{\rightleftarrows}} 1 \underset{k_{r2}}{\overset{k_{f1}}{\rightleftarrows}} \cdots \underset{k_{rN-1}}{\overset{k_{fN-2}}{\rightleftarrows}} (N-1) \underset{k_{rN}}{\overset{k_{fN-1}}{\rightleftarrows}} \mathrm{N} \text{ or } A \overset{k_F}{\rightarrow}. \quad (1)$$

Here k_F is the rate constant for molecules in the

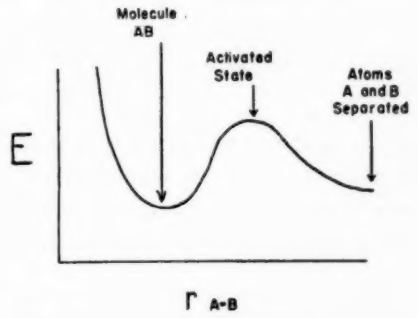

FIG. 1.

[2] Louis Kassel, *Kinetics of Homogeneous Gas Reactions* (Chemical Catalog Company, 1932), Chapter V.

activated state proceeding to the decomposition products. For simplicity of presentation we assume here that once a molecule has decomposed past the activated state it does not return. Then we can write the set of simultaneous equations for the rate of change of the concentrations, C_J, in each of the vibrational states. After a steady state is reached, the rate of change of each of these concentrations (except the C_0) is zero so that:

$$\frac{dC_A}{dt}=k_{fN-1}C_{N-1}-(k_F+k_{rN})C_A=0, \tag{2}$$

$$\frac{dC_{N-1}}{dt}=k_{fN-2}C_{N-2}-(k_{fN-1}+k_{rN-1})C_{N-1}+k_{rN}C_A=0, \tag{3}$$

$$\frac{dC_J}{dt}=k_{fJ-1}C_{J-1}-(k_{fJ}+k_{rJ})C_J+k_{rJ+1}C_{J+1}=0, \tag{4}$$

$$\frac{dC_1}{dt}=k_{f0}C_0-(k_{f1}+k_{r1})C_f+k_{r2}C_2=0. \tag{5}$$

These equations suffice to determine C_A in terms of C_0. Let us examine the simplest possible case where

$$k_{f0}=k_{f1}=k_{f2}=\cdots=k_{fN-1}\equiv k_f, \tag{6}$$

$$k_{r1}=k_{r2}=k_{r3}=\cdots k_{rN}\equiv k_r, \tag{7}$$

and

$$k_f/k_r=\exp(-\epsilon/kT). \tag{8}$$

This situation would occur if the energy jump between successive vibrational states is ϵ if all vibrational states have the same degeneracy, and if the transmission coefficients are in all cases unity. The solution to Eqs. (2) through (5) is then:*

$$\frac{C_A}{(C_A)_{\text{Eq}}}=\frac{1}{1+\frac{k_F}{k_r}\left(\frac{1-\exp(-N\epsilon/kT)}{1-\exp(-\epsilon/kT)}\right)}. \tag{9}$$

Here, $(C_A)_{\text{Eq}}$ is the concentration of molecules in the activated state which would exist if statistical equilibrium were attained between the molecules in the initial state and the molecules in the activated state. For the model which we are assuming, it is clear that

$$(C_A)_{\text{Eq}}=C_0\exp(-N\epsilon/kT). \tag{10}$$

Furthermore, with this model we can determine the ratio k_F/k_r. At complete statistical equilibrium, including back reactions, the same number of systems are moving backwards as forwards through the activated state. Since we have assumed that all transmission coefficients are unity, it follows that $k_F/k_r=1$. If, in addition, the energy of activation for the reaction, $N\epsilon$ is large compared to kT, we obtain:

$$\frac{C_A}{(C_A)_{\text{Eq}}}=\frac{1-\exp(-\epsilon/kT)}{2-\exp(-\epsilon/kT)}. \tag{11}$$

Here if ϵ is large compared to kT,

$$C_A/(C_A)_{\text{Eq}}=\tfrac{1}{2}. \tag{12}$$

If ϵ is equal to kT,

$$C_A/(C_A)_{\text{Eq}}=(e-1)/(2e-1)=0.3873. \tag{13}$$

And if ϵ is small compared to kT, $C_A/(C_A)_{\text{Eq}}$ becomes correspondingly small. However, it is likely that if the energy between successive vibrational states were small compared to kT, the motion would become classical and in the degree of freedom along which the molecule decomposes, the average energy change on successive surges would remain of the order of kT. We conclude that for this simple model of a hypothetical polyatomic molecule the concentration of molecules in the activated state is roughly between 0.5 and 0.38 times the value expected on the basis of statistical equilibrium. Thus, for this case, the rate of the unimolecular decomposition is smaller by this same factor than would be expected on the basis of the usual theory of absolute reaction rates.

The model considered in this paper is admittedly crude, but it is gratifying in that it leads to a concentration of molecules in the activated state only slightly smaller than the equilibrium concentration assumed in the usual theory of absolute reaction rates. This superficial examination does not uncover any evidence that the theory of absolute reaction rates would lead to any large errors in the rate of unimolecular decompositions of polyatomic molecules. How-

* The author wishes to thank the Journal of Chemical Physics reviewer for pointing out this simple form for the solution.

ever, the use of this theory leaves much to be desired from the logical standpoint. Real progress in the theory of unimolecular reactions requires the evaluation of the specific transition probabilities in the Ramsperger-Rice-Kassel treatment. Until this is done, the theory of unimolecular decompositions must remain on a semiquantitative basis.

The author wishes to express his thanks to the Navy Bureau of Ordnance for financial assistance during the course of this work through NOrd Contract 9938 with the University of Wisconsin.

THE JOURNAL OF CHEMICAL PHYSICS VOLUME 16, NUMBER 1 JANUARY, 1948

Statistical Thermodynamics of the Sorption of Vapors by Solids

MALCOLM DOLE
Department of Chemistry, Northwestern University, Evanston, Illinois
(Received July 1, 1947)

The statistical method of treating the sorption of vapors, begun by Fowler and Guggenheim and extended to multilayer sorption by Cassie and Hill, is further generalized to include variable heats of sorption in different layers. It is shown under what conditions multilayer sorption can lead to a linear isotherm and to various modifications of the BET equation. The treatment is also extended to the case of interaction between sorbed molecules in the same layer.

IN a previous paper[1] methods of calculating the free energy and heats of sorption of water vapor by proteins and high polymers were discussed for the cases of linear, Langmuir, and BET[2] sorption isotherms. At first sight it might appear unsound to apply equations derived on the basis of a kinetic picture of equilibrium between gas molecules colliding with and evaporating from a solid surface to the sorption of water by solids such as proteins and high polymers where the water molecules must diffuse through the solid to reach the points of sorption, but when it is realized that Fowler and Guggenheim[3] and Cassie[4] and Hill[5] have derived both the Langmuir monolayer adsorption and the BET multilayer adsorption equations on the basis of statistical reasoning, the theoretical justification for this procedure becomes apparent.

At this point we wish to emphasize that application of the BET equation to the sorption isotherms of water sorbed by high polymers in no way implies any estimate of a surface. In fact, by a careful study of the statistical derivation it is realized that the BET equation gives as one of its parameters the number of adsorption sites, not the surface. The surface can only be obtained by a further calculation in which a value for the area per site is assumed. Thus the area is a derived quantity. By adsorption we mean adsorption on a free surface, where the gas molecule can collide directly with the adsorbing site, while by sorption we mean the increase of weight of the solid as the result of the penetration and sorption of water vapor within the solid, at sorption sites where there is no free surface. Justification of the application of the BET equation to the sorption of water vapor by high polymers depends upon the existence of a real reversible equilibrium, no hysteresis, upon the negligible contribution of change of volume to the free energy of the sorption process, upon the sorption sites of the polymer remaining fixed in space during sorption (otherwise the process would be that of mixing two liquids), and upon the absence of interaction between sorbed molecules. In a later paper giving new data on the sorption of water by certain experimental polymers we shall discuss the applicability of the

[1] M. Dole and A. D. McLaren, J. Am. Chem. Soc. **69**, 651 (1947).
[2] S. Brunauer, P. H. Emmett, and E. Teller, J. Am. Chem. Soc. **60**, 309 (1938).
[3] R. H. Fowler and E. A. Guggenheim, *Statistical Thermodynamics* (University Press, Cambridge, 1939), p. 426.
[4] A. B. D. Cassie, Trans. Faraday Soc. **41**, 450 (1945).
[5] T. L. Hill, J. Chem. Phys. **14**, 263 (1946). The treatment of Hill is a correction to and extension of that of Cassie.

BET equation more fully and compare the theory presented here with that of Barrer.[6]

In this paper we extend the statistical treatment to consider cases of varying heats of sorption between layers and of multilayer sorption with interaction between molecules in the same layer. The nomenclature of Fowler and Guggenheim will be used for the most part.

GENERAL STATISTICAL TREATMENT

Let

S_0 = number of sites having no sorbed molecules,
S_1 = number of sites having one sorbed molecule,
S_2 = number of sites having two sorbed molecules, etc.,
N_1 = total number of sorbed molecules in the first layer,
N_2 = total number of sorbed molecules in the second layer, etc.,
N_S = total number of sorption sites,
N = total number of sorbed molecules,
a_1 = internal partition function for sorbed molecules in the first layer,
a_2 = internal partition function for sorbed molecule in the second layer, etc.,
a_L = internal partition function for molecule in the liquid state,
$x = p/p_0$, partial pressure ratio of sorbate in the vapor phase,
Q = total partition function of all sorbed molecules, and
n = total number of layers.

As a result of these definitions,

$$S_0 = N_S - N_1, \quad S_1 = N_1 - N_2, \quad \text{etc.},$$

$$\sum_{i=1}^{n} N_i = N.$$

The total partition function is given by the equation

$$Q = \frac{N_S!}{\prod_0^n S_i!} \prod_{i=1}^{n} (a_i)^{N_i}, \tag{1}$$

or

$$Q = \frac{N_S!}{(N_S-N_1)!(N_1-N_2)!\cdots(N_{n-1}-N_n)!N_n!} \cdot a_1^{N_1}\cdots a_n^{N_n}. \tag{2}$$

[6] R. M. Barrer, Trans. Faraday Soc. **43**, 3 (1947).

The Helmholtz free energy, F, then follows from (2), after approximating the factorials by Stirling's theorem.

$$-\frac{F}{RT} = \ln Q = N_S \ln N_S - (N_S - N_1)\ln(N_S - N_1) - \cdots (N_{n-1} - N_n)\ln(N_{n-1} - N_n) - N_n \ln N_n + \sum_{i=1}^{n} N_i \ln a_i. \tag{3}$$

For the conditions of equilibrium between the first and second layers, similarly to Hill,[2] we obtain

$$\frac{N_S - N_1}{N_1 - N_2} = \frac{N_1 - N_2}{N_2 - N_3}\cdot\frac{a_2}{a_1}, \tag{4}$$

and for equilibrium between the second and third layers, etc.,

$$\frac{N_1 - N_2}{N_2 - N_3} = \frac{N_2 - N_3}{N_3 - N_4}\cdot\frac{a_3}{a_2}, \quad \text{etc.} \tag{5}$$

In Hill's treatment

$$a_3 = a_2,$$

with a consequent simplification of (5) and similar relationships.

Finding the variation of the free energy with respect to N and setting the result equal to the chemical potential of the pure liquid phase, we deduce that

$$\frac{N_n}{N_{n-1} - N_n} = x\cdot\frac{a_n}{a_L}. \tag{6}$$

Substituting (6) into (4), (5) and similar relations, we find, also similarly to Hill,

$$N_1 - N_2 = (N_S - N_1)x\cdot\frac{a_1}{a_L},$$

$$N_2 - N_3 = (N_S - N_1)\frac{x^2}{a_L^2}\cdot a_1 \cdot a_2,$$

$$\vdots \qquad \vdots$$

$$N_n = (N_S - N_1)\frac{x^n}{a_L^n} a_1 \cdots a_n, \tag{7}$$

except that in Hill's case (the BET model)

$$a_2=a_3=\cdots=a_n=a_L.$$

Making use of (7), the generalized sorption equation results for the model used here, that is, localized sorption on definite sites with no interaction between molecules on adjacent sites, namely,

$$\frac{N}{N_S}=\frac{y(a_1+2ya_1\cdot a_2+3y^2a_1\cdot a_2\cdot a_3+\cdots)}{1+ya_1+y^2a_1\cdot a_2+y^3a_1\cdot a_2\cdot a_3+\cdots}, \quad (8)$$

where

$$y=\frac{x}{a_L}.$$

Letting

$$\phi=1+ya_1+y^2a_1a_2+\cdots,$$

it is readily seen that

$$\frac{N}{N_S}=y\frac{\phi'}{\phi}. \quad (9)$$

SPECIAL SOLUTIONS

1. Partition Functions in All Layers Equal

The simplest assumption is that the a_i's are all equal, and are some fraction, k, of the pure liquid-state partition function a_L. For an infinite number of layers the solution is

$$\frac{N}{N_S}=\frac{kx}{1-kx}, \quad (10)$$

and for a finite number n,

$$\frac{N}{N_S}=kx\frac{[1-(n+1)(kx)^n+n(kx)^{n+1}]}{(1-kx)[1-(kx)^{n+1}]}. \quad (11)$$

In case k is equal to unity, which would be true for an ideal solution, then (10) reduces to

$$\text{N}=x, \quad (12)$$

which is Raoult's law (N is the mole fraction of the vapor in the solid).

2. Partition Functions All Equal Beyond the First Layer

If

$$\frac{a_1}{k}=a_2=a_3=\cdots=a_n=a_L,$$

the BET equations result.

If

$$a_2=ka_1=a_3=a_4=\cdots=a_n\neq a_L,$$

and if n is limited to a finite number, we obtain

$$\frac{N}{N_S}=\frac{cx[1-(n+1)(ckx)^n+n(ckx)^{n+1}]}{[1-ckx][1+cx\{1-k-(ckx)^n\}]}, \quad (13)$$

where $c=a_1/a_L$. When n goes to infinity

$$\frac{N}{N_S}=\frac{xc}{[1-ckx][1+cx(1-k)]}, \quad (14)$$

which becomes identical to the BET equations on setting $k=a_L/a_1$. Equation (14) is closely similar to that deduced by Anderson[7] (Anderson's Eq. (6)) which in our terminology can be written

$$\frac{N}{N_S}=\frac{cxk}{[1-kx][1+(c-1)kx]}. \quad (15)$$

When Eqs. (14) and (15) are put into a linear form and solved for N_S and c, it can be seen that in Anderson's case

$$N_S=\frac{1}{Ik+S},$$

where I and S are the intercept at x equal to zero and the slope, respectively, and in our case

$$N_S=\frac{1}{Ick+S}. \quad (16)$$

As the functions plotted are

$$\frac{x}{N(1-ckx)} \text{ against } x \quad \text{and} \quad \frac{x}{N(1-kx)} \text{ against } x$$

in the two cases, it is obvious that both Anderson's and our treatment will yield equal values of N_S. However, if the constant c is solved for

$$c=\frac{Ick+S}{I}$$

in our case, and

$$c=\frac{Ik+S}{Ik}$$

[7] R. B. Anderson, J. Am. Chem. Soc. **68**, 686 (1946).

in Anderson's case, it is evident that a difference results. As Anderson derived his equation for a heat of adsorption in the second to the ninth layer different from that in the first layer as well as different from the heat of condensation in the pure liquid, one would not expect his and our equation to be identical (Anderson did not give details of derivation).

It should be noted that our equation reduces to the Langmuir isotherm on setting k equal to zero, whereas Anderson's equation does not.

3. Partition Functions Decreasing Harmonically

Let us make the arbitrary assumption that

$$a_2=1/2a_1, \quad a_3=1/3a_1, \quad \text{etc.}, \tag{17}$$

then

$$\phi=1+ya_1+\frac{y^2a_1^2}{2!}+\frac{y^3a_1^3}{3!}+\cdots,$$

$$=e^{ya_1}$$

and

$$\frac{N}{N_S}=x\cdot\frac{a_1}{a_L}=cx. \tag{18}$$

This demonstrates that given the proper decrease in the internal partition function with increasing number of sorbed layers, a linear sorption isotherm can be obtained. In the case of the sorption of water by high polymers there are a number of examples of the sorption following a linear relationship with the pressure up to 50 to 60 percent relative humidity. There is no *a priori* reason in these cases why the partition function should not fall to zero in the limit. In fact, the Langmuir isotherm can be obtained from (8) by setting all partition functions except a_1 equal to zero.

MULTILAYER SORPTION WITH INTERACTION

Fowler and Guggenheim[8] have shown how the Langmuir treatment is to be modified if interaction between adjacent molecules forming a number of pairs, N_{ii}, in any layer is taken into account. If the contribution to the internal partition function for such pairs is a_{ii}, then the total partition function for multilayer sorption becomes

$$Q=\frac{N_S!}{\prod_{i=0}^{n} S_i!}\prod_{i=1}^{n}(a_i)^{N_i}(a_{ii})^{N_{ii}'} \tag{19}$$

where N_{ii}' is a statistical average number of pairs when N_i molecules are adsorbed. Making the assumption of a completely random arrangement, Fowler and Guggenheim deduce the equation

$$N_{ii}'=\tfrac{1}{2}z\frac{N_i^2}{N_S}, \tag{20}$$

where z is the number of nearest neighbors in any layer. The contribution of the interaction energy, W, to the total energy can be expressed by the equation,

$$E^{\text{int.}}=\frac{N_i^2}{N_S}\cdot W. \tag{21}$$

(This follows from the assumption that the excess energy resulting from interaction can be expressed by the factor $N_{ii}[2W/z]$.)

The free energy of the adsorbed material and other relations follow immediately from (19)

$$\frac{F}{RT}=-N_S\ln N_S+(N_S-N_1)\ln(N_S-N_1)$$

$$+(N_1-N_2)\ln(N_1-N_2)+\cdots$$

$$+N_n\ln N_n-\sum_{i=1}^{n}N_i\ln a_i$$

$$-\sum_{i=1}^{n}\frac{N_i^2}{N_S}\cdot\frac{z}{2}\ln a_{ii}, \tag{22}$$

$$\frac{N_S-N_1}{N_1-N_2}=\frac{N_1-N_2}{N_2-N_3}\frac{a_2}{a_1}\cdot\frac{a_{22}^{N_{22}z/N_S}}{a_{11}^{N_{12}z/N_S}}, \tag{23}$$

$$\frac{N_S-N_1}{N_1-N_2}=\frac{N_{n-1}-N_n}{N_n}\frac{a_n}{a_1}\left[\frac{a_{nn}^{N_n}}{a_{11}^{N_1}}\right]^{z/N_S}, \tag{24}$$

$$\frac{N_n}{N_{n-1}-N_n}=x\frac{a_n}{a_L}a_{nn}^{N_n\cdot(z/N_S)}, \tag{25}$$

[8] See reference 3, p. 429.

and, finally,

$$\frac{N}{N_S}=\frac{x\cdot\frac{a_1}{a_L}a_{11}^{N_1\cdot(z/NS)}+2\left[\frac{x}{a_L}\right]^2 a_1\cdot a_{11}^{N_1\cdot(z/NS)}\cdot a_2\cdot a_{22}^{N_2\cdot(z/NS)}+\cdots}{1+x\frac{a_1}{a_L}a_{11}^{N_1\cdot(z/NS)}+\left(\frac{x}{a_L}\right)^2 a_1\cdot a_{11}^{N_1\cdot(z/NS)}\cdot a_2\cdot a_{22}^{N_2\cdot(z/NS)}+\cdots}. \tag{26}$$

Fowler and Guggenheim[8] point out that the assumption of interaction leads at certain values of the temperature to the splitting of the adsorbed layer into two phases. Hill[5,9] suggests that in the case of multilayer sorption this region of instability, corresponding to a sudden jump in the value of N/N_S, is to be conceived physically as capillary condensation, and he concludes that the multilayer adsorption and capillary condensation points of view are therefore really not in conflict.

In the case of the sorption of water vapor by solids, the present author prefers to consider the sudden increase in N/N_S at constant vapor pressure as analogous to compound formation such as occurs in the hydration of crystals when the percentage of water in the solid (water of hydration) rises from a low to a high value without change of vapor pressure. Such hydration may occur occasionally with very little change in the x-ray diagram of the solid.[10]

Let us consider the application of Eq. (26) to the phenomena of hydration of crystals. When a higher and lower hydrated form of the crystal are simultaneously in equilibrium with a certain vapor pressure of water, then the percentage of water in the crystal will rise without change in the chemical potential, μ, of the water, or

$$\frac{\partial\mu}{\partial N}=0. \tag{27}$$

It is interesting to find the value of N_n corresponding to condition (27). Letting N_n^0 represent this value, we obtain

$$N_n^0=\frac{1+x\frac{a_n}{a_L}a_{nn}^{N_n\cdot(z/NS)}}{q}, \tag{28}$$

where

$$q=\frac{z}{N_S}\ln a_{nn}.$$

Differentiating N_n^0 with respect to x, we find

$$\frac{\partial N_n^0}{\partial x}=\frac{a_n\cdot a_{nn}^{N_n\cdot(z/NS)}}{q\cdot a_L\left[1-x\frac{a_n}{a_L}a_{nn}^{N_n\cdot(z/N_S)}\right]}, \tag{29}$$

so that for $\partial N_n^0/\partial x$ to be equal to infinity as it must in the case of formation of hydrates at constant vapor pressure,

$$x\cdot\frac{a_n}{a_L}a_{nn}^{N_n\cdot(z/NS)}=1. \tag{30}$$

Hence

$$N_n^0=\frac{2}{q}. \tag{31}$$

For the layer immediately under the outer layer we obtain, on rearranging (25),

$$N_{n-1}=N_n\frac{\left[1+x\frac{a_n}{a_L}a_{nn}^{N_n\cdot(z/NS)}\right]}{x\cdot\frac{a_n}{a_L}a_{nn}^{N_n\cdot(z/NS)}},$$

which for $N_n=N_n^0$ becomes

$$N_{n-1}=2N_n^0.$$

If N_n^0 equals $1/2N_S$, which it will at the critical

[9] In a paper in press Dr. Hill has gone considerably deeper into the mathematics of the unstable region than he did in the paper quoted in reference (5). We are greatly indebted to him for the opportunity of seeing his paper in advance of publication.

[10] See, for example, the interesting paper by W. O. Milligan and H. B. Weiser, J. Phys. Chem. **41**, 1029 (1937), where x-ray diffraction patterns are given for a number of hydrated zeolites. In their case they heated the hydrated crystals at constant vapor pressure and observed a stepwise decrease in the percentage of water in the crystal.

temperature when

$$W=-2kT$$

or

$$q=\frac{4}{N_S},$$

then

$$N_{n-1}=N_S.$$

In other words, the sorption in the next layer below the outer layer is complete when the top layer is half-covered, as would be expected when the hydration of a crystal proceeds in steps. It would appear, then, that the physical fact which distinguishes between sorption of the types represented by the Langmuir, BET, or other equations and hydrate formation is the interaction energy between the sorbed molecules. When the sorbed molecules are so far apart that no or insufficient interaction energy exists, no region of increase of water sorbed at constant vapor pressure can exist, no separation of the solid into two phases will occur; on the other hand, a gradual increase of the amount sorbed with increase of vapor pressure will be observed.

Application of the equations contained in this paper to new data on the sorption of water by certain high polymers will be carried out at a later date. The work given here is part of a general program of study of the thermodynamics of high polymers for which grants have been gratefully received from the du Pont Corporation, the Research Corporation,[11] the Richardson Company, and the Visking Corporation.

[11] Frederick Gardner Cottrell grant.

THE JOURNAL OF CHEMICAL PHYSICS VOLUME 16, NUMBER 1 JANUARY, 1948

Rotation-Vibration Spectra of Diatomic and Simple Polyatomic Molecules with Long Absorbing Paths.

I. The Spectrum of Fluoroform (CHF_3) from 2.4μ to 0.7μ

H. J. BERNSTEIN* AND G. HERZBERG
Yerkes Observatory of the University of Chicago, Williams Bay, Wisconsin

(Received August 25, 1947)

The spectrum of fluoroform has been investigated under high resolution (21-ft. grating) in the photographic infra-red with an absorbing path of up to 60 meters, obtained by multiple reflection according to the method of J. U. White. In addition, with the same path length the spectrum from 1.2 to 2.4μ was obtained under low resolution with a photoelectric infra-red spectrometer. A large number of overtone and combination bands, 47 in all, were found. Two parallel bands in the photographic region were well resolved and analyzed, yielding, for the moment of inertia about an axis perpendicular to the symmetry axis,

$$I_B^{[0]}=81.08\times10^{-40}\text{ g cm}^2$$

From this value, assuming tetrahedral angles and a C−H distance as in methane, the C−F distance in fluoroform is found to be 1.329A, a value that is appreciably lower than that found in methyl fluoride, 1.380A. A provisional vibrational assignment of all the bands is given.

A. INTRODUCTION

THE investigation of the rotation-vibration spectra of diatomic and polyatomic molecules in the photographic infra-red by means of large diffraction gratings makes possible a determination of molecular constants (moments of inertia, internuclear distances, etc.) of very high precision. Indeed it was only during the last year that this precision has been surpassed by the data obtained from microwave-absorption spectra. The microwave technique is applicable only to a certain group of molecules and to certain molecular constants. Therefore, it remains imperative to continue the study of photographic infra-red spectra. It appears that there are still a number of diatomic and simple poly-

* Division of Chemistry, National Research Laboratories, Ottawa, Canada.

atomic molecules which ought to be studied in the photographic region, and others for which the information available at present could be greatly extended with improved technique. The present series of investigations is directed at this aim.

The study of molecular absorption spectra in the photographic infra-red entails the use of long absorbing paths. Particularly long paths are required for molecules not containing hydrogen, since their vibrational frequencies are small and therefore only rather high overtones fall into the photographic region. Indeed up to now only for one molecule of this type (CO_2) have photographic infra-red spectra been obtained.[1]

In most infra-red work interest is centered on the fundamentals, and only comparatively short path lengths are used. If long paths are used many overtone and combination bands may be expected in the near infra-red as well as in the photographic region. It seems important to locate as many of these overtone and combination bands as possible in order to obtain a reliable representation of all the vibrational levels of the molecule under consideration and in order to study its potential function. Toward this end, in the present series low dispersion spectra up to 2.4μ have been taken with the same long path as for the photographic high resolution spectra. It is hoped that later on it will be possible to study also this spectral region with much higher resolution.

A precise knowledge of the higher vibrational levels, as well as of the rotational constants, is not only of interest in the study of molecular structure, but also for the purpose of calculating thermodynamic functions particularly at higher temperatures. This need gives added stimulus to the investigations of infra-red spectra with long absorbing paths.

The present first paper in this series gives the results of the investigation of the spectrum of fluoroform. Spectra of ketene and carbon dioxide have already been taken and are being evaluated. The study of other molecules is being prepared.

B. EXPERIMENTAL

A long absorbing path was obtained by multiple reflection in a comparatively short tube according to the ingenious method suggested by White,[2] with slight modifications. Figure 1 shows the optical arrangement. Three concave mirrors of equal radius of curvature are used. Two of these, *A* and *B*, which were cut from one circular mirror as shown in Fig. 1b, are mounted at one end of the tube while the third, *C*, of a shape indicated in Fig. 1c, is mounted at the other end at a distance equal to the radius of curvature.

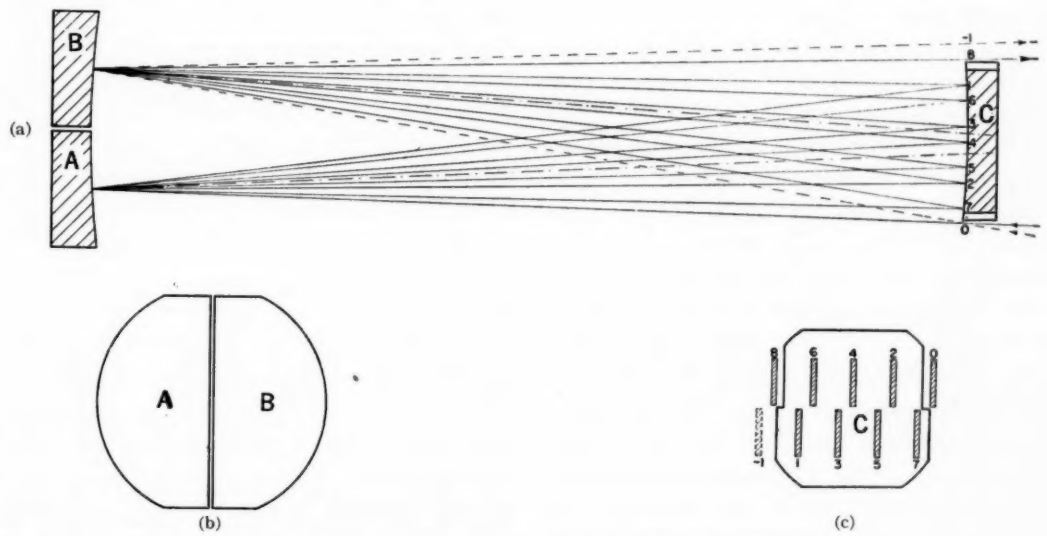

FIG. 1. Optical arrangement for obtaining a long absorbing path.

[1] In the spectrum of Venus by Adams and Dunham [Astron. Soc. Pac. **44**, 423 (1932)] in the laboratory by Herzberg and Verleger [Phys. Rev. **48**, 706 (1935)].
[2] J. U. White, J. Opt. Soc. Am. **32**, 285 (1942).

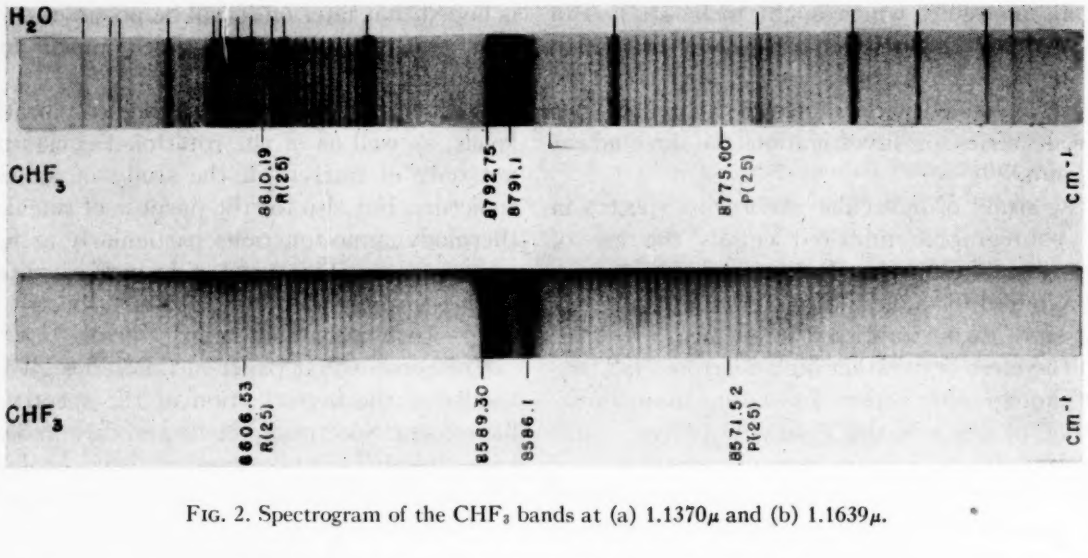

FIG. 2. Spectrogram of the CHF_3 bands at (a) 1.1370μ and (b) 1.1639μ.

Light from an automobile headlight bulb is focused on an entrance slit at 0 in Fig. 1a and c. From there the light falls on the two mirrors, A and B, which form images of the slit at 1 and -1, respectively. The image -1 is discarded but is very useful in the adjusting procedure. The mirror C is so adjusted that the light from A received at 1 is reflected to B. With proper adjustment A is imaged on B and no light is lost except by reflection losses. The mirror B then forms an image of 1 at 2, whereupon the light is reflected to A, and so on, until the light emerges at 8 after having traversed the space between the mirrors 16 times. By turning mirror A by small amounts about an axis perpendicular to the plane of the paper of Fig. 1a, the number of images on mirror C, that is, the number of traversals, can be readily changed. In order to accommodate as many images as possible on mirror C and for the purpose of simplifying the adjustment, the even and odd images are separated (by the proper adjustment of mirrors A and B) as shown in Fig. 1c. This diagram also makes it clear why the mirror C has been indented at the top half as shown. The separation of the axes (dot-dash lines) of the two mirrors A and B at C is half the separation of successive odd (or even) images. It is not necessary to have the odd images halfway between the even ones. In fact if the adjustment is made by turning mirror A only, such a symmetrical arrangement of the images will obtain only for a certain number of images depending on the orientation of mirror B.

Thus far two long paths as just described have been set up: a small one in a glass tube of 50 mm diameter, and with 150 cm radius of curvature of the mirrors, and a large one in a galvanized iron pipe of 10 inches diameter and with mirrors of 22 m radius of curvature. With the small tube up to 40 traversals have been obtained, with the large one up to 144 traversals. The resulting path lengths are 60 m and 3168 m, respectively. The limit is set only by the reflection losses and by the number of images that can be accommodated on mirror C. The spectrum of fluoroform has been taken entirely with the small absorption tube, since not enough of the gas was available for the large one.

The photographic infra-red spectra were taken in the first order of a 21-ft. grating ruled by R. W. Wood. This grating has an excellent concentration in the first order of 11,000A and is thus particularly suitable for work with the Eastman I-Z plates. The grating is mounted in a Eagle mounting. A region of 2500A in first order can be covered in one exposure. The dispersion is 2.5 A/mm. While below 9000A the exposure times (on I-N plates) were of the order of a few minutes for 20 traversals, at 11,000A the exposure times were of the order of 24 hours.

Spectra in the region from 1 to 2.4μ were taken with the new infra-red spectrometer built by Dr. G. P. Kuiper for work with the McDonald

telescope.[3] In it a photo-conductive cell is used as the receiving element. The resolving power is 800. The spectrum is recorded on an Esterline-Angus recorder. Depending on the speed of recording, the dispersion on the record varies from 20 to 100 A/mm.

The fluoroform was obtained through the kindness of Dr. A. F. Benning from the Jackson Laboratory of E. I. du Pont de Nemours and Company. It was specified as "practically pure". Pressures up to 1 atmos. were used for the weaker bands. However, for a satisfactory resolution of the fine structure of the intense bands the use of a lower pressure (about $\frac{1}{5}$ atmos.) proved of great advantage, since the pressure broadening is much reduced at these lower pressures.

C. ROTATIONAL ANALYSIS

A considerable number of photographic infrared bands were found (see below) but only two of these, at 1.1639μ and 1.1370μ, were sufficiently strong so that their fine structures could be measured. In Fig. 2 spectrograms of these two bands are reproduced as obtained at a pressure of 12 cm and a path length of 18 meters. Both bands consist of a strong central Q branch with a sharp edge at the long wave-length side and a P and R branch on either side of it. In addition, in each band a secondary Q branch occurs which is obviously caused by a difference band forming the $1-1$ band of a sequence starting with the main band (see below). The band 1.1370μ is partially overlapped by the water band at 1.135μ.

The fluoroform molecule is an oblate symmetric top with the figure axis in the direction of the C—H bond. There are parallel and perpendicular bands (with $\Delta K=0$ and ± 1, respectively). There can be no question that the two bands reproduced in Fig. 2 are parallel bands, since the central branch has a sharp edge and since there is only one P and one R branch in each band. To be sure, on account of the comparatively small difference between the moments of inertia I_B and I_C, the Q branches of the sub-bands of a perpendicular band will also form a fairly pronounced central branch; but it will not have a sharp edge, and the P and R branches of different sub-bands will not form apparently single branches of the whole band as they do for parallel bands. It should be emphasized that, on account of the variation of the rotational constants B and C with the vibrational quantum numbers, parallel bands in the photographic region do not necessarily have this simple structure. Only when the effective moments of inertia differ very slightly in the upper and lower states, can such a simple structure be expected.[4] In the

TABLE I. Wave numbers of the band lines.

J	Band at 1.1639μ $\nu_{head}(Q)=8589.30$ $P(J)$	$R(J)$	Band at 1.1370μ $\nu_{head}(Q)=8792.75$ $P(J)$	$R(J)$
4		8592.72		8796.12
5		93.33		96.73
6	8585.00	93.97	8788.52	97.42
7	84.37	94.66	87.86	98.18
8	83.64	95.35	87.16	98.84
9	82.94	96.02	86.41	8799.52
10	82.24	96.64	85.72	8800.18
11	81.52	97.31	85.03	00.90
12	80.79	98.08	84.32	01.54
13	80.10	98.76	83.60	02.14*
14	79.45	8599.43	82.91	02.84
15	78.79	8600.07	82.22	03.52
16	78.02	00.73	81.50	04.20
17	77.28	01.38	80.78	04.86
18	76.60	02.06	80.09	05.53
19	75.86	02.68	79.33	06.15
20	75.13	03.30	78.62	06.83
21	74.38	03.98	77.88	07.48
22	73.69	04.64	77.15	08.15
23	72.97	05.29	76.46	08.78
24	72.26	05.94	75.73	09.38*
25	71.52	06.53	75.00	10.09
26	70.79	07.18	74.27	10.74
27	70.02	07.81	73.56	11.43
28	69.31	08.46	72.79	12.00*
29	68.56	09.06	72.18*	— *
30	67.78	09.70	71.40*	13.38*
31	67.06	10.32	70.60	13.95*
32	66.31	10.90	69.86	14.48
33	65.52	11.50	69.12	15.14
34	64.79	12.16	68.34	15.78
35	64.06	12.73	67.63	16.39
36	63.28	13.37	66.86	16.98
37	62.54	13.97	66.08	
38	61.73	14.54	65.37	
39	60.98	15.10	64.59	
40	60.20	15.74	63.89	
41	59.46	16.29	63.13	
42	58.71	16.91	62.23	
43	57.92		61.58	
44	57.11		60.76	
45	56.40		60.10*	
46			59.33	
47			58.55	
48			57.68	
49			56.96	
50			56.20	

* An asterisk indicates overlapping by H_2O lines.

[3] G. P. Kuiper, W. Wilson, and R. J. Cashman, Astrophys. J. **106**, 243 (1947).

[4] See. G. Herzberg, *Infrared and Raman Spectra of Polyatomic Molecules* (in future referred to as *I.R.S.*), (D. Van Nostrand Company, Inc., New York, 1945), p. 418.

present case this condition is fulfilled since the vibration of the H atom which is mainly involved (see Section D) changes the moment of inertia but slightly.

In Table I the wave numbers of the lines of the P and R branches, as well as those of the Q heads of the two bands, are given. The numbering of the lines was readily obtained since the head of the Q branch gives very nearly the position of the band origin.

Table II gives the combination differences $\Delta_2F''(J)=R(J-1)-P(J+1)$ for the two bands. They agree for each J value within the accuracy of the measurements. It should be mentioned however, that an almost equally good agreement is obtained if the numbering in both bands is shifted by one unit. The reason for this insensitivity of the agreement of the combination differences to the numbering is due to the fact that the rotational constants B' in the upper states of the two bands are almost the same. It appears, however, practically certain that the numbering as obtained from the positions of the Q branches is correct. If the effect of centrifugal distortion is included[5] the rotational term values are given by

$$F(J,K)=BJ(J+1)+(C-B)K^2-D_JJ^2(J+1)^2 -D_{JK}J(J+1)K^2-D_KK^4,$$

where

$$B=\frac{h}{8\pi^2cI_B} \quad \text{and} \quad C=\frac{h}{8\pi^2cI_C}$$

and D_J, D_{JK}, and D_K are very much smaller than B and C. From this formula it follows immediately that

$$\Delta_2F(J)=F(J+1,K)-F(J-1,K) =(4B-6D_J-4D_{JK}K^2)(J+\tfrac{1}{2}) -8D_J(J+\tfrac{1}{2})^3.$$

If the effect of centrifugal distortion is neglected $\Delta_2F(J)/(J+\frac{1}{2})$ would be a constant, $4B$. Actually, as shown by Fig. 3, the observed $\Delta_2F''(J)/(J+\frac{1}{2})$ values show a slight decrease with $(J+\frac{1}{2})^2$ indicating the effect of the term $8D_J(J+\frac{1}{2})^2$. From the slope of the straight line in Fig. 3 one obtains $D_J''=3_8\times10^{-7}$ cm^{-1} while the intercept on the ordinate axis gives $4B''-6D_J''-4D_{JK}''K^2 =1.3806_4$ cm^{-1}. The term $-6D_J''-4D_{JK}''K^2$ may be neglected in view of the magnitude of D_J'' and the consideration that D_{JK}'' would be expected to be of the same order as D_J''. Thus we have

$$B''_{[0]}=0.3451_6 \text{ cm}^{-1}.$$

The rotational constants B' for the upper states can be more accurately determined from the $B'-B''$ values obtained by plotting $R(J-1)+P(J)$ against J^2. The same plots also give the band origins ν_0. The resulting B' and ν_0 values are given together with the other rotational constants in Table III. The band origins ν_0 agree very well with the positions of the Q heads given in Table I. The latter contain, of course, the error inherent in measurements of band heads.

It may be mentioned that the $R(J-1)+P(J)$ *versus* J^2 curves show a slight curvature at high

TABLE II. Combination differences.

J	$\Delta_2F''(J)$ from 1.1370μ band	$\Delta_2F''(J)$ from 1.1639μ band	$\Delta_2F''(J)$ mean
5	7.60	7.72	7.66
6	8.87	8.96	8.92
7	10.26	10.33	10.29
8	11.77	11.72	11.75
9	13.12	13.11	13.12
10	14.49	14.50	14.50
11	15.86	15.85	15.86
12	17.30	17.21	17.26
13	18.63	18.63	18.63
14	(19.92)	19.97	19.97
15	21.34	21.41	21.38
16	22.74	22.79	22.77
17	24.11	24.13	24.12
18	25.53	25.52	25.53
19	26.91	26.93	26.92
20	28.25	28.30	28.28
21	29.68	29.61	29.65
22	31.02	31.01	31.02
23	32.42	32.38	32.40
24	33.78	33.77	33.78
25	(35.11)	35.15	35.15
26	36.53	36.51	36.52
27	37.95	37.87	37.91
28	(39.25)	39.25	39.25
29	(40.60)	40.68	40.68
30	—	42.00	42.00
31	(43.52)	43.39	43.39
32	(44.83)	44.80	44.80
33	46.14	46.11	46.13
34	47.51	47.44	47.48
35	48.92	48.88	48.90
36	50.31	50.19	50.25
37	51.61	51.64	51.63
38		52.99	52.99
39		54.34	54.34
40		55.64	55.64
		57.03	57.03
		58.37	58.37
		59.80	59.80

Values in brackets are from blended lines (* in Table I) and have not been used in forming the mean.

[5] See G. Herzberg, *I.R.S.*, p. 26.

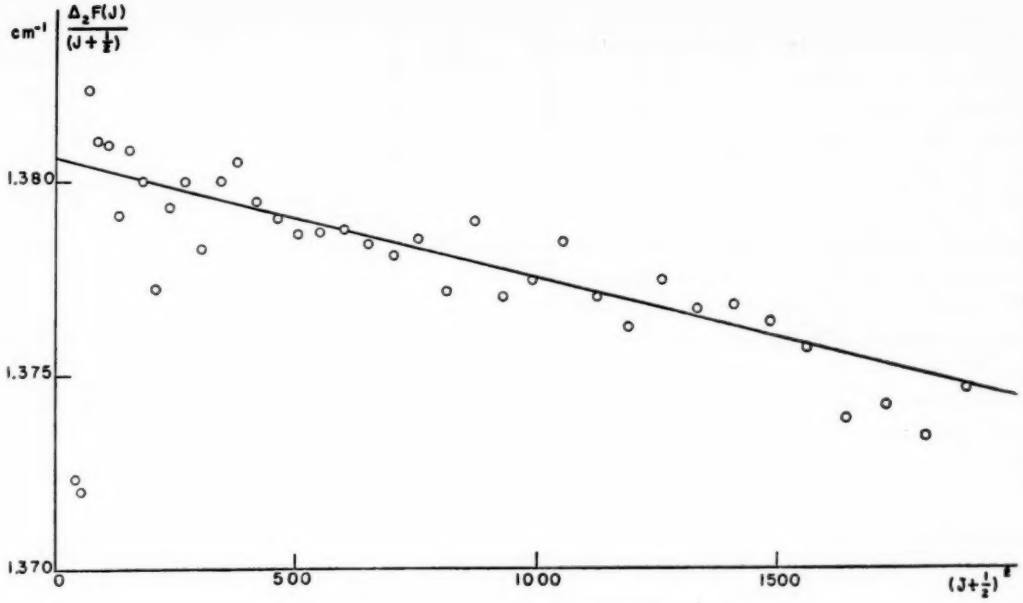

FIG. 3. Combination differences $\Delta_2F''(J)/(J+\frac{1}{2})$.

J values. This is due to the fact that each "line" is actually a superposition of $J+1$ lines corresponding to $K=0, 1, 2, \cdots J$ which spread out more and more to longer wave-lengths as J increases. Therefore in determining $B'-B''$ from the slope of these lines only the first part of these lines up to $J=30$ was used.

The rotational constants B depend on the vibrational quantum numbers v_i according to

$$B_{[v]}=B_e-\sum\alpha_i(v_i+d_i/2),$$

where $d_i=1$ or 2 depending on whether the vibration ν_i is non-degenerate or doubly degenerate. According to the vibrational analysis in Section D, the two photographic bands 1.1370μ and 1.1639μ are $3\nu_1$ and $2\nu_1+2\nu_4$, respectively. Therefore the $B'-B''$ value of the former gives $3\alpha_1$ while that of the latter gives $2\alpha_1+2\alpha_4$. In this way one obtains $\alpha_1=0.00025$ and $\alpha_4=0.00021$. Since the other α_i's have not been determined, it is not possible to obtain B_e, the rotational constant for the equilibrium position.

The $B_{[0]}$ value determined above gives the effective moment of inertia in the lowest vibrational level. One obtains, using Birge's[6] conversion factor 27.9865×10^{-40},

$$I_B^{[0]}=81.08\times10^{-40}\text{ g cm}^2.$$

[6] R. T. Birge, Rev. Mod. Phys. **13**, 233 (1941).

On account of the effect of Coriolis interaction a determination of the second moment of inertia $I_C^{[0]}$ would require the rotational analysis not only of one but of all three perpendicular fundamentals or of a perpendicular vibration in the Raman effect. Since such analyses have not been carried out, one must be satisfied with the determination of one unknown internuclear distance from $I_B^{[0]}$, assuming plausible values for the others.

It appears very probable that the C−H distance in CHF_3 is closely the same as in methane, that is

$$r(\text{C-H})=1.0936\times10^{-8}\text{ cm}.$$

But even if a value as found in ethylene (1.071) or acetylene (1.0597) would be assumed, the following conclusions would be substantially unaltered. More critical is the assumption made

TABLE III. Rotational constants of CHF_3.

$B_{[0]}$	0.3451_6 cm^{-1}
$B_{[v]}$ for $2\nu_1+2\nu_4$	0.3442_3 cm^{-1}
$B_{[v]}$ for $3\nu_1$	0.3444_0 cm^{-1}
α_1	0.00025 cm^{-1}
α_4	0.00021 cm^{-1}
D_J	$3_8\times10^{-7}$ cm^{-1}
ν_0 for $2\nu_1+2\nu_4$	8589.28 cm^{-1}
ν_0 for $3\nu_1$	8792.70 cm^{-1}
$I_B^{[0]}$	81.08×10^{-40} g cm^2
$I_C^{[0]}$, $C_{[0]}$ calculated assuming tetrahedral angles	148.67×10^{-40} g cm^2; 0.1882_5 cm^{-1}

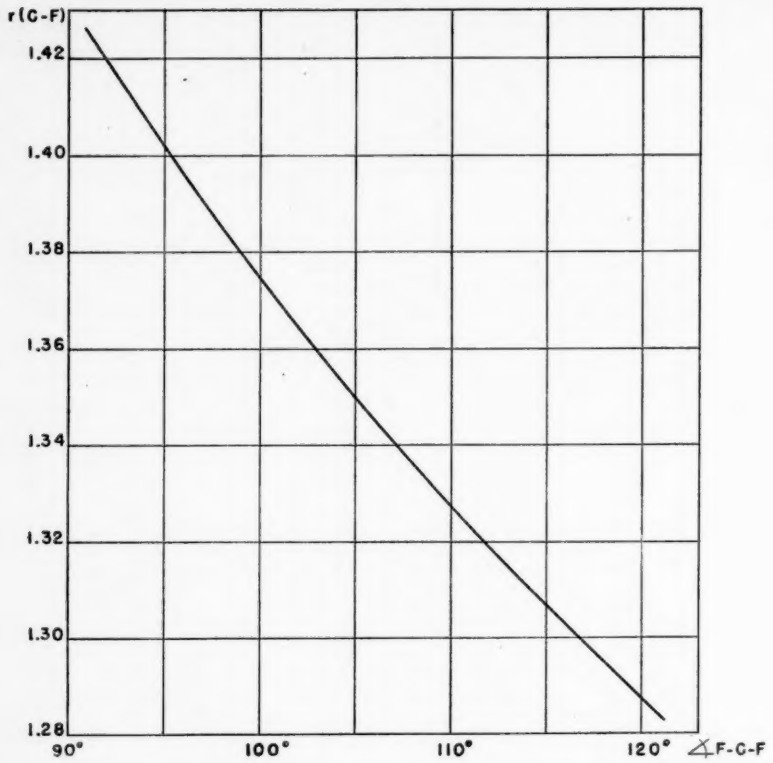

FIG. 4. Variation of the C−F, distance for various assumptions about the F-C-F angle, compatible with the observed moment of inertia $I_B^{[0]}$.

for the F-C-F angle. If one assumes a tetrahedral angle the C−F distance remains the only unknown, and one obtains

$$r(\mathrm{C-F}) = 1.329 \times 10^{-8} \text{ cm}.$$

For other values of the F-C-F valence angle Fig. 4 gives the corresponding r(C−F) values. It is seen that for F-C-F angles larger than the tetrahedral angle the r(C−F) distance is smaller than the value given above.

It is interesting to compare the C−F distance in fluoroform with that in other related molecules. This is done in Table IV where both spectroscopic and electron-diffraction data are summarized. While the electron-diffraction values are rather larger than the spectroscopic values in all cases where both are available, for either set the C−F distance in CH_3F is appreciably larger than in the molecules containing more than one fluorine atom. Of course by a proper choice of the F-C-F angle in CHF_3 it would be possible to obtain from the above $I_B^{[0]}$ value a C−F distance equal to that in CH_3F. However, the angle would have to be as low as 99°, which seems highly improbable.

An unambiguous determination of the C−F distance as well as the F-C-F angle will be possible once the moment of inertia I_B of "heavy" fluoroform (CDF_3) has been determined from its parallel bands.

The C−F distance given above and the assumption of tetrahedral angles may be used to calculate the moment of inertia $I_C^{[0]}$ about the symmetry axis as well as the rotational constant $C_{[0]}$. The values obtained are included in Table

TABLE IV. C-F distances in different molecules.

	C-F distance (in 10^{-8} cm) from spectrum	from electron diffraction	F-C-F-angle
CH_3F	1.380[a]	1.42[c]	
CH_2F_2	1.320[b]	1.36[c]	106°50′[b]
CHF_3	1.329		109°28′ (assumed)
CF_4		1.36[c]	109°28′ (assumed)
CF_3CH_3		1.37[d]	107°32′

[a] Derived from the $B_{[0]}$ value given in a recent paper by Yates and Nielsen [Phys. Rev. 71, 349 (1947)] assuming an H-C-H angle of 111°48′ (see G. Herzberg, *I.R.S.*, p. 439). The large deviation from the value given by Herzberg is due to the large change of Yates and Nielsen's $B_{[0]}$ as compared to the earlier one of Bennet and Meyer [Phys. Rev. 32, 888 (1928)].

[b] From a paper presented by W. H. Shaffer and H. Stewart at the Symposium on Molecular Structure and Spectroscopy at Ohio State University, June 1947.

[c] L. O. Brockway, J. Phys. Chem. 41, 185 (1937).

[d] W. Shand and R. A. Spurr, quoted in H. Russell, Jr., D. R. V. Golding, and D. M. Yost, J. Am. Chem. Soc. 66, 16 (1944).

TABLE V. Fundamental frequencies of gaseous CHF_3 after Price.*

Assignment	Infra-red band
$\nu_1^{CH}(a_1)$	3035.6 (s.)
$\nu_2^{CF}(a_1)$	1209 (m.)
$\nu_3(a_1)$	703.2 (m.)
$\nu_4^{CF}(e)$	1351.5 (s.)
$\nu_5^{CH}(e)$	1152.4 (v.s.)
$\nu_6(e)$	509.4
	cm^{-1}

* *Note added in proof:* New measurements by Price in the long wavelength region seem to indicate that the two low frequency fundamentals ν_3 and ν_6 have to be exchanged since the band at 509.4 cm^{-1} has the appearance of a parallel band while the band at 703.2 cm^{-1} has an indifferent appearance.

III. However, it must be remembered that these values are not a direct consequence of the measured wave numbers as are $I_B^{[0]}$, $B_{[0]}$, and the other constants of Table III.

D. VIBRATIONAL STRUCTURE

The Raman spectrum of fluoroform in the liquid phase has been studied by Glockler and Edgell.[7] The infra-red spectrum of the gas in the region of the fundamentals has been investigated by Price.[8] There is an appreciable shift of the fundamental frequencies in going from the gas to the liquid. Therefore, for the interpretation of the overtone and combination bands found here in the gas, we use the fundamentals determined by Price as given in Table V. The designation is that used by Herzberg.[9] There are three totally symmetric fundamentals (a_1) and three degenerate fundamentals (e).

In addition to the two photographic bands whose fine structure has been analyzed (Section C), a considerable number of fainter photographic bands were previously found by Mackay[10] and have been confirmed in the present work. They extend as far as 7000A. Furthermore, many strong bands were found in the region from 2.4μ to 1.2μ with the photoelectric infra-red spectrometer referred to in Section B. Figure 5 reproduces one of the recordings obtained. The wave numbers of all the observed overtone and combination bands are given in Table VI. The wave numbers measured with the infra-red instrument (marked I. in the second column) are accurate to about ± 5 cm^{-1}; those measured in the photographic region (marked P.I.) are accurate to less than 1 cm^{-1} except in the case of very diffuse bands.

The dispersion of the photoelectric spectrometer is not sufficient to distinguish parallel and perpendicular bands. But even with the high resolution possible in the photographic infra-red it is often difficult to decide whether a given weak band is a parallel or a perpendicular band. If the band has a very broad central branch without a head it is fairly certain that it is a perpendicular band. In one case of such a band, at 10154.6 cm^{-1}, the Q branches of the sub-bands forming this central branch were partially resolved into a series which even showed an indication of the proper intensity alternation (strong, weak, weak, strong) so that its identification as a perpendicular band is beyond doubt. The completely resolved parallel bands, 8589 and 8793 cm^{-1} (Fig. 2), have a sharp edge of their central branches since B' is somewhat smaller than B''. Other bands showing such heads, even

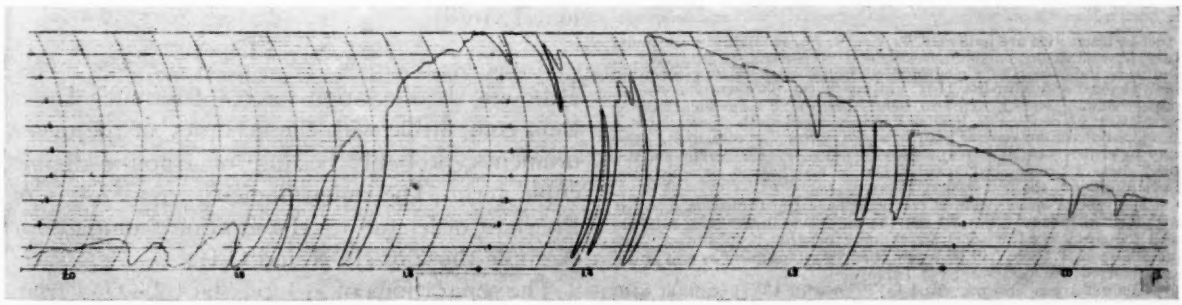

FIG. 5. Infra-red spectrum of CHF_3 obtained with the photoelectric infra-red spectrometer.

[7] G. Glockler and W. F. Edgell, J. Chem. Phys. 9, 224 (1941).
[8] W. C. Price, unpublished.
[9] G. Herzberg, *I.R.S.*, p. 316.
[10] A. E. Mackay, Master's thesis, University of Saskatchewan, 1942.

TABLE VI. Overtone and combination bands of CHF_3.

$\nu_{vac.}$ observed (cm^{-1})	Band type[a]	Assignment[b]	$\nu_{vac.}$ calculated (cm^{-1})
4340	v.s. I. ⊥[c]	$\nu_1+\nu_4(E)$	4387
4540	v.w. I.	$3\nu_4+\nu_6(A_1+3E)$	4580
4685	v.w. I.	$\nu_1+\nu_5+\nu_6(A_1+E)$	4702
4715	v.w. I.		
4770	v.w. I.	$\nu_1+\nu_2+\nu_6(E)$	4759
4872	v.w. I.	$\nu_1+\nu_4+\nu_6(A_1+E)$	4901
5047	v.w. I.	$\nu_1+\nu_3+\nu_4(E)$	5087
5186	m. I.	$\nu_1+2\nu_4-\nu_6[A_1+2E]$	5185
5330	s. I.	$\nu_1+2\nu_5(A_1+E)$	5340
5530	s. I.	$\nu_1+\nu_4+\nu_5(A_1+E)$	5539
5699	v.s. I. (doublet)	$\nu_1+2\nu_4(A_1+E)$	see text
5728	v.s. I.		
5938	v.s. I.	$\nu_1+\nu_2+\nu_3+\nu_6(A_1+E)$?	5911
5978	v.s. I. (doublet)	$2\nu_1(A_1)$	see text
6290	v.w. I.	$\nu_1+\nu_2+\nu_3+\nu_4(E)$	6296
6435	v.w. I.	$2\nu_1+\nu_6(E)$	6492
6664	w. I.	$2\nu_1+\nu_3(A_1)$	6678
6853	m. I.	$\nu_1+2\nu_4+\nu_5(A_1+2E)$	6851
6906	w. I.	$\nu_1+2\nu_4+\nu_2(A_1+E)$	6908
7023	s. I.	$\nu_1+3\nu_4(A_1+E)$	7050
7100	s. I.	$2\nu_1+\nu_5(E)$	7130
7318	v.s. I.	$2\nu_1+\nu_4(E)$	7329
8135	v.w. I.	$2\nu_1+\nu_3+\nu_4(E)$	8029
8270	m. I.	$2\nu_1+2\nu_5(A_1+E)$	8283
8551.0	v.w. P.I.	$2\nu_1+2\nu_4(E)$	see text
8589.30	m. P.I. ∥ head	$2\nu_1+2\nu_4(A_1)$	
8586.1	w. P.I. ∥ head	$2\nu_1+2\nu_4+\nu_6-\nu_6$	see text
8791.1	w. P.I. ∥ head	$3\nu_1+\nu_6-\nu_6$	
8792.75	m. P.I. ∥ head	$3\nu_1(A_1)$	see text
9540	v.w. I.	$3\nu_1+\nu_3(A_1)$	9493
9730.0	v.w. P.I. ⊥	$2\nu_1+2\nu_4+\nu_5(A_1+2E)$	9742
9881.6	w. P.I.[d]	$2\nu_1+3\nu_4(A_1+E)$	9941
9938.3	v.w. P.I. ⊥	$3\nu_1+\nu_5(E)$	9945
10154.6	w. P.I.[e] ⊥	$3\nu_1+\nu_4(E)$	10144
11109.2	v.w. P.I. line	$3\nu_1+2\nu_5(A_1+E)$	11098
11279.1	v.w. P.I. ⊥	$3\nu_1+\nu_4+\nu_5(A_1+E)$	11297
11300.2	v.w. P.I. line		
11346.2	v.w. P.I. line	$3\nu_1+2\nu_4+\nu_6-\nu_6[2A_1+4E]$	
11347.2	w. P.I.[f] line	$3\nu_1+2\nu_4(A_1+E)$	see text
11497.0	v.w. P.I. ⊥?		
11555.5	v.w. P.I. ∥ head	$4\nu_1+\nu_3-\nu_3[A_1+E]$	
11559.2	v.w. P.I. ∥ head	$4\nu_1+\nu_6-\nu_6[A_1+E]$	
11563.4	w. P.I. ∥ head	$4\nu_1(A_1)$	see text
12620.1	v.w. P.I. ⊥	$3\nu_1+3\nu_4(A_1+E)$	12699
12641.5	v.w. P.I. line		
14002.8	v.w. P.I. line	$4\nu_1+2\nu_4(A_1+E)$	see text
14037	v.w. P.I. ⊥?		

[a] The intensities are indicated by v.s., s., m., w., and v.w. meaning very strong, strong, medium, weak, and very weak, respectively. I. and P.I. indicate bands measured with the photoelectric infra-red spectrometer and with the 21-ft. grating in the photographic region, respectively. ∥ and ⊥ refer to bands that have been identified as parallel or perpendicular bands. Bands marked with "line" have a line-like but diffuse central branch whose center was measured. They may be either parallel or perpendicular bands. Parallel bands marked head show a pronounced head of the central branch to which the wave number of the first column refers.

[b] The species of the allowed components of the transition moment are given in brackets. For all but the difference bands they coincide with the species of the upper states (omitting the A_2 substates). *Note added in proof:* There will be a few changes of species if ν_3 and ν_6 are interchanged; see footnote (a) of Table V.

[c] This band was also measured by Price with 10-cm path, at 4310 cm^{-1}. The identification of the band as ⊥ band is due to him.

[d] This band has a very peculiar structure. There is a strong violet-shaded head to which the wave number given in column 1 refers; in addition there is a diffuse band shaded apparently to longer wavelengths.

[e] This band shows more clearly than any other photographic band the expected structure of a perpendicular band. The series of Q branches is partially resolved, and the appropriate intensity alternation (strong, weak, weak, strong) is just recognizable.

if the P and R branches are too weak to be observed, must also be identified as parallel bands. However, there is a considerable number of bands whose central branches (frequently the only feature observed) are like diffuse lines. They may either belong to parallel bands for which $B' \approx B''$ or to perpendicular bands for which the spacing of the sub-bands, which is $2[B-C(1-\zeta)]$, is small because the Coriolis interaction constant ζ happens to be close to -0.84.

It was expected that the series of bands ν_1, $2\nu_1$, $3\nu_1$, $4\nu_1$, $\cdots$ (that is the overtones of the C−H vibration) would be the most prominent feature of the near infra-red spectrum of fluoroform, as it is for chloroform. Actually there are in each case two neighboring parallel bands of similar intensity rather than one. The two bands analyzed in Section C (see Fig. 2) form one such pair, namely, the one corresponding to $3\nu_1$ It is readily seen that these pairs of bands can be interpreted as $v_1\nu_1$ and $(v_1-1)\nu_1+2\nu_4$, since $2\nu_4$ has a magnitude similar to ν_1, particularly to the latter's higher vibrational quanta, and since one substate of $2\nu_4$ has the same species as ν_1, that is A_1. The separation of the two components of a pair is larger than 200 cm^{-1} and therefore Fermi resonance will affect the positions of the levels only slightly, even though it may affect the intensities to an appreciable extent. The shortward components of each pair which represent ν_1, $2\nu_1$, $3\nu_1$, $4\nu_1$, are 3035.6, 5978, 8792.7, and 11563.4, respectively. The separations of successive vibrational levels of the CH vibration are, therefore, 3035.6, 2942.$_4$, 2824.$_7$, and 2770.7 cm^{-1}. The levels can be represented approximately by

$$3088.0v_1-52.4v_1^2,$$

although the deviation for $v_1=4$ is much larger than compatible with the accuracy of the measurements, probably because of a non-negligible cubic term. The anharmonicity $x_{11}=52.4$ is of the right order for a CH vibration (compare for example those of HCN and C_2H_2).

The separations of $\nu_1+2\nu_4$, $2\nu_1+2\nu_4$, $\cdots$ from ν_1, $2\nu_1$, $\cdots$, respectively, are 2663.$_4$, 2611.$_3$, 2554.5, and 2439.4 cm^{-1}. The accelerated de-

[f] Accompanied by a diffuse fine structure on both long and short wave-length sides.

[g] These were calculated with old values, 700 and 514 cm^{-1}, for ν_3 and ν_6.

crease again points to a cubic term in the energy expression. Neglecting this, the anharmonic term x_{14} comes out to be approximately 28 cm^{-1}. However, this anharmonic coefficient does not represent very well bands of the type $v_1\nu_1+\nu_4$ and $v_1\nu_1+3\nu_4$. This is probably because the observed bands $v_1\nu_4+2\nu_4$ are parallel bands, having the A_1 component level as upper state while the bands $v_1\nu_1+\nu_4$ are perpendicular bands, the upper state having the species E only. For $v_1\nu_1+3\nu_4$ the situation is more complicated.

The vibrational data here obtained are not sufficient to determine all the anharmonicity coefficients x_{ik}. Since, in addition, the effect of cubic terms and of Fermi resonance is difficult to take into account accurately at the present stage, we give in the last column of Table VI, for all bands other than those just discussed, the wave numbers computed by simply adding to the observed wave numbers of the bands of type $v_1\nu_1$ and $v_1\nu_1+2\nu_4$ the fundamental or sum of fundamentals involved according to the assignments given.[11] On account of the effect of anharmonicity and the other reasons mentioned above, one should not expect a very close agreement of calculated and observed wave numbers. The only reason for listing the calculated values is as support for the assignments given in the third column.

[11] See footnote (g) of Table VI.

The central branches of the strong photographic bands are accompanied by weaker companions which must clearly be interpreted as difference bands of the type $\nu+\nu_i-\nu_i$ in which a low frequency fundamental is excited in both upper and lower state of the main band. Their positions relative to the main band are determined by the anharmonicity constants and cannot be predicted.

We are greatly indebted to Dr. A. F. Benning of the Jackson Laboratory of E. I. du Pont de Nemours and Company for putting at our disposal the fluoroform used in this investigation. Grateful thanks are due Dr. G. P. Kuiper for his cooperation in taking the infra-red spectra of fluoroform with his new photoelectric infra-red spectrometer. We also wish to thank Dr. W. C. Price for letting us have his data about the fundamentals of CHF_3 in advance of publication. Finally, we would like to express our appreciation to Professor R. W. Wood for supplying us with the remarkable grating with which the high resolution work was carried out.

THE JOURNAL OF CHEMICAL PHYSICS VOLUME 16, NUMBER 1 JANUARY, 1948

The Mercury Photosensitized Reactions of Ethylene Oxide*

M. K. PHIBBS, B. DE B. DARWENT, AND E. W. R. STEACIE
Divison of Chemistry, National Research Laboratories, Ottawa, Canada

(Received September 29, 1947)

The reactions of ethylene oxide with $Hg(^3P_1)$ atoms have been investigated at 25°C at pressures between 10- and 600-mm Hg, and at 200°C and 300°C at 100-mm Hg. The principal products are H_2, CO, CH_3CHO and a polymer; smaller amounts of CH_4, C_2 hydrocarbons and formaldehyde are also formed. The nature of the products and the very small effect of pressure on the reaction are best explained by a mechanism based principally on the formation of the activated ethylene oxide molecule, with a minor portion of the reaction proceeding via a C−H split.

INTRODUCTION

THE reactions between $Hg(^3P_1)$ atoms and the lower hydrocarbons have been studied in some detail.[1] It appears that, in general, the unsaturated hydrocarbons react principally by the transfer of energy from the excited mercury

* Contribution No. 1602 from the National Research Laboratories, Ottawa, Canada.

[1] See E. W. R. Steacie, *Atomic and Free Radical Reactions* (Reinhold Publishing Corporation, New York, 1946).

atom to the hydrocarbon molecule, leading to the formation of an excited hydrocarbon from which the products arise; on the other hand, the saturated hydrocarbons appear to react by a direct C—H split, which may or may not involve the formation of HgH, leading to the formation of the corresponding alkyl radical and an H atom. It has recently been shown that diethyl-ether[2] probably reacts with $Hg(^3P_1)$ atoms in a manner similar to the paraffins, whereas acetone[3] appears to behave like the olefins, and to react by the transfer of energy. The mercury photo-sensitized reactions of ethylene oxide are of interest in connection with the photo-chemical reactions of the simple oxygen containing organic compounds, since the oxygen atom may form part of a ring structure.[4]

EXPERIMENTAL

The ethylene oxide used was obtained from the Matheson Company, East Rutherford, New Jersey. It was used after repeated melting and freezing in vacuum followed by a simple bulb to bulb distillation. No impurities were detectable by the analytical methods used. The absorption spectrum was checked at atmospheric pressure on a Beckmann quartz spectrophotometer (10-cm path), and it was found to be completely transparent to 2200A.

The reaction was investigated in a circulatory system in which all of the ethylene oxide was present in the gas phase, no attempt being made to remove the higher boiling products of the reaction by means of cold traps since very small conversions were used. The gases were circulated by means of a pump of the type described by Puddington[5] over warm mercury, through a mercury desaturator and a cylindrical quartz vessel with plane ends in which the reactants were illuminated with the unfiltered light from a low pressure mercury lamp with neon (3 mm) as carrier gas. Since the incident light traveled through a distance of about 12 inches in air, it is reasonably certain that only traces of λ1849 could have reached the reactor.

The products of the reaction were separated by pumping off a trap kept successively at −183°, −126°, and −80°C. The products volatile at −183°C (H_2, CO, and CH_4) and at −126°C (C_2 hydrocarbons) were analyzed by conventional methods. The residual ethylene oxide (volatile at −80°C) was estimated by $P-V$ relations and by titration as recommended by Lubatti.[6] Specific tests showed formaldehyde[7] to be absent from the C_2 (−183° to −126°C) fraction but to be present in the "ethylene oxide" fraction. Acetaldehyde was also found[8] in the "ethylene oxide" fraction in which it was estimated by the sodium bisulfite—iodine—sodium thiosulfate titration[9] after correction for formaldehyde which was estimated colorimetrically.[10] A small blank correction was necessary when acetaldehyde was estimated after the titration for ethylene oxide. The correction was negligible and the reproducibility better when the ethylene oxide titration was omitted; in these cases the residual ethylene oxide was determined by $P-V$ relation by correcting for the total aldehyde present. No detectable pressure developed on allowing the trap to warm up, after removal of ethylene oxide, from −80° to room temperature.

A non-volatile white solid was visible on the walls of the reaction vessel at the end of each experiment at room temperature. It was also found that under these conditions a large proportion of the ethylene oxide reacted could not be accounted for by the gaseous products and aldehydes. Accordingly, experiments were conducted in a single-pass system to obtain enough of the heavy products for identification. In these experiments a much more intense light source was used and the flow rate of the ethylene oxide adjusted to permit 10–20 percent reaction per pass. No white solid was deposited on the walls, but droplets of a relatively high boiling liquid appeared early in these experiments. The products obtained

[2] B. de B. Darwent, E. W. R. Steacie, and A. F. van Winckel, J. Chem. Phys. **14**, 551 (1946).
[3] E. W. R. Steacie and B. de B. Darwent, unpublished.
[4] For opinions on the structure of ethylene oxide see, however, P. V. Zimakov, J. Phys. Chem. (U.S.S.R.) **20**, 133 (1946); A. D. Walsh, Nature **159**, 165, 712 (1947); R. Robinson, *ibid.* **159**, 400 (1947), **160**, 162 (1947).
[5] I. E. Puddington, Ind. Eng. Chem. (Anal. Ed.) **17**, 592 (1945).
[6] O. F. Lubatti, J. Soc. Chem. Ind. **54**, 424 (1935).
[7] S. B. Schryver, Proc. Roy. Soc. (London) **82B**, 226 (1910).
[8] A. Ley, J. pharm. chim. (6) **22**, 107 (1897).
[9] I. M. Kolkoff and N. H. Furman, *Volumetric Analysis* (John Wiley and Sons, Inc., New York, 1929), Vol. II, p. 450.
[10] D. Matukawa, J. Biochem. (Tokyo) **30**, 386 (1939).

from one experiment separated on cooling into two layers, the upper of which boiled at about 165°C and the lower at about 99°C. Fractional distillation of the products of further experiments gave three fractions, the identifications of which were unsuccessful, but tests showed them to be aldehydic in nature and showed the absence of such plausible compounds as dioxanes, dioxolanes, 1,3-diepoxybutane, and alcohols. The white polymer produced in the low intensity circulating runs was found to be water soluble and aldehydic in nature; it was easily removable from the walls by warming or by flaming in an oxygen atmosphere, the latter being the procedure adopted for cleaning the cell before each run. It is worthy of note that this white polymer was not formed on the incident face, but rather on the cylindrical side walls of the cell, and started about 1 mm from the incident face.

Some experiments were carried out at higher temperatures. In these runs the quartz reactor was enclosed in a furnace fitted with a quartz window. All other conditions were unaltered. No visible polymer was formed in these experiments, and the material balance was satisfactory at 200°C and higher temperatures.

The light intensity was measured by the rate of hydrolysis of monochloracetic acid (0.5*N*) in the cell. The corrections as given by Smith, Leighton, and Leighton[11] for the dark reaction were applied.

RESULTS

Details of the experimental conditions and results on which subsequent discussion will be based are given in Table I. From these results it is evident that the rates of production and composition of the gaseous products at any given pressure are independent of time. The data for the amount of ethylene oxide reacted are much more variable, being small differences of two large quantities, but the rate here may also be taken as independent of time within the limits of accuracy of the determination. The rate of production of aldehydes is not independent of time (Fig. 1); however, it seems likely that the initial rate of production of aldehydes is approximately independent of the initial pressure of ethylene oxide. By basing the discussion on the initial rates the complications connected with

TABLE I. The mercury photosensitized decomposition of ethylene oxide.

Experimental conditions and results
Volume of system—726 cc, λ2537 absorbed—9.82×10^{-5} einstein/hr.
Volume of reaction vessel—230 cc, Hg pressure, 1.2×10^{-3} mm.
Circulation rate—400 cc/min. at prevailing pressure.

Expt. No.	Duration, hours	Ethylene oxide reacted cc 25°C	Products cc at 25°C H_2	CO	CH_4	C_2	Total ald.
I. Experiments at room temperature—25±2°C							
A. Initial pressure of ethylene oxide = 10±1 mm							
29	1.0	0.5	0.27	0.46	0.09	0.16	—
28	2.0	1.8	0.48_5	0.92	0.19	0.28	—
33	5.1	2.4	0.98_5	1.91	0.39	0.52	—
B. Initial pressure of ethylene oxide = 40 mm							
44	0.25	—	—	—	—	—	0.05
45	0.5	—	—	—	—	—	0.16
9	0.5	0.5	0.19	0.26	0.05	0.08	0.18
3	1.0	1.7	0.38	0.58	0.10	0.15	0.16
46	1.0	—	—	—	—	—	0.16
1	2.0	2.5	0.72	1.06	0.20	0.33	0.10
2	4.0	3.9	1.36	2.04	0.37	0.55	0.07
11	4.0	—	—	—	—	—	0.09
C. Initial pressure of ethylene oxide = 100 mm							
43	0.25	—	—	—	—	—	0.10
32	0.25	0.6	—	—	—	—	—
42	0.5	—	—	—	—	—	0.15
25	1.0	2.2	0.39	0.52	0.09	0.12	—
41	2.0	—	—	—	—	—	0.47
23	4.0	5.2	1.52	2.00	0.32	0.46	—
40	4.3	—	—	—	—	—	0.61
24	8.0	8.88	2.78	3.57	0.59	0.66	—
D. Initial pressure of ethylene oxide = 200 mm							
14	0.17	—	—	—	—	—	0.15
10(*A*)	0.5	—	0.21	0.24	0.05	0.08	—
12(*A*)	0.5	—	—	—	—	—	0.27
8	1.0	1.7	0.42	0.48	0.09	0.11	0.20
11(*A*)	1.0	—	—	—	—	—	0.42
4	2.0	2.9	0.88	1.04	0.16	0.20	0.48
6	4.0	6.3	1.72	1.94	0.31	0.31	0.81
13	6.0	—	—	—	—	—	0.91
5	8.0	10.4	3.12	3.66	0.57	0.55	0.75
E. Initial pressure of ethylene oxide = 600 mm							
18	1.0	2.2	0.45	0.43	0.09	0.10	—
21	1.0	2.6	—	—	—	—	—
15	2.0	—	0.89	0.91	0.14	0.18	0.42
20	3.0	5.1	—	—	—	—	—
16	4.0	—	1.83	1.78	0.28	0.24	—
16(*A*)	6.0	9.7	2.57	2.42	0.37	0.42	0.99
22	10.0	12.9	4.48	3.94	0.67	0.64	—
II. Experiments at 200°C and an ethylene oxide pressure of 100 mm							
36	1.0	2.5	0.70	1.29	0.30	0.37	1.66
37	3.0	4.5	2.03	4.09	0.95	1.19	1.74
III. Experiments at 300°C and an ethylene oxide pressure of 100 mm							
38	1.0	3.1	0.85	2.03	0.71	0.53	1.57
38(*A*)	1.0	(Blank—lamp off—total non-condensible gas = 0.043 cc)					1.41

[11] R. N. Smith, P. A. Leighton, and W. G. Leighton, J. Am. Chem. Soc. **61**, 2299 (1939).

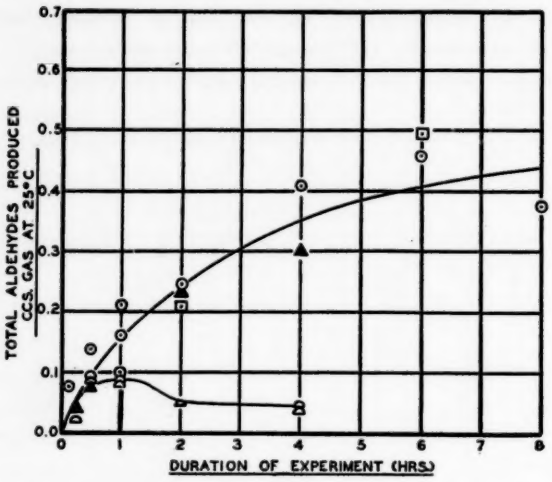

FIG. 1. The production of aldehydes at 25°C; initial pressure of ethylene oxide as follows: squares—600 mm; circles—200 mm; triangles—100 mm; half-circles—40 mm. (In experiments at 40, 200, and 600 mm the ethylene oxide was estimated by titration before the aldehydes were determined; the aldehyde content was less accurate than in the experiments at 100 mm in which no titration for ethylene oxide was attempted.

the disappearance of aldehydes in the later stages of the reaction may be eliminated.

The effect of pressure on the initial rates is shown in Table II. The data given here show that the gaseous and aldehydic products do not account for all the material reacted except at the lowest pressure. It has been mentioned previously that a white solid polymer was formed during the experiments. The effect of pressure on the rate of polymerization has been calculated (Table III) from material balances, and the results show the increase in the extent of the polymerization reaction with pressure. The composition of the polymer (ratios H/C and C/O) is given in columns 11 and 12 of Table III. The H/C ratio is constant, within experimental error, at 2.0 and is approximately independent of pressure, whereas the C/O ratio decreases, indicating increasing oxygenation, with increasing pressure. The above results and the fact that two immiscible liquids were found in the single-pass experiments lends plausibility to the suggestion that the total polymer consisted of two types of substance $((CH_2)_2O)_n$ and $(CH_x)_n$, in which X lies between 1.2 and 2.1 with an average value of 1.8, as shown in Table IV.

TABLE II. Effect of pressure on the mercury photosensitized decomposition of ethylene oxide at 25°C.

A. Experiments at room temperature						
Initial pressure mm	Rates—cc/hr. (25°)					
	$-(CH_2)_2O$	H_2	CO	CH_4	C_2	ald.
10	0.56	0.21	0.42	0.082	0.118	0.45
40	1.02	.35	.53	.094	.145	.45
100	1.30	.36	.475	.076	.093	.45
200	1.44	.411	.47	.074	.081	.45
600	1.50	.445	.42	.070	.067	.45

The effect of pressure is shown in Fig. 2 in which the rates given in Tables II and IV are plotted against the reciprocal of the pressure. The relationship between pressure and the rates shown in Fig. 2 for the experiments at room temperature is as follows:

$$\frac{d}{dt}(H_2) = 0.450 - \frac{5.5}{p},$$

$$\frac{d}{dt}(CO) = 0.425 + \frac{4.5}{p},$$

$$\frac{d}{dt}[((CH_2)_2O)_n] = 0.660 - \frac{25.0}{p},$$

$$\frac{d}{dt}(C_2) = 0.060 + \frac{3.1}{p},$$

$$\frac{d}{dt}(CH_4) = 0.064 + \frac{1.0}{p},$$

where the rates are in cc (25°C) per hour and p = pressure (mm Hg) of ethylene oxide. The lowest pressure investigated (10 mm) has not been included in Fig. 2 because the results indicate that quenching was incomplete below about 40 mm.

DISCUSSION

The following processes have been shown to occur in the mercury photosensitized reactions of ethylene oxide at room temperature:

(a) Isomerisation to acetaldehyde: the initial rate of production of acetaldehyde being independent of the ethylene oxide pressure.

(b) Decomposition to H_2, CO, CH_4, C_2 hydrocarbons and formaldehyde. The rates of production of the above substances (except formaldehyde) are linear functions of the reciprocal pressure such that the rates are finite even as $p \to \infty$, the pressure dependence in all cases being small.

TABLE III. Effect of pressure on the mercury photosensitized polymerisation of ethylene oxide at 25°C.

Pressure mm	Reaction rates cc atom/hr. (25°C) C	H	O	Gases and aldehydes+ cc atom/hr. (25°C) C	H	O	Polymer (by diff.) cc atom/hr. (25°C) C	H	O	Comp. of polymer H/C	C/O
10	1.12	2.24	0.56	1.52	2.92	0.87	−0.40	0.00	−0.31	—	—
40	2.04	4.08	1.02	1.70	3.38	0.98	0.34	0.70	0.04	2.1	8.5
100	2.60	5.20	1.30	1.52	3.04	0.92	1.08	2.16	0.38	2.0	2.8
200	2.88	5.76	1.44	1.48	3.08	0.92	1.40	2.68	0.52	1.9	2.7
600	3.00	6.00	1.50	1.40	3.09	0.87	1.60	2.91	0.63	1.8	2.5

+ The average composition of the aldehydes was 75 percent $CH_3{\cdot}CHO$, 25 percent HCHO.

(c) Polymerization to yield substances of the types $((CH_2)_2O)_n$ and $(CH_2)_n$—the rate of production of the former being quite strongly pressure dependent, whereas the latter is approximately independent of pressure.

The occurrence of an isomerisation reaction, by which acetaldehyde is formed as a major product, and the pressure independence of that reaction, indicate that an active ethylene oxide molecule is formed in the primary act:

$$Hg(^1S_0)+h\nu_{2537}\rightarrow Hg(^3P_1), \quad (0)$$

$$Hg(^3P_1)+(CH_2)_2O\rightarrow C_2H_4O^*+Hg(^1S_0), \quad (1)$$

from which acetaldehyde is produced by either a first or second order process:

$$C_2H_4O^*\rightarrow CH_3CHO, \quad (2)$$

$$C_2H_4O^*+(CH_2)_2O\rightarrow CH_3CHO+(CH_2)_2O. \quad (2^1)$$

The above reactions (2) and (2¹) are energetically possible since the active molecule may possess as much energy as 112 kcal. per mole, and thermal investigations[12] indicate that only 52 kcal. per mole are necessary for isomerization. Any process by which acetaldehyde could be formed by atomic and/or radical recombination, providing that the atoms or radicals also react with ethylene oxide, would lead to kinetics such that the rate of formation of acetaldehyde would be inversely proportional to the concentration of ethylene oxide.

The effect of pressure on the decomposition to hydrogen and carbon monoxide is also in agreement with the supposition that an active molecule plays the predominant role in the initial step of this reaction. If the decomposition were largely due to a C−H split followed by "atomic cracking," the type of process frequently postulated to account for C−C splitting in the photosensitized reactions of the paraffin hydrocarbons, it would be expected that, since H atoms react with ethylene oxide[13] at about the

TABLE IV. Effect of pressure on the composition of the polymer.

Pressure mm	cc $((CH_2)_2O)_n$ per hour	cc $(CH_x)_n$ per hour	X
10	—	—	—
40	0.04	0.26	2.1
100	0.38	0.32	2.0
200	0.52	0.36	1.7
600	0.63	0.34	1.2

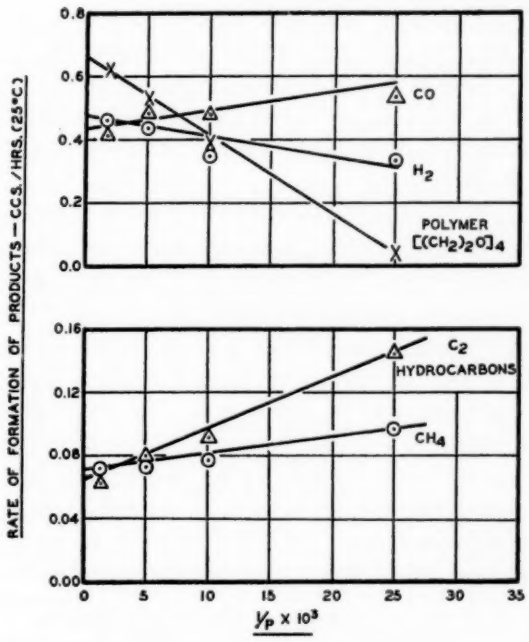

FIG. 2. The effect of pressure on the decomposition and polymerization reactions at 25°C.

[12] W. W. Heckert and E. Mack, J. Am. Chem. Soc. **51**, 2706 (1929).

[13] W. R. Trost and E. W. R. Steacie, unpublished.

same rate at room temperature as they do with the paraffins, the rate of decomposition would approach zero as the concentration of ethylene oxide approaches infinity. Since such a relationship has not been found, it must be concluded that a C−H split cannot play an important role in the mechanism. The decomposition of the excited molecule may be first or second order:

$$C_2H_4O^* \rightarrow H_2+CO+CH_2, \qquad (3)$$

$$C_2H_4O^*+(CH_2)_2O \rightarrow H_2+CO+CH_2+(CH_2)_2O. \qquad (3^1)$$

An alternative process by which the decomposition proceeds by virtue of acetaldehyde in the stable or activated state, such as was found for the thermal and H-atom reactions[13] of ethylene oxide, does not agree with the results of the present investigation. That type of process would lead either to an induction period or to a pressure dependence such that the rate of decomposition would approach zero at higher pressures.

If the excited molecule acquires almost all of the energy of the $Hg(^3P_1)$ atom (112 kcal. per mole), it will be possible for reactions (2^1) and (3^1) to occur in a single step leading to the isomerization of one molecule and to the decomposition of the other in the collision between one excited and one ground-state ethylene oxide molecule.

The results obtained do not allow of a choice between the first- and second-order processes outlined above. The limiting high pressure rates, obtained by extrapolation in Fig. 2, give the following quantum yields:

$$\phi \text{ Decomp.} = 0.18,$$
$$\phi \text{ Isom.} = 0.12,$$
$$\phi \text{ Polym.} = 0.36,$$
$$\phi \text{ Total} = 0.66.$$

Hence only 0.30 mole of ethylene oxide isomerizes or decomposes per einstein absorbed. This inefficiency may be due to either a first- or second-order process:

$$C_2H_4O^* \rightarrow (CH_2)_2O+h\nu \qquad (4)$$

$$C_2H_4O^*+(CH_2)_2O \rightarrow 2(CH_2)_2O. \qquad (4^1)$$

Since no investigation of fluorescence was made, it is not possible to decide between the alternatives since either a short-lived excited molecule with fluorescence or a long-lived one which on collision always either reacts or is deactivated will explain the results.

The very small effect of pressure on the rate of production of the minor products (CH_4, C_2 hydrocarbons and formaldehyde) indicates that they also arise in some way from the decomposition of the excited molecule.

The above mechanism accounts for the major characteristics of the isomerization and decomposition reactions but not for the pressure dependence, small though it is, of the decomposition. Also the fact that polymerization is important at high pressures, and that more hydrogen than carbon monoxide is formed at high pressures show that a small portion of the reaction probably proceeds by a free radical mechanism. The following type of process

$$Hg(^3P_1)+(CH_2)_2O \rightarrow C_2H_3O+H+Hg(^1S_0), \qquad (1^1)$$

is well known in photosensitized reactions and is probably responsible for this aspect of the reaction. The nature of the polymer is consistent with the initiation of polymerization by the C_2H_3O radical, and the increase in "atomic cracking" with the decreasing pressure explains the small pressure dependence, providing that the major portion of the initial act is reaction (1) rather than (1^1). The effect of temperature can be explained by the decomposition of the C_2H_3O radical leading to increasing CO and decreasing polymer at high temperatures.

The Use of Tritium in the Determination of the Solubility of Water in Solvents. The Solubility of Water in Benzene

G. G. JORIS* AND H. S. TAYLOR
Frick Chemical Laboratory, Princeton University, Princeton, New Jersey

(Received July 14, 1947)

A new method for determination of the solubility of water in hydrocarbons is based on the use of radioactive hydrogen isotope, tritium, as tracer for the dissolved water. This method is applicable to the determination of the solubility of water in compounds in which it is sparingly soluble.

ALTHOUGH numerous methods have been used or proposed for the determination of water solubility in hydrocarbons, the number of hydrocarbons studied has been singularly limited. Solubility of water has been measured only in benzene,[1–5] toluene,[2,5] cyclohexane,[2] various gasolines,[1,4,6,7] and oils.[8–10] The synthetic or sealed-tube method employed by Groschuff,[1] and by Tarassenkow and Poloshinzewa[2] consisted in observing the temperature at which a measured amount of water is visually soluble in a measured weight of hydrocarbon. This is done by superheating the mixture sufficiently to bring all the water into solution and then cooling until a fine mist is formed; from the temperature of appearance and disappearance of this fine mist, solubility data may be obtained. The saturated solutions were, in another method, volatilized and absorbed in a dehydrating agent which does not absorb or react with organic solvent (calcium chloride).[4,6] The water dissolved in the hydrocarbons has also been determined by converting it to hydrogen through addition of calcium hydride[5] or a sodium-potassium alloy[7] to the solution. The method used by Hill[8] is based upon the property of silver perchlorate of being exceptionally soluble in water and somewhat soluble in various organic solvents; the amount of water present in the hydrocarbon is estimated from the solubility of silver perchlorate in the solution, reference curves having been previously obtained using synthetic mixtures of water and hydrocarbon. The Karl Fischer method[11,12] has also been applied for the measurement of water solubility in oils.[8–10,13]

The most serious disadvantage of all these methods is that they require large amounts of hydrocarbons if any accuracy is to be obtained. There was need for a method, accurate as well as general, which would require small amounts of solvent and therefore permit the study of solvents only available in the pure state in small quantities. The recent availability of water containing radioactive hydrogen rendered possible the development of a new method for the measurement of water solubility based on saturating the solvent with radioactive water and measuring the radioactivity of the solution. For radioactive hydrogen or tritium, having a half-life of 31 ± 8 years,[14] there is no appreciable change in the radioactivity of the water during the course of the solubility measurement. The radioactive water used in this study was prepared in the Berkeley cyclotron by bombardment of heavy water with high speed deuterons; it was therefore necessary to correct the experimental

* Present address: Allied Chemical and Dye Central Research Laboratory, Morristown, New Jersey.

[1] Groschuff, Zeits. f. Elektrochemie **17**, 348 (1911).

[2] N. D. Tarassenkow and E. N. Poloshinzewa, Zhur. obshchei Khim., Khim. Ser. **1**, 71 (1931); Chem. Abs. **25**, 4762 (1931); Chem. Abs. **26**, 2363 (1932); Ber. d. d. Chem. Ges. **65B**, 184 (1932).

[3] A. E. Hill, J. Am. Chem. Soc. **45**, 1143 (1923).

[4] C. W. Clifford, Ind. Eng. Chem. **13**, 631 (1921).

[5] C. K. Rosenbaum and J. H. Walton, J. Am. Chem. Soc. **52**, 3568 (1930).

[6] Seidell, *Solubilities of Inorganic and Metal Organic Compounds* (D. Van Nostrand Company, New York, 1940), 3rd edition, Vol. I, p. 587.

[7] E. W. Aldrich, Ind. Eng. Chem., Anal. Ed., **3**, 348 (1931).

[8] R. N. Evans and J. E. Davenport, Ind. Eng. Chem., Anal. Ed., **14**, 732 (1942).

[9] G. Wernimant and F. J. Hopkinson, Ind. Eng. Chem., Anal. Ed., **15**, 272 (1943).

[10] M. M. Acker and H. A. Frediani, Ind. Eng. Chem., Anal. Ed., **17**, 793 (1945).

[11] Brouckere and Gillet, Bull. Soc. Chem. Belg. **44**, 473 (1935).

[12] D. M. Smith, W. N. D. Bryant, and J. Mitchell, Jr., J. Am. Chem. Soc. **61**, 240 (1939).

[13] K. Fischer, Angew. Chemie **48**, 394 (1935).

[14] R. D. O'Neal and H. Goldhaber, Phys. Rev. **58**, 574 (1940).

results to obtain the solubility data of ordinary water in the solvents. Since the concentration of tritium in the water used was only of the order of 10^{-12} mole tritium per mole of heavy water, the radioactive isotope is essentially all in molecules of TDO. The isotope effect due to tritium is correspondingly reduced. The mode of calculation from this isotopic species to H_2O solubility will be detailed later.

EXPERIMENTAL METHOD AND TECHNIQUE

The experimental technique consists in a series of successive operations: (a) the saturation of the hydrocarbon sample with radioactive water at the desired temperature by bubbling air, saturated with radioactive water vapor, through the hydrocarbon sample until saturation is attained; (b) the taking of an aliquot portion of the saturated solution; (c) the measurement of the radioactivity present in the sample.

APPARATUS AND OPERATING PROCEDURE

1. Saturation and Sampling

A unidirectional flow of air, saturated with radioactive water vapor and hydrocarbon vapor, is effected in the closed circulatory system represented in Fig. 1 by the combined action of a mercury-filled reciprocating pump and the two mercury valves, V and V'. The removable chamber A contains the liquid hydrocarbon solvent; its temperature is kept constant during saturation by means of the water-filled Dewar flask, N. The circulating air has to go through trap C before entering the saturator A; the temperature of trap C is held at about 0.1°C below the temperature of saturator A by means of the water-filled Dewar flask, M. This temperature differential is important and has to be carefully maintained since it prevents the condensation of water on the inlet tube walls of the saturator and on the hydrocarbon itself. In order also to avoid condensation of liquid in parts of the apparatus other than the trap C the whole circulatory system is kept at a temperature higher than that of the Dewar flasks by enclosure in an electrically heated air thermostat. In addition, the vertical tube, L, is electrically heated to prevent condensation of the vapors over the cool mercury.

After complete evacuation (10^{-5} mm Hg) and flaming of the apparatus, dry air is introduced, trap C being at liquid air temperature. When the system is at atmospheric pressure, it is isolated and the circulating pump is started. A small amount (about 0.1 cc) of radioactive water is then distilled from its storage chamber into the apparatus where it is trapped in cylinder C.

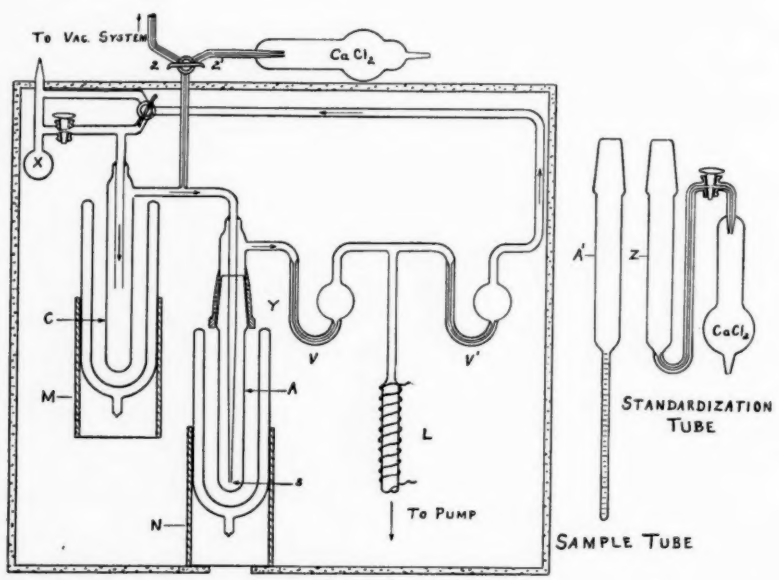

Fig. 1.

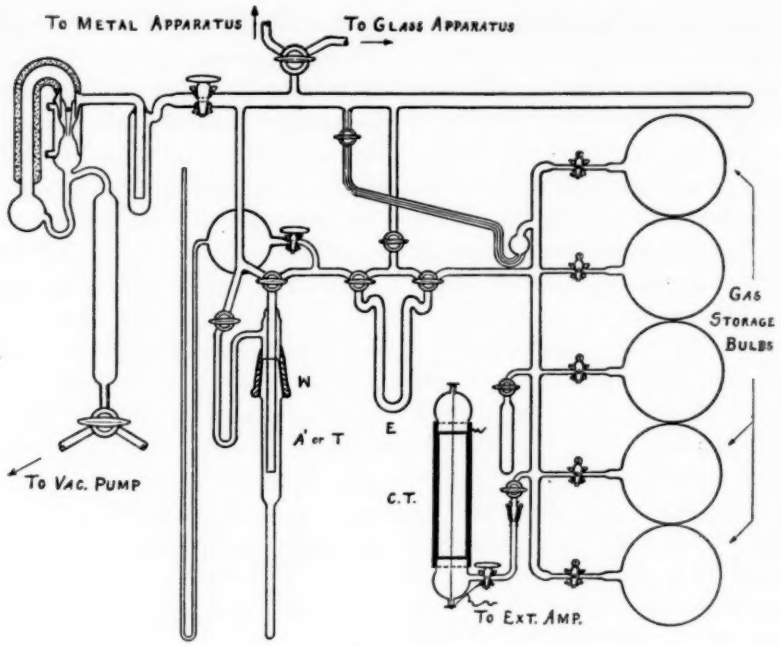

FIG. 2.

The circulation is stopped and about five cubic centimeters of liquid hydrocarbon solvent are added to the removable saturator A. Temperatures of the trap C and saturator A are adjusted to the desired level by means of the water-filled Dewar flasks, stopcock 2 being opened to the atmosphere to permit the elimination of the air in excess. When the conditions of temperature are attained, stopcock 2 is closed and the air is circulated. Results indicate that about four hours of circulation at the rate of approximately 300 cc per minute will effect complete saturation.

When saturation has been completed and circulation stopped, part of the saturated sample is drawn up into the inlet tube S by opening stopcock 2 to the vacuum system. Saturator A is then detached from the apparatus at Y. The outside of the tube S is carefully wiped with absorbent cotton moistened with alcohol to remove all traces of radioactive water and then dried. The calibrated sample tube A' (see Fig. 1) is attached at the joint Y and by turning stopcock 2 to the atmosphere the saturated sample is delivered into tube A'. The sample tube A' is then removed and transferred to the other section of the apparatus where its radioactivity can be measured.

2. Measurement of the Radioactivity of the Saturated Sample

Tritium emits soft beta-radiations[15] whose intensity is best measured by direct introduction of the radioactive sample into the Geiger-Müller counter. This was most conveniently done by separating the radioactive water in solution from the hydrocarbon solvent through absorption on calcium oxide and by subsequently transferring the tritium in the counter through equilibration with ethanol vapor. The analytical apparatus is schematized in Fig. 2.

When the volume of the saturated hydrocarbon sample, taken in the calibrated sample tube A', has been measured at an observed temperature, the sample tube A' is connected to the analytical apparatus by means of the ground-glass joint at W. The sample is solidified by cooling A' with liquid air and the apparatus is evacuated in its entirety to remove the non-condensable gases. The sample is then transferred into the U-tube E which contains freshly dehydrated calcium oxide and is cooled with liquid air while the temperature of A' is warmed slowly up to room temperature.

When the transfer is visually completed the

[15] R. D. O'Neal, Phys. Rev. 60, 359 (1941).

U-tube is isolated from the rest of the apparatus and brought back to room temperature; water is allowed to react with calcium oxide. The radioactive water left adsorbed on the walls of the sample tube is transferred into the Geiger counter for counting through equilibration with ethanol vapor and introduction of the latter into the counter. This is most conveniently done by evaporating into the sample tube section small amounts of ethanol vapor and expanding them into the counter until the total pressure reaches 5 mm of mercury. Small amounts of argon gas are then similarly introduced into the sample tube section and expanded into the counter until the total pressure is 2 cm of mercury. The radioactivity of the mixture is then measured. The same operation is repeated until the radioactivity becomes negligible.

After absorption of the water by the calcium oxide the hydrocarbon is removed by vacuum distillation. The first distillation fractions are introduced into the Geiger counter to ascertain the amount of possibly unreacted water they may carry. When the distillation fractions are exempt from radioactivity the hydrocarbons are condensed again into the sample tube A'. The bulk of the water in the hydrocarbon sample is now present as calcium hydroxide from which tritium is extracted for counting, again through exchange reaction with ethanol vapor. This is effected by introducing into the U-tube a quantity of ethanol such that when expanded into the evacuated Geiger counter it has a pressure of 5 mm; the U-tube is heated to 250°C and kept at that temperature for 30 minutes. The radioactive ethanol vapors are then expanded into the Geiger counter; small amounts of argon gas are successively introduced into the U-tube and expanded into the Geiger counter until the total pressure in the latter reaches 20 mm. The radioactivity of the ethanol vapors is determined. Since the equilibrium constant for the isotopic hydrogen exchange between calcium hydroxide and ethanol is of the order of unity at 250°C, the process of extraction of tritium from the hydroxide has to be repeated until the radioactivity of the ethanol vapor washings is small.

3. Detecting Unit

The Geiger-Müller counter employed consisted of a brass cylinder 25 cm in length and 5 cm in diameter with glass ends waxed into place with Piceine cement. A five-mil tungsten wire, cemented at the center of each glass end, was used as anode. The standard counter gas mixture was constituted of one part of ethanol and three parts of argon at a total pressure of 2 cm of mercury. The actual counting was operated by a "high speed Geiger-Müller counter Set Model G.L. 532" manufactured by Herbach and Rademan. This instrument permits the counting of 0 to 300 discharges per second. The amplification system consists of a five-stage high gain short time constant amplifier. The scaling system contains circuits employing five pairs of thyratron tubes yielding scales of 2, 4, 8, 16, and 32. An electromechanical watch recording every second impulse was used as registering instrument.

Under the actual conditions of radioactivity measurement, a plateau of about 100 volts was observed where the number of counts is practically constant with increasing voltages. Measurements were carried out 50 volts above the threshold voltage.

4. Estimation of Corrections

(*a*) *Coincidence correction.* The Slay cut-off coincidence correction formula has been used.

(*b*) *Background correction.* The background correction was determined by counting a gas mixture containing inactive ethanol vapor and argon.

(*c*) *Sensitivity correction.* The sensitivity of the counter was checked after each series of counts by measurement of the added radioactivity caused by the introduction of a radioactive material, a bottle of uranium acetate, in a definite position near the Geiger-Müller counter.

5. Standardization of the Radioactive Water

Air was saturated with radioactive water at a definite temperature (20°C) and, employing pressure-volume relationships, a measured quantity of the saturated air was introduced into the Geiger-Müller counter. Ethanol vapor and argon were then successively used, as before, as flushing agent until the total pressure in the counter was 2 cm of Hg. The radioactivity of the standardized water was 8.84×10^8 counts per minute per mole.

EXPERIMENTAL RESULTS

1. As an example illustrating the method, the experimental data leading to the calculation of the solubility of water in benzene saturated at 20°C are reported below. The sample of saturated benzene taken for analysis had a volume of 1.10 cc. All the following counts have been adjusted to a standard sensitivity of 1000.

(*a*) *Background correction 383 counts per minute.*

(*b*) *Ethanol vapor washing of the sample tube section.* 743 − 383 = 360 c/m.

(*c*) *Radioactivity of first portions of hydrocarbon volatilized from CaO U-tube (0.5 cm Hg in G.M. counter each).* 1st portion: 1915 − 383 = 1532 c/m. 2nd portion: 843 − 383 = 460 c/m.

(*d*) *Radioactivity of washings of CaO oxide with ethanol vapor.* 1st washing: 8360 − 383 = 7977 c/m; 2nd washing: 4040 − 383 = 3657 c/m; 3rd washing: 2770 − 383 = 2387 c/m; 4th washing: 1172 − 383 = 789 c/m; 5th washing: 900 − 383 = 517 c/m. Estimated radioactivity remaining 520 c/m. Total radioactivity 18200 c/m.

Thus the 1.10 cm³ of benzene saturated at 20°C contain an amount of water corresponding to 18200 c/m or 16550 c/m/cc of benzene.

Measurement of the water radioactivity. The amount of water introduced in counters: 2.62×10^{-6} moles. Number of discharges: 2697 − 383 = 2314 c/m. Number of discharges per mole of D_2O water: 8.84×10^{-8} c/m.

Calculation of solubility of ordinary water at 20°C. This calculation actually requires the assumption of the validity of Henry's Law, a knowledge of the Henry's Law constants and also the vapor pressures of the isotopic species TDO and H_2O. We have assumed the validity of Henry's Law because of the extreme dilutions that are here involved. In the absence of data we further assume that the Henry's Law constant $k = p_1/n_1$ is the same for TDO and H_2O. We can proceed in the absence of data on the vapor pressure of TDO in the following manner.

The molar concentration of TDO present in the sample (volume = 33.4 cc; $p = 7$ cm; $t = 22$°C) used in the preceding section for measurement of the radioactivity is

$$\frac{33.4 \times 7 \times 273 \times p_1}{22400 \times 76 \times 298 \times 760} = 1.685 \times 10^{-7} p_1 \text{ moles TDO/mole,} \quad (1)$$

where p_1 is the pressure in mm of the TDO in the gas sample measured. This is also the pressure of TDO in the gas phase in equilibrium with the solution when the benzene is saturated with water.

Let A be the number of counts/min./mole of TDO which is used. The number of moles in question is defined by Eq. (1). The observed activity of the sample was 2314 c/m. Hence,

$$\frac{2314}{A} = 1.685 \times 10^{-7} p_1 \quad \text{or} \quad p_1 = \frac{2314}{1.685A} 10^7,$$

$$p_1 = \frac{1.375}{A} 10^{10} \text{ mm.}$$

In 1 cc of benzene, saturated at 20°C, we found 16550 c/m. The molar concentration of TDO in the benzene solution is therefore

$$\frac{16550}{A} \cdot \frac{78.05}{0.895} = \frac{1.445}{A} 10^6 \text{ mole TDO/mole benzene.}$$

The Henry's Law constant, k, for TDO becomes therefore

$$k = \frac{p_1}{n_1} = \frac{1.375A^{-1} \times 10^{10}}{1.445A^{-1} \times 10^6} = 0.952 \times 10^4.$$

If the assumption is now made that the Henry's Law constant is the same for H_2O as for TDO the solubility of H_2O at 20°C is, therefore,

$$n_2 = \frac{p_2}{0.952 \times 10^4}$$

where p_2 is the vapor pressure of H_2O at 20°C, i.e., $p_2 = 17.535$ mm.[16,17]

Inserting this value for p_2 we receive

$$n_2 = \frac{17.535}{0.952 \times 10^4} = 18.4 \times 10^{-4} \text{ mole } H_2O/\text{mole } C_6H_6.$$

The corresponding solubilities in other units are:

(a) solubility per 100 cc benzene = 2.105×10^{-3} mole or 3.80×10^{-2}g H_2O;

(b) solubility per 100g benzene = 4.25×10^{-2}g H_2O.

[16] F. T. Miles and A. W. C. Menzies, J. Am. Chem. Soc. **58**, 1065 (1936).

[17] G. N. Lewis and R. T. McDonald, J. Am. Chem. Soc. **55**, 3057 (1933).

TABLE I.

Temperature °C	This work	References 3	1	2	4	5
10	0.030	0.043	0.040	0.035	0.032	0.045
20	{0.0425 0.0445	0.057	0.056	0.055	0.044	0.057
26	0.054	0.070	0.070	0.069	0.057	0.067

TABLE II.

p/p_0	0.60	0.77	0.92	0.95	1.00
t (monolayers)	1	7.2	46	70	184

2. Solubilities at 10, 20, and 26°C

The available literature data on the solubility of benzene at 10, 20, and 26°C, extrapolated or interpolated when necessary, are reported in Table I along with our actual results.

Examination of Table I reveals that our results are in good agreement with those of Clifford[4] who measured the water of solution by volatilization and absorption by calcium chloride, but that those obtained using the other methods, synthetic or chemical, are somewhat higher. It had been suggested that Clifford's results were possibly too low because the volatilization of the water may have been incomplete. Such a possibility has been eliminated in our method since we have measured the residual radioactivity of the sample tube section after distillation of the liquid sample. It should also be noted that the chemical and synthetic methods tend to yield high solubility results. First, any water, from atmosphere or other sources, introduced during the analytical procedure will increase the measured solubility since physical adsorption of water on glass surfaces is far from negligible at ordinary temperatures. McHaffie and Lenher[18] among others, have shown that the adsorbed water film on glass surfaces is multimolecular. Table II summarizes their results; p is the vapor pressure of the water in equilibrium with the surface film of thickness t at the adsorption temperature, and p_0 is the vapor pressure of the water at the same temperature. The thickness t is expressed in number of monolayers calculated assuming that the surface of adsorption is the geometrical surface of glass.

[18] T. R. McHaffie and S. Lenher, J. Chem. Soc. **127**, 1559 (1925).

These measurements were carried out in the temperature interval 25–37°C and it was observed that the thickness of the film is only a function of the water partial pressure. Recent investigations[19,20] have shown that the real surface area of glass varies with chemical, thermal, and other treatments of the glass. Brunauer suggests that the actual surface area of a glass may be from three to ten times greater than the apparent or geometrical area. Therefore, according to Brunauer, the water film thickness reported by McHaffie and Lenher would be 18 to 62 monolayers thick at $p:p_0=1$. It may be assumed that desorption and adsorption of water on glass are reversible except for the first unimolecular layer which is chemisorbed and can only be desorbed at high temperature. The washings of the sample tube with ethanol vapor indicate that there was always a minimum of residual radioactivity of the order of 360 to 400 counts per minute even after transfer as complete as possible of the hydrocarbon sample into the calcium oxide tube. This corresponds to about 4.3×10^{-7} moles of water or 2.59×10^{17} molecules of water. Assuming $11A^2$ as the area occupied by one water molecule, the unimolecular layer would be 285 cm². The estimated geometrical surface area of the sample tube section of the apparatus is about 60 cm² which gives a roughness factor of 4.75, in good agreement with Brunauer's suggestion.

The amount of water adsorbed on the walls of the glass vessel at saturation pressure will be especially important when the solubility is small and the ratio of volume of the sample to surface area of containing vessel is small.

When the synthetic method is used, colloidally dispersed water may be included with the dissolved water. In the method based on the hydrogen liberated by addition of calcium hydride, Rosenbaum and Walton appear to have neglected to consider the amount of gas dissolved in the hydrocarbon sample.

The purity of the benzene employed is another factor which may influence the solubility ob-

[19] P. Emmett, *Advances in Colloid Science* (Interscience Publishers, Inc., New York, 1942) edited by E. O. Kremer, Volume 1, Chapter 1.

[20] Brunauer, *The Adsorption of Gases and Vapors. Physical Adsorption* (Princeton University Press, Princeton, New Jersey, 1943), p. 323.

tained. The benzene which was used in our determination was prepared by the Pure Hydrocarbon Research Program of the Ohio University and had the following physical characteristics:[21]

Density at 20°C,	$d_4^{20}=0.87893$.
Refraction index,	$n_D^{20}=1.5012$.
Dielectric constant,	$E^{20}=2.2933$.

Preliminary results obtained by use of commercial benzene during the development of the technique indicated solubility results somewhat higher than those reported in Table I. The increase of solubility due to the presence of impurities has been noted by other investigators[5,12] and will be more fully discussed in a subsequent paper.

The reproducibility of the results is indicated by the two determinations at 20°C. The logarithm of the solubilities when plotted against the reciprocal of the absolute temperature shows a quite satisfactory linear relationship. The heat of solution thus obtained is 6.1 Kcal. per mole of water.

Limitations of the Method

The results are subject to certain sources of error. The probable error in determining a sample size of the order of about 1 cc may reach several percent. The exchange procedure used in the determination of the radioactivity is never theoretically complete and estimation of the residual radioactivity is necessary if an exceedingly time-consuming operation is to be avoided. The probable error arising in the counting procedure itself may also be of the order of a few percent being the function of the total radioactivity; this error can be minimized by longer periods of counting or the use of water with higher tritium content, or both.

[21] Private communication from Dr. C. P. Smyth.

CONCLUSION

Fractions of one milligram of water containing tritium oxide at a molar concentration of the order of 10^{-12} can be measured with accuracy. This is of particular interest in the determination of solubility of water in hydrocarbons available only in small quantities in the pure state. This method is generally applicable to a wide variety of materials but is obviously limited to solvents in which no exchange takes place between the hydrogen atoms of the water and the solvent under the conditions of saturation and analysis. It may be applied to determinations over an extremely varied solubility range by employing water containing adequate tritium contents. It has the additional advantage of being easily adaptable to high pressure measurements when required, as in the case of the lower hydrocarbons at room temperature.

ACKNOWLEDGMENT

We wish to express our indebtedness to the Texaco Company for a grant-in-aid which made this and other work on the solubility of water in hydrocarbons possible. Our thanks are also due Dr. E. O. Lawrence of the University of California for a gift of tritium water. To Dr. W. F. Libby we are indebted for assistance in the development of the counter and the techniques involved in this research.

THE JOURNAL OF CHEMICAL PHYSICS VOLUME 16, NUMBER 1 JANUARY, 1948

The Influence of Internal Stress on the Structure of Electro-Deposits

M. R. J. WYLLIE
Department of Chemistry, The Johns Hopkins University, Baltimore, Maryland
(Received July 22, 1947)

The author's data on the properties of chromium electro-deposited from a standard chromic acid electrolyte are examined in the light of a theory first proposed by Bozorth. It is shown that the data fit well the assumption that the preferred orientation found in these chromium electro-deposits is the result of a slipping process, analogous to cold-working, which occurs during deposition when internal contractile stress reaches a certain critical value. It is further shown that the type of orientation found in chromium deposits is in accord with the theory and it is stated that (111) orientation is to be expected generally for body-centered cubic metals electro-deposited in a state of contractile stress, while (110) or (100) is to be anticipated for face-centered cubic metals deposited with the same type of stress. The orientations of a number of electro-deposited metals are shown to be in agreement with this expectation. Certain anomalies in the stress and orientation results for silver, nickel, and aluminum deposits have also been studied experimentally, and the results explained on the basis of the above theory. In conclusion, the possible mechanism of internal stress formation in electro-deposits is examined.

I. INTRODUCTION

IT was first shown in 1924 by Glocker and Kaupp,[1] as the result of x-ray diffraction analysis, that metals formed by electro-deposition could under certain conditions possess an orientated structure. The orientations observed were of a type known as fiber textures, the metal crystals of the deposits being aligned with a particular crystallographic axis perpendicular to the surface of the cathode but possessing freedom of rotation through 360° about this axis. Subsequent investigations by other workers have extended the range of electro-deposited metals examined by x-ray diffraction and have shown that the majority of the commonly deposited metals may possess a fiber texture of the type first noted by Glocker and Kaupp. These investigations have also proved that the extent of the preferred orientation and to some extent the nature of the orientation are both dependent upon such variables as composition of electrolyte, temperature and current density at which the electro-deposition took place, and nature of the cathode material. The effect of the cathode metal, however, and its influence on the orientation of deposits can frequently be ignored. While under certain favorable conditions a deposit is able to reproduce the structure and lattice spacing of the basis metal on which it is produced for some distance, this effect is generally very limited, particularly if the deposit itself has a strong orientating tendency. Finch and Sun[2] have shown that where the deposition conditions themselves give rise to orientations the effect of the substrate does not extend to a distance of more than 1000A. Orientation results considered in this discussion are limited to those found at thicknesses much greater than 1000A, results which are dependent solely on the deposition conditions and do not result from any substrate influence. The orientation results for chromium, given below, were found to be entirely independent of the nature of the substrate, whether the substrate was itself orientated or unorientated or whether it was a face-centered or body-centered cubic crystal structure being quite immaterial.

Fiber textures have been generally ascribed to a crystal growth process occurring during electrolysis, and the general conception of the mechanism was admirably summed up by Blum, Beckman, and Meyer[3] when they stated "One might expect that preferred orientation would tend to occur generally in electro-deposits because of the highly anisotropic nature of the process—the direction of current flow and diffusion restrictions."

The existence in electro-deposited metals of residual stresses, often of very considerable magnitude, was first reported in 1877 by Mills[4]

[1] R. Glocker and E. Kaupp, Zeits. f. Physik **24**, 121 (1924).

[2] G. E. Finch and C. H. Sun, Trans. Faraday Soc. **32**, 852 (1936).

[3] W. Blum, A. O. Beckman, and W. R. Meyer, Trans. Electrochem. Soc. **80**, 409 (1941).

[4] E. J. Mills, Proc. Roy. Soc. **26**, 504 (1877).

who showed, by preparing deposits on the bulb of a thermometer and noting the movement of the mercury thread caused by the distortion of the bulb, that deposits of iron, copper, nickel, and silver were formed in a state of contractile stress, i.e., were apparently endeavoring to shrink and thereby causing the mercury thread to rise, while the exact reverse was the case with deposits of cadmium and zinc, an expansive stress being shown and the mercury thread tending to sink. Mills showed that the forces involved were considerable, the contractile effect of copper on the bulb being as great as a uniformly applied hydrostatic pressure of over one hundred atmospheres. Stoney[5] investigated quantitatively the contractile stresses in certain nickel deposits and showed them to be as much as 19.2 tons per square inch parallel to the plane of the cathode. More recently, Hume-Rothery and Wyllie[6,7] reported that the contractile stresses in chromium deposits may reach values of nearly 30 tons per square inch. Much other valuable work on the effect of electro-deposition conditions on stress has been carried out.[8–11]

Relatively little attention has been paid to the possible effects of these internal stresses on the properties of electro-deposits. It was found by Hume-Rothery and Wyllie, however, that in the case of chromium deposits there appeared to be a clear connection between the internal stress and the extent of preferred orientation, and between stress and such physical properties as hardness and ductility. This paper will seek to explain the preferred orientation and properties of chromium electro-deposits in terms of a plastic deformation process caused by internal stress and will endeavor to show that the theory may be extended to other electro-deposited metals. An attempt will also be made to explain the mechanism of the formation of both contractile and expansive stresses in electro-deposits.

[5] G. G. Stoney, Proc. Roy. Soc. **A82**, 172 (1909).
[6] W. Hume-Rothery and M. R. J. Wyllie, Proc. Roy. Soc. **A181**, 331 (1943).
[7] W. Hume-Rothery and M. R. J. Wyllie, Proc. Roy. Soc. **A182**, 415 (1943).
[8] V. Kohlschutter and E. A. Vuilleumier, Zeits. f. Elektrochemie **24**, 300 (1918).
[9] V. Kohlschutter and F. Jakober, Zeits. f. Elektrochemie **33**, 290 (1927).
[10] E. A. Vuilleumier, Trans. Am. Electrochem. Soc. **42**, 99 (1922).
[11] C. Marie and N. Thon, Comptes rendus **193**, 31 (1931).

II. THE DATA FOR ELECTRO-DEPOSITED CHROMIUM

Hume-Rothery and Wyllie[6] showed that the hardness of chromium electro-deposits produced from an electrolyte comprising 250 grams per liter chromic acid and with a CrO_3 to sulphate ion ratio of 100:1 was a property solely dependent on the structures of the deposits as revealed by x-rays and was independent of the exact conditions under which the structure of a given type was produced. Further work has shown that the principle holds good for the two other physical properties of ductility and internal stress. Thus with increasing temperature of deposition a sequence of structures is found at constant current density, each structure being characterized by its own value for hardness, ductility, and internal stress. With increasing current density the temperature at which a given structure occurs increases, and it appears that the relationship between the temperature and current density producing a structure of a particular type is an exponential one. This relationship, in the case of the most highly preferred type of chromium deposit, has already been pointed out.[6]

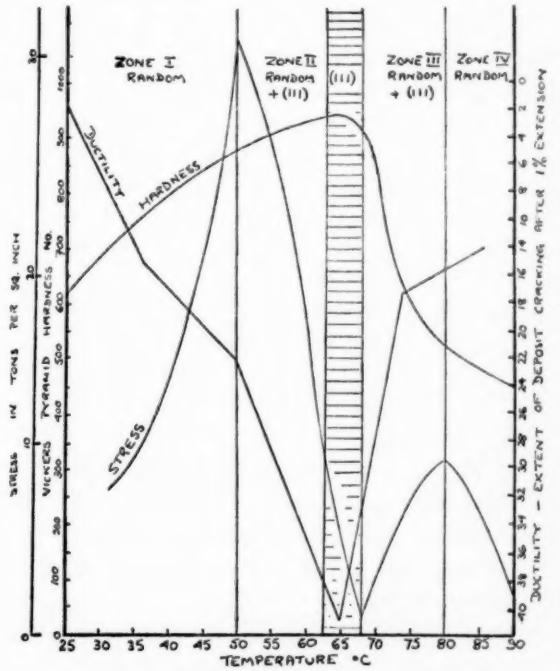

FIG. 1. Properties of chromium electro-deposits; electrolyte 250 g per liter CrO_3: 2.5 g per liter [SO_4'']; current density: 1000 amp. per square foot.

The structure and properties of chromium deposits produced over a wide range of temperature at a constant current density may thus be taken as representative of all deposits obtainable from the particular chromic acid electrolyte used in the experiments. Figure 1, which has been adapted from the papers of Hume-Rothery and Wyllie, and Wyllie,[12] shows on the same diagram curves for the hardness, ductility, and internal stress of electro-deposits produced on a basis metal of carbon steel with increasing temperature of deposition at the constant current density of 1000 amp. per square foot. The diagram has also been divided into four zones to represent the changes in the orientation of deposits 10 microns thick which, as revealed by x-rays, occur with increasing temperature. In Zone I the deposits have a random orientation, but at the border of Zone I and Zone II a trace of orientation of the (111) type is first noticed. With increasing temperature in Zone II two effects are apparent: (a) the number of particles with purely random orientation decreases and (b) the perfection of the alignment of crystals with the (111) orientation increases. In the shaded zone lying between 62½°C and 67½°C there are no crystals with random orientation. In this region the appearance of the crystals is very bright and they all have a very strong (111) orientation, the deviation from a perfect (111) orientation not exceeding ∓7½°.

In Zone III effects precisely opposite from those operating in Zone II are evident. Here increase of temperature brings about a progressive decrease in the exactness of alignment of the (111) orientation and an increase in the number of particles with a purely random orientation. At the border Zone III/Zone IV all orientation effects finally disappear, and the high temperature Zone IV deposits have a random structure.

The changes of structure revealed by x-rays are followed, particularly noticeably, by the curve giving the values for the residual contractile internal stress in deposits of the same 10-microns thickness. In Zone I stress goes up rapidly to a peak of nearly 30 tons per square inch at about the Zone I/Zone II border. In Zone II it decreases to a minimum and almost zero value for the deposits of maximum (111) orientation. In Zone III the stress increases again to a smaller maximum of about one-third the previous value at the Zone III/Zone IV border, and then decreases again rapidly in Zone IV.

Ductility values are also at a minimum in the case of the most orientated deposits, but ductility increases rapidly in the case of deposits prepared on both the high and low temperature sides of the region of maximum orientation. Hardness, too, has a maximum value coincident with the region of maximum orientation and falls off in value at both higher and lower temperatures—the more rapidly, however, to the high temperature side.

These data appear to indicate that there is some definite correlation between the physical properties of chromium electro-deposits and their preferred orientation and particularly between the internal stress and orientation. The correlation appeared to the writer to exceed any effects which might be attributable merely to an inherent tendency for the deposit to grow preferentially under certain deposition conditions in a (111) direction, and an attempt is therefore made to explain the correlation on the basis of internal stress.

III. THE RELATIONSHIP BETWEEN STRESS AND TYPE OF ORIENTATION IN ELECTRO-DEPOSITS

A theory attributing the formation of preferred orientation in electro-deposits to internal stress was first put forward by Bozorth.[13] A similar idea had earlier been incorporated in a paper by Greaves,[14] but Greaves had claimed that preferred orientations would be expected only in deposits produced at low current densities while the fine-grained hard deposits resulting from high current density deposition would be entirely random in structure. Greaves attributed internal stress to the effect of the electric field operating during deposition and claimed that only at low current densities, when the atoms had had time to arrange themselves, would orientation effects ensue. The data for chromium are entirely out

[12] M. R. J. Wyllie, Trans Electrochem. Soc. Preprint 92–5 (1947).

[13] R. M. Bozorth, Phys. Rev. 26, 390 (1925).

[14] R. H. Greaves, Metallurgist 1, 141 (1925).

of accord with the views of Greaves, since in the case of chromium it is the hardest deposits of minimum grain size which exhibit the maximum preferred orientation. Bozorth considered that since deformation produced in metals by cold-working gave rise to special orientations, it was natural to suppose that the tension known to be present in many electro-deposited metals produced orientations in them in a manner similar to that in which orientations were produced in hard-drawn wires or rolled sheets. Bozorth considered that the stress was produced by co-deposited hydrogen which diffused out of the metal as the deposit thickened, thus leaving the metal in a state of tension. He supposed that as the process of deposition went on the stress difference between the innermost and outermost layers of the deposit increased and that ultimately the compressive stress in the layers next to the cathode became so great that the crystals were crushed, thus forming new crystals of very small dimensions. In the outer layers, however, where the crystals were formed under greatest tension, the orientations would be most marked. Bozorth's idea thus also accounts for the experimental observation that preferred orientation tends to increase with increasing deposit thickness. Experimentally, Bozorth examined some deposits of iron, nickel, copper, zinc, and cadmium and found marked orientation effects only in iron and nickel. These two metals were found to be much harder than the deposits of random orientation, and this fact Bozorth interpreted as lending support to his view that the orientations observed in the iron and nickel were produced by some sort of cold-working mechanism.

The theory of Bozorth, although clear in its general implications, i.e., that stress in electro-deposits is produced by co-deposited hydrogen and that this stress is responsible for the production of preferred orientation in the deposits by a mechanism analogous to the cold-working of metals, was put forward in a somewhat qualitative manner and was based on rather scanty experimental data. The more comprehensive results available for chromium deposition enable the writer to carry Bozorth's theory a step further.

The deposition of chromium is an extremely inefficient process, and in no case were efficiencies greater than 35 percent noted, the most orientated deposits being characterized by an efficiency of about 9 percent.[6] The bulk of the current is thus consumed in the liberation of hydrogen, and for every atom of chromium laid down at the cathode numerous atoms of hydrogen are simultaneously liberated. It may be assumed that some of these hydrogen atoms are initially entangled in the growing crystal lattice of chromium, causing the lattice to be abnormally expanded. As deposition proceeds the major portion of the hydrogen in the lattice diffuses out, thus leaving the lattice in an expanded and unstable condition. The chromium atoms, therefore, attempt to contract together to their normal interatomic positions. This contraction, however, is opposed by the adhesion of the deposited atoms to the layers below, and a state of strain is thereby set up. It is not suggested that all the hydrogen initially contained in the lattice is lost since a residual expansion of the lattice of electro-deposited chromium has been reported[15] and Hume-Rothery and Wyllie, although unable to determine the lattice parameter of chromium in the "as-deposited" condition because of the extreme diffuseness of the lines on a Debye-Scherrer film, nevertheless found a parameter of 2.8861A at 23°C, as against the normal value of 2.8786A, in the case of a highly orientated deposit annealed in vacuum for 4 hours at 750°C. The suggestion is put forward, however, that immediately after deposition, when the bulk of the hydrogen escapes, the lattice is considerably strained and that this strain is relieved, when it reaches a certain critical value, by an actual slipping or yielding of the metal crystals which are thus left in a condition somewhat analogous to that of a cold-worked metal. On this assumption it may be understood why the temperature and current densities leading to deposits with the most highly preferred orientations are those which lead also to the lowest residual stress, and why such deposits are hard and brittle, since it is known that cold-work increases the hardness and decreases the ductility of a metal. It has been shown that the stresses involved in chromium deposition are very high, and at the moment of

[15] W. A. Wood, Phil. Mag. **23**, 984 (1937).

deposition these may well be sufficient to produce plastic deformation. While the stresses involved are thus of sufficient magnitude to justify the concept of plastic distortion occurring, the amount of actual strain involved in the process is more difficult to assess. The distortion necessary to account for stresses of the magnitude actually observed experimentally in deposits would result from an enforced straining of the deposit amounting to perhaps 0.7 percent in directions parallel to the plane of the cathode. This order of magnitude of straining would not normally account for very appreciable internal slip in the crystals of the deposits, and certainly would not be expected to yield the slip into preferred orientations which is postulated below. Reduction in volume of the order of 60 percent is necessary if a block of massive metal is to be so distorted by slip as to show evidence of a preferred orientation. While it is realized that this fact constitutes a potent argument against the slip theory of Bozorth and the writer, it may be argued that the exact mechanism of slip is still obscure and that in the case of a massive block of polycrystalline metal considerable reduction in volume may be essential before the influence of the strain on small crystals becomes sufficiently appreciable and directed so as to produce orientation effects. It is possible that the separating action of co-deposited hydrogen produces during deposition a very much greater strain throughout very small crystals than can ever be detected in a deposit completed and removed from the electrolyte. If this be so, it is suggested that during the contraction of these expanded crystals to approximately normal interatomic distances after loss of hydrogen slip occurs over shorter ranges and very much more freely than in a massive metal, this slip resulting both in a harder and more orientated state of the material than can be achieved by any ordinary cold-working process. On this theory slip-bands would not normally be visible in an electro-deposited metal, and the so-called slip bands observed by Hughes[16] and Tamman[17] in iron and copper deposits, as well as the rhythmic banding observed in nickel,[18] would be susceptible to explanations other than as confirmation of the internal slip theory suggested.

On the theory outlined above, the data shown in Fig. 1 are readily explicable. Across Zone I the residual stress resulting from the lattice strain caused during deposition is increasing, and the general distortion of the crystal lattice causes both an increase in deposit hardness and a diminution in ductility, but not until the Zone I/Zone II boundary is reached does the lattice strain during deposition attain the critical value for sufficient slip to occur to manifest itself in preferred orientation. In Zone II it may be presumed that the strain set up during deposition steadily increases to reach a maximum value in the shaded region. In this zone, therefore, orientation increases and the residual stress, indicative of strain unrelieved by slip, decreases. Hardness correspondingly increases and ductility further decreases. In Zone III it would appear that the strain resulting immediately after deposition begins to decrease, possibly because of the effects of increased thermal vibration enabling the co-deposited hydrogen to escape more readily. As the strain decreases in magnitude less slip, and therefore preferred orientation, results and more unrelieved strain is left in the lattice to show itself as residual stress. In Zone IV the strain never reaches a value sufficient to cause any orientation and appears to fall off rapidly with increasing temperature. In Zones III and IV hardness also decreases and ductility increases as would be anticipated on the basis of the strain effects postulated.

It remains to be seen what effect the slipping process suggested would have on the crystal orientation, and here an apparent correlation has been found between the textures of electro-deposited metals and of the same metals in the drawn state.

It is well known that when a metal is drawn the resulting texture is such that one or more crystallographic directions lie in the direction of drawing. It has been found that if for a particular metal the drawn texture is such that one or more crystallographic directions lie in the direction of drawing, then the texture of the electro-

[16] W. E. Hughes, J. Iron and Steel Inst. **103**(1), 356 (1921).

[17] G. Tamman, *Lehrbuch der Metallkunde* (Leopold Voss, Leipzig, 1932).

[18] See, for example, W. A. Wesley and E. J. Roehl, Trans. Am. Electrochem. Soc. **82**, 37 (1942).

deposit, if the latter involves formation with contractile stress, is such that the maximum number of the same directions lie in the plane of the deposit. If, however, the electro-deposit involves expansive stress, the texture is related to the compression texture of the metal.

In the case of body-centered cubic metals it is known that the drawing texture is such that a [110] direction lines in the drawing direction, and the above principles therefore require the maximum number of [110] directions to lie in the plane of the deposit. This condition is satisfied by a (111) orientation since the (111) planes contain three [110] directions and this is the maximum possible. The preferred orientations of body-centered cubic chromium and of iron agree with this principle. That the orientation in iron is (111) has been shown,[13,19] and that the stress is contractile has also been demonstrated.[4,9]

With face-centered cubic metals, drawing produces one of two different textures, or both, with the [100] or [111] directions parallel to the direction of drawing.* The above principle leads to the expectation that electro-deposited face-centered cubic metals will possess preferred orientations with the greatest number of [100] and [111] directions in the plane of the cathode if the deposits are formed with contractile stress. Taking the different planes in order it is found:

Plane parallel to cathode surface	No. of [100] directions in cathode surface	No. of [111] directions in cathode surface
(100)	2	0
(110)	1	2
(111)	0	0
(210)	1	0
(211)	0	1

The planes of the higher indices are all less favorable as regards the number of [100] and [111] directions they contain.

It should be expected that the preferred orientations of electro-deposited face-centered cubic metals will be (100) or (110) if the deposits involve contractile stress. In agreement with this principle electro-deposits of cobalt formed under conditions likely to give rise to contractile stress[9] have been found with a (110) orientation.[19] Similarly deposits of copper have a (110) or (100) orientation[1,20] when formed under conditions giving rise to contractile stresses.[4,10] Deposits of nickel exhibit very strong contractile stress,[4,5] and the orientations generally reported are (110) or (100), although (211) has been noted.[13] It has been stated[21] that a (100) orientation is always obtained if the electrolyte is stirred by rotating the cathode. The orientation of gold electro-deposits has been shown to be (110),[19] but no reference to the nature of the internal stress appears to exist. The data for silver are more complicated. Glocker and Kaupp stated[1] that both [100] and [111] orientations were observed. On the theory above a [111] orientation would not be expected from a silver deposit possessing contractile stress. However, it has been demonstrated[9] that, depending on the current density of deposition, silver deposits formed from the same solution may have either contractile or expansive stress. Since the compression texture of silver is such that the [110] direction is the direction of compression, a silver deposit formed under conditions of expansive stress might be expected to possess a (111) orientation since the (111) plane, as previously observed, contains three [110] directions.

Experiments, described below, were therefore undertaken to investigate the connection between the direction of stress and orientation in silver deposits. Some experiments involving the deposition of nickel from a nickel chloride solution under various conditions, as well as aluminum from an organic electrolyte, are also noted.

IV. STRESS AND ORIENTATION IN SOME SILVER, NICKEL, AND ALUMINUM DEPOSITS

Silver

Kohlschutter and Jakober[9] showed that silver deposits produced on a platinum cathode from a

[19] G. I. Finch, A. G. Quarrell, and H. Wilman, Trans. Faraday Soc. **31**, 1051 (1935).

* With aluminum the texture is almost entirely [111] whilst copper gives a mixed texture 40 percent [100] and 60 percent [111] and silver a mixed texture 75 percent [100] and only 25 percent [111]. Nickel resembles copper.

[20] H. Hirata and Y. Tanaka, Mem. Coll. Sci. Kyoto Imp. Univ. **A15**, 9 (1932).

[21] W. G. Burgers and H. E. Quanjel, Rec. trav. chim. **61**, 353 (1942).

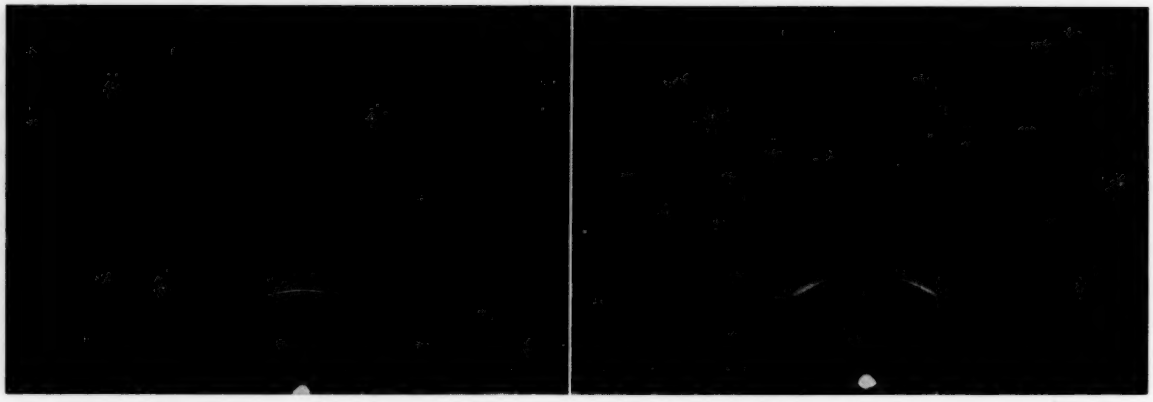

(a) (b)

FIG. 2. (a) Silver deposit showing (111) orientation; expansive stress; current density 5 M.A./cm²; temperature 18°C electrolyte: 0.2 *M* AgCN, 0.4 *M* KCN. (b) Silver deposit showing (110) orientation; contractile stress; current density 5 M.A./cm²; temperature 18°C; electrolyte: 0.2 *M* AgCN, 0.2 *M* KNO_3, 0.4 *M* KCN.

solution comprising 0.2 *M* AgCN and 0.4 *M* KCN possessed strong expansive stress at a current density of 5 milliamp. per square centimeter and considerable contractile stress at a current density of 15 milliamp. per square centimeter. It was decided to reproduce their results and to examine the deposits by the glancing beam x-ray method.[22] One liter of electrolyte was made up 0.2 *M* AgCN and 0.4 *M* KCN from British Drug Houses "Analar" silver cyanide and potassium cyanide. The container used was a liter glass beaker. The anode, which closely fitted the whole interior wall of the beaker, was silver foil of 99.99 percent purity. The cathode was silver foil of the same quality as the anode and was 0.05 mm thick and 5 cm wide. This foil had been delivered by its manufacturers in the form of a tight roll and was naturally smooth and springy. When a length of 11 cm was cut from the roll, it curled into a circular segment of about 3 cm diameter, there being a gap of just over 1 cm between the edges of the split cylinder thus formed. Advantage was taken of this phenomenon to measure conveniently the type of stress in deposits. A copper lead was soldered to the inside of the cylinder at a point diametrically opposite the split, and the entire inside of the silver foil as well as the copper wire was stopped off with cellulose varnish. The cylinder was then suspended in the electrolyte by means of the wire so that it was roughly concentric with the silver anode around the wall of the beaker. With this arrangement, since deposition can take place only on the outside of the split cylinder, it is clear that any expansive or contractile stresses in silver deposits formed will manifest themselves in a closing or opening of the gap in the cylinder.

At a current density of 5 milliamp. per square centimeter and at 18°C a definite closing of the gap was noted. The effect was not very large, amounting to about 1-cm movement for a deposit thickness of 10 microns. At 10 milliamp. per square centimeter no stress was perceptible, and this was also the case of 15 milliamp. per square centimeter. The latter deposit was a dirty yellow in color, nodular, and rather nonadherent. No evidence of the contractile stress claimed by Kohlschutter and Jakober for a deposit formed at this current density could be detected. X-ray evidence revealed that the deposit produced at 5 milliamp. per square centimeter had a marked (111) orientation (Fig. 2a) but those formed at 10 and 15 milliamp. per square centimeter were random in orientation.

Further investigation showed that contractile stress in silver deposits on a silver cathode could be formed from a solution containing 0.2 *M* AgCN, 0.2 *M* KNO_3, and 0.4 *M* KCN. This solution was made from the previous one by addition of "Analar" brand potassium nitrate. Using the same arrangement of anode and cathode as described previously the following results were obtained at a current density of 5

[22] M. R. J. Wyllie, Rev. Sci. Insts. **18**, 425 (1947).

milliamp. per square centimeter and an electrolyte temperature of 18°C:

Time (minutes)	Distance between the sides of the gap in the split cylinder (millimeters)	Expansion (millimeters)
0	16.21	——
6	18.54	2.32
12	23.70	5.16
18	29.38	5.68
31	38.27	8.89
	Total expansion	22.06

X-ray investigation of this deposit (Fig. 2b) showed that it possessed a marked (110) orientation. These data for silver thus tend to substantiate the theory outlined above, insomuch as deposits with contractile stress show a (110) orientation and those with expansive stress a (111) orientation.

Further experiments in silver deposition were conducted to ascertain whether or not the lattice parameter and crystal form of deposits were the same during deposition, i.e., while the current was flowing, as they were after deposition was complete. A possible cause of internal stress may be the deposition of one allotropic form of a metal, this form reverting to a more stable modification of different volume either during deposition or after removal of the specimen from the electrolyte. Such changes would normally escape detection as deposits are examined some considerable time after deposition has ceased. The allotropic modification theory for stress will be further discussed below.

The apparatus used is shown diagramatically in Fig. 3. The electrolyte was 0.2 *M* AgCN and 0.4 *M* KCN contained in a rectangular glass vessel 10 cm×6 cm×8 cm. The anode was of 99.99 percent silver sheet 10 cm×8 cm in area arranged against the side of the vessel as shown in the figure. The cathode was a 99.99 percent silver disk 0.2 cm thick and 6 cm in diameter and was screwed to the shaft of an electric motor. The disk was rotated at 1 r.p.m. The bottom of the disk was 2 cm below the surface of the electrolyte. With this arrangement, deposition of silver at 18°C was carried on at a constant current density of 5 milliamp. per square centimeter on the area of the cathode immersed. The portion of disk plated, of course, changed all the time as the disk revolved, but since the portion of the disk not in the electrolyte remained covered with a film of electrolyte as it revolved, it is possible that some slight deposition always occurred on this portion as well as on the immersed portion. It was, in fact, hoped that this was the case. Normal back reflection photographs, using a revolving circular cassette holder with 120° masks and unscreened cobalt radiation, were taken of (a) the pure silver cathode, (b) the deposit while depositing, and (c) the deposit after deposition ceased. The disk was not touched during this sequence of photographs nor was the electrolyte removed. The beam was arranged to impinge 0.5 cm from the edge of the disk and 1 cm above the electrolyte surface, and the direction of disk rotation was such that the portion of deposit diffracting was that which had just emerged from the electrolyte. Disk to film distance was approximately 3 cm.

Figure 4 shows the result obtained. It is evident that under these conditions there is no difference between the lines given by the deposit during deposition or after deposition has ceased. The lines from the deposit are, however, more diffuse than those from the basis metal, and

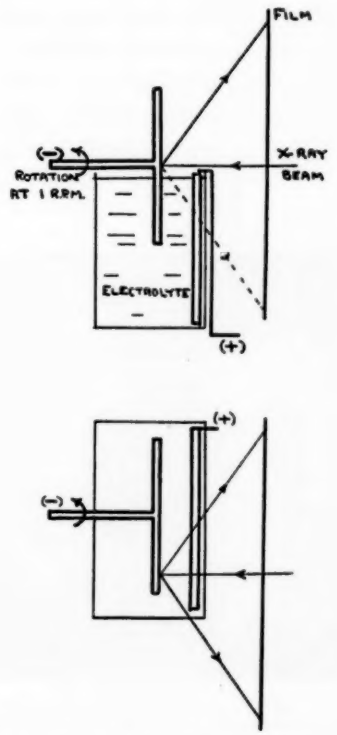

FIG. 3. Schematic drawing of apparatus for taking back reflection x-ray photographs of silver electro-deposits immediately after deposition.

there is possibly a very slight general increase in the lattice parameter of the deposited silver. The effect is not large. It is suggested that the method outlined above deserves wider application to the study of electro-deposition processes generally.

Nickel

The solution chosen was one which has been stated[18] to show particularly large values of contractile stress. It comprised 205 g per liter of $NiCl_2 \cdot 6H_2O$, 8 g per liter of KCl and 17 g per liter of NH_4Cl. The salts used were "Baker's Analysed" reagents, the cobalt content being 0.10 percent, the copper 0.003 percent, and the iron 0.003 percent. Measurement of stress was carried out by depositing nickel on one side of a flexible high carbon steel strip and measuring the direction and magnitude of the curvature of the strip after the deposition was complete. The steel used was of Swedish manufacture and remarkably uniform in its properties. It was 0.25 in. wide and 0.002 in. thick. Bending was measured by determining the distance between the free end of a 14 cm long strip (12 cm being immersed in the electrolyte) relative to a fixed glass pointer when the other end of the strip was clamped in a brass holder. Before deposition the strip was cleaned by cathodic etching in a solution of sodium carbonate followed by an anodic etch of 30-seconds duration at a current density of 200 amp. per square foot in a 30 percent sulfuric acid solution. The reverse side of the strip was insulated with cellulose varnish. Deposits were prepared in all cases at a thickness of 10 microns, this figure being checked by weighing. A pH of 5.0, measured with a commercial glass electrode, was standardized.

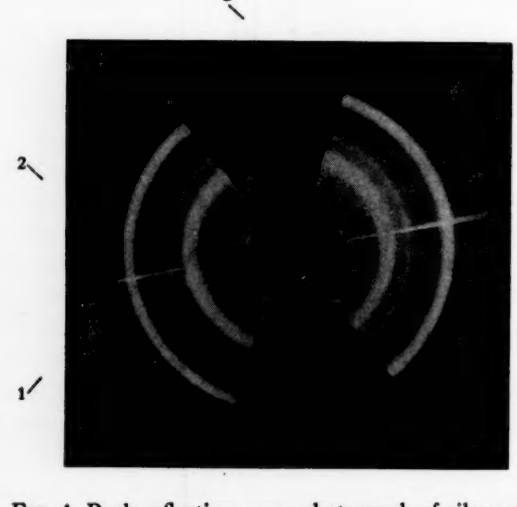

FIG. 4. Back reflection x-ray photograph of silver while depositing; current density 5 M.A./cm² temp. 18°C; electrolyte: 0.2 *M* AgCN, 0.4 *M* KCN; segment 1: deposition proceeding, current on; segment 2: deposition concluded, current off; segment 3: pure silver basis metal.

The electrolyte was contained in a glass vessel 10 cm×5 cm×15 cm, the temperature being controlled to 0.1°C by a constant temperature bath. The nickel anodes used were 14 cm×5 cm in area and were of high purity, the material being donated by the International Nickel Company.

Initial experiments were carried out at a current density of 5 amp. per square decimeter and were made to ascertain the effect of temperature on stress. Figure 5 shows the results obtained. It is obvious that, while the stress tends to fall off steadily with increasing temperature of deposition about 25°C, there is a very rapid and immediate decrease below 25°C. Figures of stress are given in millimeters of deflection of the tip of the strip, but it may be pointed out that a deflection of 1 mm represents a contractile stress of about 6 tons per square inch parallel to the plane of the cathode. X-ray investigations showed that in all cases the orientation of these nickel deposits was random.

In terms of the theory outlined above the sudden change of stress below 25°C would be attributable to an internal relief of strain by slip into a preferred orientation. No orientation was found. However, under the microscope the deposits below 25°C all showed numerous cracks, and it was evident that stress was being relieved in these deposits by rupturing of the metal film and not by any possible internal mechanism. The cracking of deposits, with consequent relief of stress, has been pointed out[23] to be a source of error in the measurement of stress in nickel deposits. It was a complication not noticed in the case of chromium.

The hardness of nickel deposits has been attributed largely to co-deposited basic nickel

[23] D. J. MacNaughtan and A. W. Hothersall, Trans. Faraday Soc. 31, 1168 (1935).

salts,[24,25] and considerable evidence to justify this belief has been presented. At an operating *p*H of 5.0 the *p*H of the cathode film is undoubtedly much higher, as has been experimentally observed,[26] and co-deposition of nickel hydroxide, formed as a sol adjacent to the cathode surface, is almost inevitable. It was considered that the effect of co-deposited basic material highly dispersed in the deposit might be to weaken, to some extent, intergranular cohesion and therefore to promote cracking as well as to inhibit plastic deformation. It is known that the effect of a finely divided second phase in a matrix is to make plastic deformation, and therefore the occurrence of orientation, more difficult.

The only logical method of cutting down the deposition of basic material appeared to be by decreasing the thickness of the cathode film, and this was achieved by affixing anode and cathode, facing each other, at the end of an arm 5 cm in length and rotating this arm about its center in the electrolyte at 25 r.p.m. Under these conditions at 5 amp. per square decimeter, crack-free deposits of low stress values could be fairly reproducibly obtained below 25°C, and these uncracked, fine-grained deposits showed evidence of a (110) orientation. Deposits obtained by the rotating anode and cathode method at temperatures above 25°C did not differ appreciably either in appearance, internal stress, or orientation from those prepared under the same conditions of current density and electrolyte in the absence of rotation.

A point of interest noted when determining stress was the fact that in many cases when the deposit was being soaked in an alcohol/acetone mixture to remove stop-off varnish prior to the bending of the strip being measured, a visible evolution of gas from the deposit occurred, while at the same time further bending of the strip, i.e., contraction of the deposit, took place. It was often necessary to wait several hours before the strip bending reached a final equilibrium value.

The results for nickel deposited from a nickel chloride electrolyte under these conditions indicate that very high values of contractile stress can occur and that a peak stress is reached at about 25°C whether the electrolyte is stationary or flowing past the cathode. Stress relief below 25°C is generally caused by cracking of the deposit, but if rotation is used the stress is still low and an orientation is observed. This result tends to confirm the statement[21] that nickel deposits from a nickel acetate electrolyte cannot be produced with a definite (100) orientation on a circular cathode of 6-mm diameter unless the cathode is rotated at 100 r.p.m. or more. It was found impossible to obtain satisfactory x-ray photographs of nickel deposits while deposition was being carried on.

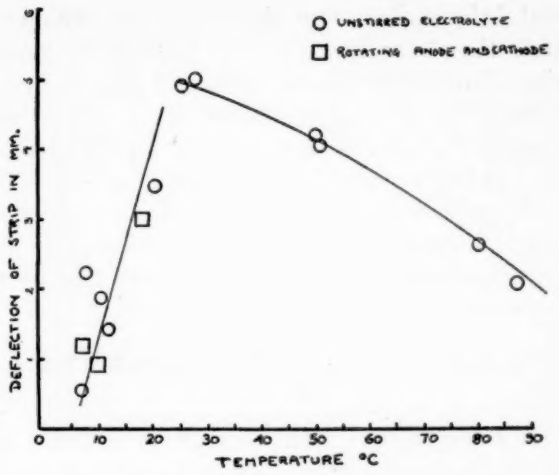

FIG. 5. Stress in nickel deposits from nickel chloride electrolyte; current density 5 amp. per square decimeter *p*H 5.0.

Aluminum

Aluminum was deposited on steel strips cleaned in precisely the same way as that used previously for nickel deposition. The non-aqueous electrolyte, essentially aluminum bromide and ethylene bromide, was made up in the manner suggested by Blue and Mathers.[27] Pure aluminum was used as anode and the electrolyte, anode, and steel cathode were enclosed in an airtight cell 4 cm in diameter and 16 cm high. Using a current density of 1 amp. per square decimeter at room temperature, good adherent

[24] D. J. MacNaughtan and R. A. F. Hammond, Trans. Faraday Soc. **27**, 633 (1931).
[25] D. J. MacNaughtan, G. E. Gardam, and R. A. F. Hammond, Trans. Faraday Soc. **29**, 729 (1933).
[26] A. Brenner, Proc. Am. Electroplaters Soc. 28 (1941).
[27] R. D. Blue and F. C. Mathers, Trans. Am. Electrochem. Soc. **65**, 339 (1934).

and bright aluminum deposits were obtained after the electrolyte had been worked for some time. No perceptible stress, either expansive or contractile, was recorded, and x-ray diffraction showed that the deposits were of a grain size of 10^{-2} to 10^{-3} cm and were random in orientation. This appears to be the first occasion on which a determination of the stress and orientation of deposits from non-aqueous solvents has been attempted.

V. THE ORIGIN OF STRESS IN ELECTRO-DEPOSITS

A theory which attributes the orientation of many electro-deposits to stress has already been given, and a mechanism for the possible formation of the contractile stress in chromium electro-deposits has been outlined. The deposition of chromium from an aqueous chromic acid electrolyte is, however, unique among the commonly deposited metals insomuch as the deposition efficiency is extraordinarily low and in all cases liberation of chromium is accompanied by the evolution of very considerable quantities of hydrogen. It remains to be considered whether the co-deposited hydrogen theory is capable of explaining contractile stresses generally, and whether any analogous theory can account for the formation of expansive stresses in certain electro-deposited metals.

Although a number of papers have been published on the experimental determination of stress in deposits, stress data are still scanty. Certain generalizations on the basis of existing results may, however, be made.

(1) Only contractile stresses are exhibited by metals of the transitional groups unless very considerable quantities of organic addition agents are added. E.g., the addition of sufficient sodium napthalene trisulfonate to a nickel bath may eventually produce a slight expansive stress.

(2) Metals such as copper and silver, which are closely related to transitional metals, may exhibit either contractile or expansive stresses depending on the deposition conditions.

(3) Non-transitional metals such as lead, zinc, and cadmium, if stressed at all, show only expansive stresses.

It would also appear that contractile stresses tend to be of considerably greater magnitude than expansive stresses.

The fact that hydrogen is associated with the formation of contractile stresses appears to derive support from a number of considerations. It is well known that transitional metals, and under certain conditions semitransitional metals such as copper and silver, tend most readily to form stable or metastable alloys with hydrogen. Expansion of the lattices of such metals during deposition and their subsequent contraction is therefore quite feasible. Residual expansions in electro-deposited chromium have been found in this work, and the same is certainly true for palladium.[28,29] Depolarizers and alternating current superimposed on the direct plating current both serve markedly to reduce contractile stress,[9] and their action is almost certainly the oxidation of hydrogen shortly after it is liberated cathodically and before it can exert any considerable effect on the growing metal lattice. The work of Marie and Thon[11] shows that copper deposited from a neutral solution of copper sulphate exhibits expansive stress on bright platinum, silver, and gold substrates but a contraction on a dull platinum base. When the addition of 1 percent sulphuric acid is made contractions occur on both dull and bright platinum, and in the presence of 2 percent H_2SO_4 contractions are observed on all the substrates. These data point both to an over-voltage effect and the relative ease of liberation of hydrogen and metal. Contractile effects increase with time after removal of the deposit from the electrolyte and are accompanied by the liberation of a gas which is almost certainly hydrogen. The annealing of highly stressed deposits at low temperatures frequently increases contractile stress,[23] and gas is evolved. There is, nevertheless, no direct connection between magnitude of stress and amount of co-deposited hydrogen. Thus in Fig. 1 the efficiency of deposition at 1000 amp. per square foot is about 30 percent at 30°C falling to only 5 percent at 85°C, while the values for stress vary as shown. A similar lack of obvious relationship exists in the case of nickel.[30] It has recently been shown[31] that the stress in nickel deposits increases with increase in the *p*H, and on these data it was claimed that co-deposited

[28] L. McKeehan, Phys. Rev. (2) **21**, 334 (1923).
[29] G. Chaudron, J. Bérnard, and A. Michel, Comptes rendus **218**, 913 (1944).
[30] D. J. MacNaughtan and A. W. Hothersall, Trans. Faraday Soc. **24**, 387 (1928).
[31] B. Martin, Proc. Am. Electroplaters Soc. 207 (1944).

basic material is the cause of stress. Nevertheless, it would appear that some hydrogen is always evolved if contractile stress is to result, and nickel deposits prepared at a *p*H of as much as 5.7 have been found by direct analysis to contain hydrogen.[32] A tentative conclusion appears to be that hydrogen must be evolved before contractile stress manifests itself, but that there is an optimum amount of hydrogen necessary to produce maximum stress, the amount varying with temperature, the rate of deposition, and other factors not readily capable of quantitative evaluation.

The formation of expansive stresses in silver, copper, zinc, cadmium, and lead deposits under appropriate conditions is more difficult to explain. It may be that both contractile and expansive stresses result from the deposition of one allotropic modification of a metal, this modification reverting to a more stable form, with a consequent volume change, while deposition proceeds. No direct experimental evidence has yet been found to justify this theory, but it is perhaps noteworthy that metals such as nickel, chromium, iron, and cobalt, which all show heavy contractile stresses, can all exist in another crystalline form. The beta-modification of chromium, for example, can be formed from a chromic acid electrolyte if more than 18 percent trivalent chromium exists in the solution,[33] and this modification reverts readily to the normal alpha-form. It is possible that the concentration of trivalent chromium may reach 18 percent in the cathode film by reduction of the hexavalent ion by liberated hydrogen. The beta-form is, however, more close packed than the alpha-modification, and a transformation should cause an expansive rather than a contractile stress. However, the same is true for nickel where the normal beta-nickel is a face-centered cube and the alpha-form a close-packed hexagonal structure. Nevertheless the density of the close-packed nickel when formed by sputtering in hydrogen was estimated as 7.04 against the normal value of 8.9.[34] Here a change from alpha- to beta-form would cause a contraction of a metal film.

The data of Marie and Thon, given above for copper deposition, show that the stress in the deposits changes from expansive to contractile as the over-voltage of the cathode is lowered or the acidity of the electrolyte is increased. The change from expansive to contractile stress found in silver deposits on platinum[9] formed from the same solution of potassium argento-cyanide takes place with increase of current density. It would appear that in these cases there are two processes at work, one endeavoring to give expansive stress and one contractile. Under conditions giving rise to the liberation of a large quantity of hydrogen the second effect prevails over the first, and contractile stresses result.

It is now suggested that in almost all deposited metals there is a tendency to form expansive stress, but in the case of transitional metals this tendency is always overcome, and in the case of borderline transitional metals it may be overcome by the formation of contractile stress resulting from interference by hydrogen in the growing lattice. Only in the case of non-transitional metals such as lead, zinc, and cadmium is the expansive tendency always greater than the contractile. The proposed mechanism for the formation of the expansive stress is based on the observation that in every stressed deposit investigated the $\Delta F°$ value for the reduction to metal of the metal ion in solution by monatomic hydrogen is favorable to the reaction taking place. Thus the $\Delta F°$ values are -61524 calories for zinc, -90820 for lead, and -112610 for copper for reduction from their divalent ions, and -42120 calories for the reduction of silver from the $Ag(CN)_2^-$ complex.[35] Iron, nickel, cobalt, and palladium theoretically may also be reduced. These $\Delta F°$ values, of course, only indicate that the reduction is possible, since the precise concentration of ions and hydrogen in the cathode film cannot be calculated. Assuming, however, that reduction of the metal ion by monatomic hydrogen takes place, metal atoms will be produced at the cathode by two separate and distinct electron-transfer mechanisms. It is suggested that the metal formed by the hydrogen

[32] A. Brenner, J. Research Nat. Bur. Stand. **18**, 565 (1937).
[33] L. Wright, H. Hirst, and J. Riley, Trans. Faraday Soc. **31**, 1253 (1935).
[34] G. Bredig and R. Allolio, Zeits. f. physik. Chemie **126**, 41 (1927).
[35] Values calculated from W. M. Latimer, *Oxidation Potentials* (Prentice-Hall, Inc., New York, 1938).

reduction has little tendency to continue the lattice structure of the nuclei resulting from the deposition of metal by electron gain from the cathode, and that it tends to grow between these nuclei. What may be envisaged crudely as a shouldering apart of the growing deposit occurs, and expansive stress ensues. Under conditions where more monatomic hydrogen than can reduce the metallic ions is being formed, contractile stresses will occur if the metal being deposited is capable of absorbing hydrogen. Thus with silver at 5 milliamp. per square centimeter the stress is expansive; at 15 milliamp. per square centimeter it is contractile. With copper contractile stress occurs only when hydrogen is more readily evolved. The inability of non-transitional metals to form systems with hydrogen causes the stress in electro-deposits of these metals always to be expansive.

VI. LIMITATIONS OF THE STRESS-ORIENTATION THEORY

The theory proposed satisfactorily fits the data for chromium. Experimental findings are limited in the case of other metals, and insufficient data exist to permit a detailed correlation of stress, orientation, and physical properties. For nickel deposits, however, this lack of data is not entirely true. Many papers on nickel deposits have been published, but because of the wide number of electrolyte compositions used and the complicating variable of *p*H in addition to current density and temperature, it is not easy to generalize the results. It would appear, however, that the internal cold-working mechanism suggested to account largely for the hardness of chromium (supplemented by extremely small grain size and possibly by the effects of a residual interstitial solid solution of hydrogen), can account only for part of the hardness of many deposits of nickel. It is possible that the major portion of the hardness of these deposits results from very finely dispersed basic material contained in the lattice. The hardness of all very hard electro-deposits is greater than that which could be engendered by cold-working the same massive metal or by the known effects of precipitation hardening, alloy formation, or diminution in particle size. It is possible that internal cold-working taking place within small grains immediately after their deposition might produce greater effects than those resulting from ordinary cold-working processes, but on the whole it is felt that the anomalous hardness figures for electro-deposits result from a combination of all the hardening factors outlined above. The degree to which each contributes may vary from metal to metal, i.e., primarily cold-work in chromium and precipitation hardening by co-deposited basic material in nickel deposits.

It is not suggested that growth mechanisms can never be responsible for orientations in electro-deposits since some experiments[36,37] clearly show that, particularly at low current densities, preferential growth of distinct crystal planes may take place. It is, however, suggested that orientations in hard, fine-grained electro-deposits are the result of an internal cold-working mechanism occurring during deposition.

ACKNOWLEDGMENT

The writer's thanks are due the President and Academic Council of the Johns Hopkins University for the grant of a Courtesy Fellowship, and to Professor Walter A. Patrick for his interest and assistance in this work.

---

[36] T. Erdey-Gruz, Zeits. f. physik. Chemie **A172**, 157 (1935).

[37] T. Erdey-Gruz and E. Frankl, Zeits. f. physik. Chemie **A178**, 266 (1937).

On the Thermodynamic Substitution Group and Its Representation by the Rotations of a Square

J. A. PRINS
Laboratorium voor technische physica, Techniche Hogeschool, Delft, Holland
(Received September 2, 1947)

TO the general reader the *rule* concluding this article will be of more interest than its derivation. It is slightly different from Koenigs original statement[1] and is perhaps more easily grasped. The major part of this article is, however, concerned with the group-theoretical and physical *foundation* of this rule.[2]

By way of introduction, consider Maxwell's equations for the electromagnetic field. This set of well-known equations is invariant for:

a. simultaneous changes in sign of E, H, D, and B,
b. simultaneous interchanges (E, H), (D, B), and (ϵ, μ),
c. other transformations, not to be considered here.

The physical interpretation of *a* is the rather trivial fact that the positive sense of all vectors may be reversed; of more importance is the meaning of *b* that nature is symmetrical with regard to electricity and magnetism, as far as the *general* field equations for insulators go (*not* meaning, of course, that for a *definite* substance $\epsilon(E)$ should always equal $\mu(H)$).

In much the same way a set of transformations exists that leaves the set of all *general* thermodynamic relations invariant. If for succinctness the argument is confined to a single homogeneous substance, and the Nernst law is disregarded, all general formulae may be deduced from the fundamental set:

$$\begin{aligned} &\text{energy} && =U, && dU=TdS-PdV,\\ &\text{enthalpy} && U+PV=W, && dW=TdS+VdP,\\ &\text{free energy} && U-TS=F, && dF=-SdT-PdV,\\ &\text{fr. enth.} && U+PV-TS=G, && dG=-SdT+VdP. \end{aligned} \tag{1}$$

The symmetry of this set with respect to changes of sign of the "primary" variables P, V, T, S and the "secondary" variables or characteristic functions U, W, F, G is summarized in (2) and (3). Each horizontal line of simultaneous changes is allowed:

	P	V	T	S	U	G	W	F	
E	+	+	+	+	+	+	+	+	
A	−	−	+	+	+	+	+	+	
B	+	+	−	−	+	+	+	+	(2)
C	−	−	−	−	+	+	+	+	
a	−	+	−	+	−	−	−	−	
b	+	−	+	−	−	−	−	−	
α	−	+	+	−	−	−	−	−	(3)
β	+	−	−	+	−	−	−	−	

Physically, this table expresses little more than that the characteristic functions depend on products of "intensive" variables (P, T) and "extensive" variables (V, S). Another symmetry with respect to the *interchanging* of variables is again much more important. It is approximately summarized by the next set of eight substitutions (including unity E=no change):

E	P	V	T	S	U	G	W	F
I	$-V$	P	T	S	W	F	U	G
II	P	V	$-S$	T	F	W	G	U
III	$-V$	P	$-S$	T	G	U	F	W
IV	S	T	V	P	G	U	W	F
V	S	T	P	$-V$	F	W	U	G
VI	T	$-S$	V	P	W	F	G	U
VII	T	$-S$	P	$-V$	U	G	F	W

(4)

It should be noted that "conjugated pairs" of variables keep together, not only (P, V) and (T, S), but also (U, G) and (W, F). Physically, this set expresses that in *general* thermodynamic relations (disregarding signs) no distinction is present between mechanical and thermal variables nor between intensive and extensive variables, a rather unexpected fact.

A not very important but unpleasant complication is offered by the fact that the set (4) does *not* form a group and can only be made to do so either by disregarding the signs (which is

[1] F. O. Koenig, J. Chem. Phys. **3**, 29 (1935); Professor M. Born informs me that the subject was also treated in his lectures at Göttingen and that a poem was made for memorizing the substitutions.
[2] J. A. Prins, Physica **13**, 417 (1947).

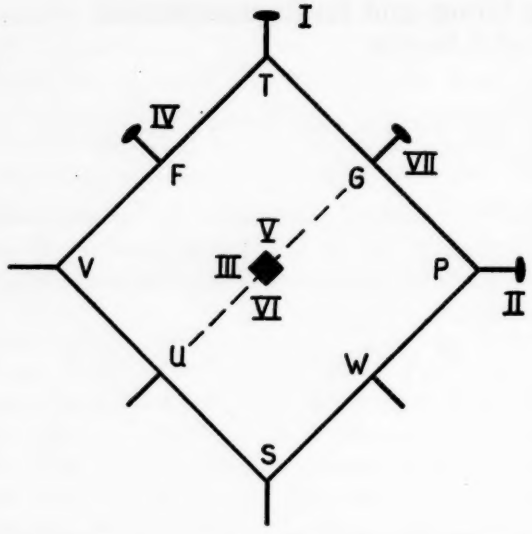

FIG. 1. Modification of Koenig's thermodynamic square. The seven principal thermodynamic substitutions are found by rotating the square over 180° around its digonal axis and over 90°, 180°, and 270° around its tetragonal axis.

inadmissible) or extending the number of transformations from eight to 32 (which is cumbersome) by multiplication of (4) by (2). One may even raise it to 64 by multiplying (4) by (2) and (3), or by (2) and a.

In the total group of 64 transformations the 32 form a maximal invariant sub-group. Its factor group is C_2. In the group of 32 the only maximal invariant sub-group is (2), which is isomorphous with Klein's "*Vierergruppe*," V_4. Its factor group is found to be Klein's dihedral group for the square, which is usually called D_4 but will here be called D_8 to indicate the number of its elements. So the composition of the total thermodynamic substitution group[3] of 64 elements is $G_{64}=C_2V_4D_8$. The unpleasant fact remains that D_8 itself does not occur as a subgroup in the 64 or 32 substitutions, though, on the other hand, its hidden presence lends the most important feature to the group, *viz.* the *interchanges* of variables.

To sail between the scylla of non-group character and the charybdis of too many elements, Koenig[1] and McKay,[4] although they do not state the dilemma so explicitly, have resorted to different devices. With a view to simplicity I suggest, however, the following

Rule: *In Fig. 1 a square is in its normal position with T at the top and P to the right, the conjugate variables being opposite and the characteristic functions occurring between those variables wherein they are normally expressed, as shown for instance by the differentials in (1). The operations indicated by the four diagonal axes and the one tetragonal axis transform the square into itself and in doing so substitute the letters in such a way, (4), that all general thermodynamic relations remain true after transformation. For the extensive variables V and S the additional rule must be observed that they change sign in passing the dotted line.*

As an example the reader may apply the transformations to one of Maxwell's thermodynamic equations, getting the other ones, or to the formula for the Joule effect, getting that for the Joule-Kelvin effect:

$$(\partial T/\partial V)_U=\frac{P-T(\partial P/\partial T)_V}{C_V}\rightarrow$$

$$(\partial T/\partial P)_W=\frac{-V+T(\partial V/\partial T)_P}{C_P},$$

C standing for $T\partial S/\partial T$.

[3] The group considered in this article, G_{64} may be represented in a totally different way by the 64 linear transformations (matrices), working on the two complex variables $P+iV$ and $T+iS$:

$$c\begin{vmatrix} a & 0 \\ 0 & b \end{vmatrix} \quad \text{and} \quad c\begin{vmatrix} 0 & a \\ b & 0 \end{vmatrix},$$

where c stands for either taking the complex conjugate or not, and independently a and b stand for either 1, -1, i, or $-i$.

The composition given in the text, $G_{64}=C_2V_4D_8$, is not the only one possible. By taking (2)+(3) as first maximal invariant sub-group the composition $D_8C_2V_4$ is found. By Hölders theorem the two compositions differ, of course, only in the sequence of the factors.

[4] H. A. C. McKay, J. Chem. Phys. **3**, 715 (1935).

THE JOURNAL OF CHEMICAL PHYSICS VOLUME 16, NUMBER 1 JANUARY, 1948

The Infra-Red Absorption Spectrum of Hexafluoroethane Gas*

J. RUD NIELSEN AND C. M. RICHARDS
Department of Physics, University of Oklahoma, Norman, Oklahoma

AND

H. L. MCMURRY
Phillips Petroleum Company, Bartlesville, Oklahoma

(Received October 28, 1947)

The infra-red absorption of gaseous hexafluoroethane between 2 and 25μ has been investigated with prism spectrometers of high resolution. On the basis of normal vibration calculations and the known Raman frequencies it has been possible to interpret all but 3 of the 51 observed absorption maxima. Only combination bands permitted for both the staggered (D_{3d}) and the eclipsed (D_{3h}) model were used in the assignment of bands. Five fundamental frequencies have been determined in addition to the six obtained from the Raman spectrum. No combination band involving the remaining frequency, associated with the torsional oscillation of one CF_3 group relative to the other, could be identified. An attempt to determine the moments of inertia of the C_2F_6 molecule from the envelope of the strongest parallel band gave unsatisfactory results.

INTRODUCTION

A NUMBER of fluorocarbons have recently been prepared.[1] Their unique physical and chemical properties make the investigation of their infra-red and Raman spectra of considerable theoretical interest, as well as of practical value in providing data for analytical applications. Because of the structural analogy between fluorocarbons and hydrocarbons it may be expected, moreover, that a study of the spectra of the former will throw light upon the vibrational problems presented by compounds of the latter important class.

The Raman and infra-red spectra of tetrafluoromethane, which has been available for some time, have been studied by several workers.[2,3] P. Torkington and H. W. Thompson[4] have investigated the infra-red spectrum of tetrafluoroethylene. Recently, Rank and Pace[5] have observed the Raman spectrum of liquid hexafluoroethane. In the present paper a study of the infra-red absorption spectrum of gaseous hexafluoroethane will be reported.

EXPERIMENTAL

The sample of hexafluoroethane was prepared and purified in the Fluorine Laboratory of the Pennsylvania State College and was kindly made available by Professor J. H. Simons. It was part of a sample on which thermodynamic measurements have been made by Aston and Pace.[6] Its purity, as estimated by these workers, was 99.6 mole percent. The small amount of the impurity was found by Aston and Pace to be low-boiling, and a subsequent distillation raised the purity to 99.9 mole percent. A part of this latter sample was used by Rank and Pace[5] for obtaining the Raman spectrum.

The infra-red absorption spectrum was recorded, from 2 to 15μ, by means of a spectrometer similar to one described by Wright.[7] The 60° rocksalt prism, in Littrow mounting, has faces 10 by 8 cm and the collimating parabolic mirror a focal length of 91.4 cm. A Pfund-type compensated vacuum thermocouple serves as receiver, and the galvanometer deflections are amplified by a balanced barrier-layer photo-cell device and recorded on bromide paper whose

* Presented at the Symposium on Molecular Structure and Spectroscopy held at Ohio State University, Columbus, Ohio, June 9 to 14, 1947.

[1] Compare March 1947 issues of Ind. and Eng. Chem. and Anal. Chem.

[2] D. M. Yost, E. N. Lassettre, and S. T. Grosse, J. Chem. Phys. **4**, 325 (1936).

[3] C. R. Bailey, J. B. Hale, and J. W. Thompson, Proc. Roy. Soc. London **167A**, 555 (1938).

[4] P. Torkington and H. W. Thompson, Trans. Faraday Soc. **41**, 236 (1945).

[5] D. H. Rank and E. L. Pace, J. Chem. Phys. **15**, 39 (1947).

[6] J. G. Aston and E. L. Pace, to appear shortly in J. Am. Chem. Soc.

[7] N. Wright, Ind. Eng. Chem., Anal. Ed. **13**, 1 (1941).

motion is synchronized with that of the Littrow mirror. The cell length was 43 cm. Several pressures up to 194 mm of mercury were used, the temperature of the gas being about 30°C.

Through the courtesy of Mr. D. C. Smith of the Naval Research Laboratory, a few records were made with a spectrometer of higher resolving power.[8] In particular, the absorption in the region from 15 to 25μ was determined with this instrument. A 10-cm cell was used with the NRL spectrometer. The pressure ranged from less than one millimeter to 800 mm.

RESULTS

The infra-red absorption of hexafluoroethane gas from 2 to 15μ is shown in Fig. 1 which gives complete percent transmission curves on a uniform wave-length scale for three different pressures, as well as partial transmission curves for the two strongest bands obtained at a pressure of less than one millimeter. The curves are based on the records made with the University of Oklahoma spectrometer but have been checked against the data obtained with the NRL instrument and have been slightly improved in a few places. The scale of the drawing is not quite large enough to show all of the details revealed by the NRL spectrometer.

Faint bands, at 2890, 2967, and 3060 cm^{-1}, appeared on the first records obtained with hexafluoroethane at pressures of 6 and 48 mm but were absent, or at least greatly reduced in intensity, on the last records obtained at a pressure of 194 mm. Before the last records were made the material was frozen several times and the remaining vapor removed by pumping. It appears, therefore, that the bands mentioned are caused by a volatile impurity. Their wave numbers lie close to the Raman frequencies, 2885, 2974, and 3040 cm^{-1}, observed by Hatcher and Yost[9] for liquid CH_3CF_3. The band of highest frequency nearly coincides with the intense

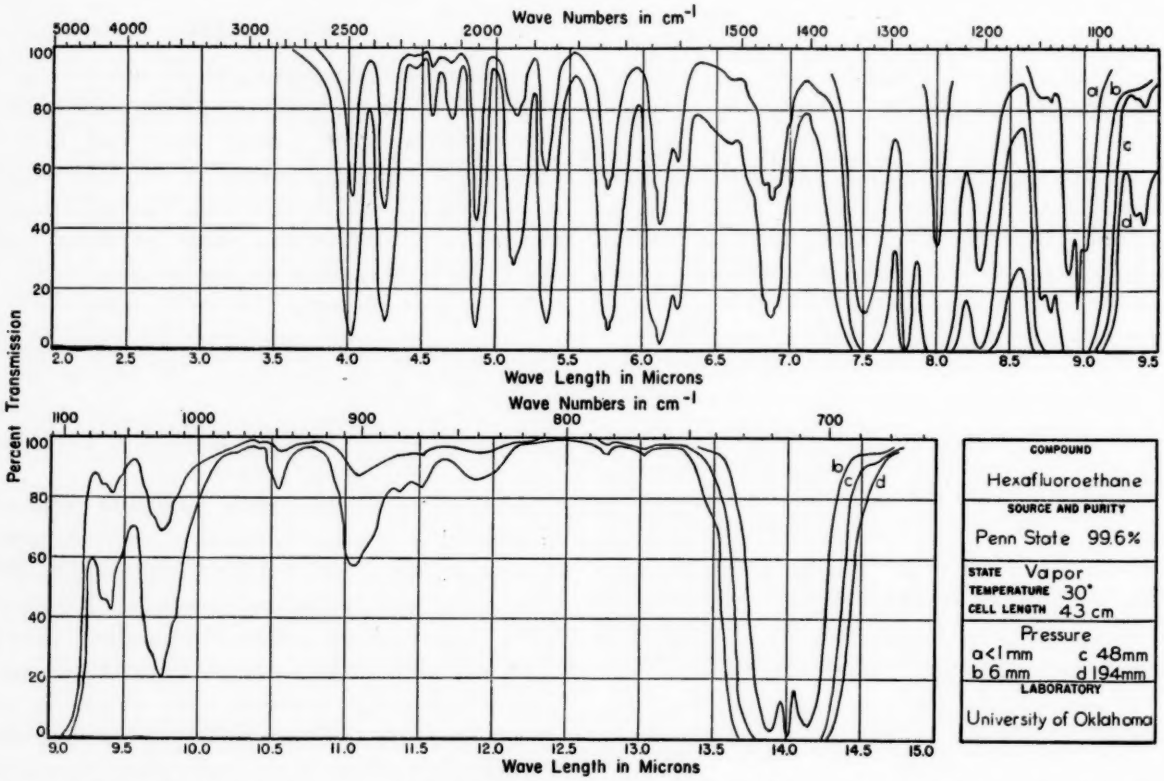
Wave Numbers in cm⁻¹
5000 4000 3000 2500 2000 1500 1400 1300 1200 1100
Percent Transmission
100 80 60 40 20 0
a b c d
2.0 2.5 3.0 3.5 4.0 4.5 5.0 5.5 6.0 6.5 7.0 7.5 8.0 8.5 9.0 9.5
Wave Length in Microns
Wave Numbers in cm⁻¹
1100 1000 900 800 700
b c d
9.0 9.5 10.0 10.5 11.0 11.5 12.0 12.5 13.0 13.5 14.0 14.5 15.0
Wave Length in Microns
COMPOUND
Hexafluoroethane
SOURCE AND PURITY
Penn State 99.6%
STATE Vapor
TEMPERATURE 30°
CELL LENGTH 43 cm
Pressure
a<1mm c 48mm
b 6 mm d 194mm
LABORATORY
University of Oklahoma

FIG. 1. Infra-red absorption spectrum of hexafluoroethane gas from 2 to 15μ. Percent transmission is plotted against wave-length on a uniform wave-length scale. Cell length: 43 cm. Pressures: 6, 48, and 194 mm. Temperature 30°C.

[8] J. Rud Nielsen, F. W. Crawford, and D. C. Smith, J. Opt. Soc. Am. **37**, 296 (1947).
[9] W. H. Hatcher and D. M. Yost, J. Chem. Phys. **5**, 992 (1937).

Raman band, 3062.0 cm^{-1} found by Glockler and Edgell[10] for liquid fluoroform. When the cell was being evacuated after the first filling, a weak band was observed at 1267 cm^{-1}, close to the most intense hexafluoroethane band, 1250.5 cm^{-1}. After the material had been frozen several times, the ratio between the intensities of 1267 cm^{-1} and 1250.5 cm^{-1} had fallen off very greatly. It was concluded, therefore, that the former band belonged to a volatile impurity. Since Bailey, Hale, and Thompson[3] have found the most intense band of CF_4 to lie at 1265 cm^{-1}, the impurity causing the 1267 cm^{-1} band is evidently tetrafluoromethane.

Beyond 15μ, only three bands were observed: a strong diffuse band with maximum at 522.5 cm^{-1}, a weak band with Q-branch at 632.5 cm^{-1}, and P- and R-branches at 613 and 649 cm^{-1}, and a very faint band at 599 cm^{-1}. The band at 632.5 cm^{-1} was at first not regarded as an impurity band (but was interpreted as $\nu_7-\nu_{11}$, although with misgivings because of what seemed to be an abnormally large separation of the rotational branches). However, when it was noted that this band agrees closely, both as regards frequency and intensity distribution, with the second strongest infra-red absorption band found by Bailey, Hale, and Thompson[3] for tetrafluoromethane, and when the 1267 cm^{-1} band had been interpreted as caused by this impurity, it became clear that the 632.5 cm^{-1} band must also be ascribed to the presence of a small amount of CF_4.

The wave-lengths of the observed absorption maxima (or "shoulders"), after elimination of the impurity bands mentioned, are listed in the first column of Table I and the corresponding wave numbers in the fourth column. Rough indications of the intensities and shapes of the bands are given in the second and third columns under the joint heading "Description." The following abbreviations are used: *vvs* extremely strong, *vs* very strong, *s* strong, *m* medium, *w* weak, *vw* very weak, *vvw* extremely weak, *vvvw* barely observable, *d* diffuse, and *sh* sharp. In many cases, especially at shorter wave-lengths, it is not possible to designate bands as either diffuse or sharp.

[10] G. Glockler and W. F. Edgell, J. Chem. Phys. 9, 224 (1941).

TABLE I. Infra-red absorption spectrum of hexafluoroethane gas.

Wave-length	Description		Frequency	Assignment		Calculated frequency
19.14μ	*s*	*d*	522.5 cm^{-1}	$\perp$	ν_8	——
16.7	*vvw*	*d*	599	$\parallel\perp$	$\nu_9+\nu_{12}$	596 cm^{-1}
14.13	*vs*	*d*	707.3		P	
14.005	*vs*	*sh*	714.03	$\parallel$	ν_8	——
13.89	*vs*	*d*	720.2		R	
13.04	*vvvw*		766.9	$\parallel$	$\nu_5-\nu_3$	768
12.78	*vvvw*		782.5			
11.88	*vvw*	*d*	842	$\parallel\perp$	$\nu_9+\nu_{11}$	836
11.52	*vvw*	*d*	868	$\parallel\perp$	$\nu_7-\nu_{12}$	871
11.38	*vvvw*	*d*	879	$\perp$	$\nu_3+\nu_8$	872
11.19	*vw*	*d*	894	$\perp$	$\nu_1-\nu_8$	897
11.08	*m*		903	$\parallel\perp$	$\nu_8+\nu_{12}$	903
10.56	*vw*		947			
9.756	*m*	*d*	1025.0	$\perp$	$\nu_2+\nu_9$	——
9.50	*vvw*		1053		P	
9.410	*vw*	*sh*	1062.7	$\parallel$	$\nu_3+\nu_8$	1063
9.35	*vvw*	*d*	1070		R	
9.01	*s*	*d*	1110		P	
8.953	*vvs*	*sh*	1116.9	$\parallel$	ν_3	——
8.89	*vs*	*d*	1125		R	
8.771	*m*	*sh*	1140.1	$\parallel\perp$	$\nu_8+\nu_{11}$	1143
8.75	*vw*	*d*	1143		R	
8.714	*m*		1147.6	$\parallel\perp$	$\nu_8+2\nu_9$	1146
8.298	*m*	*d*	1205.1	$\perp$	$\nu_1-\nu_9$	1204
7.997	*vvs*	*d*	1250.5	$\perp$	ν_7	——
7.799	*m*		1282.2	$\parallel\perp$	$(\nu_8+2\nu_{12}+\nu_{\delta})-\nu_{\delta}$	
7.787	*m*		1284.2	$\parallel\perp$	$\nu_8+2\nu_{12}$	1283
7.528	*m*	*d*	1328.4	$\perp$	$\nu_3+\nu_8$	1332
6.92	*vvw*		1445		P	
6.882	*m*	*sh*	1453.1	$\parallel\perp$	$\nu_9+\nu_{10}$	1453
6.83	*vw*		1464	$\parallel$	$\nu_5+\nu_8$ or R	1466
6.57	*vvw*	*sh*	1522	$\parallel$	$\nu_6+\nu_3$	1523
6.246	*m*		1601.0	$\perp$	$\nu_3+\nu_7$	1600
6.238	*m*		1603.1	$\perp$	$(\nu_3+\nu_7+\nu_9)-\nu_9$	
6.130	*m*	*sh*	1631.3	$\parallel\perp$	$\nu_7+\nu_{12}$	1631
6.10	*vvvw*		1639	$\perp$	$\nu_1+\nu_9$ or R	1636
5.770	*m*	*d*	1733.1	$\perp$	$\nu_8+\nu_{11}$	1737
5.64	*vvw*		1773	$\parallel\perp$	$\nu_8+\nu_{10}$	1760
5.357	*m*		1866.7	$\parallel\perp$	$\nu_7+\nu_{11}$	1871
5.198	*vvw*		1924	$\parallel$	$\nu_3+\nu_5$	1926
5.151	*m*		1941.4	$\perp$	$\nu_1+\nu_8$	1943
5.115	*vw*	*d*	1955	$\perp$	$\nu_8+\nu_{10}$	1951
4.867	*w*		2055	$\perp$	$\nu_3+\nu_7$	2060
4.69	*vvw*		2132	$\parallel$	$\nu_1+\nu_8$	2134
4.572	*vvw*		2187			
4.44	*vvvw*		2252	$\parallel\perp$	$\nu_7+\nu_{11}+\nu_{12}$	2251
4.252	*m*		2352	$\perp$	$\nu_5+\nu_{10}$	2354
4.033	*m*		2480	$\parallel\perp$	$\nu_7+\nu_{10}$	2488
4.01	*m*		2494	$\parallel\perp$	$\nu_7+2\nu_{11}$	2491
3.734	*m*		2678	$\perp$	$\nu_1+\nu_7$	2671
3.64	*vvw*	*d*	2750	$\perp$	$\nu_1+\nu_3+\nu_8$	2752

INTERPRETATION

Two equilibrium configurations must be considered for the hexafluoroethane molecule, the "staggered" model of symmetry D_{3d} and the "eclipsed" form of symmetry D_{3h}. The symmetry species and selection rules for the twelve fundamental vibration frequencies are shown, for either of these models, in Table II. The number-

TABLE II. Normal vibrations of ethane-like molecules.

	D_{3d}		D_{3h}	
Designation	Species	Activity	Species	Activity
ν_1	A_{1g}	$R\cdot p$	A_1'	$R\cdot p$
ν_2	A_{1g}	$R\cdot p$	A_1'	$R\cdot p$
ν_3	A_{1g}	$R\cdot p$	A_1'	$R\cdot p$
ν_4	A_{1u}	inactive	A_1''	inactive
ν_5	A_{2u}	$I \parallel$	A_2''	$I \parallel$
ν_6	A_{2u}	$I \parallel$	A_2''	$I \parallel$
ν_7	E_u	$I \perp$	E'	$I \perp$, $R\cdot dp$
ν_8	E_u	$I \perp$	E'	$I \perp$, $R\cdot dp$
ν_9	E_u	$I \perp$	E'	$I \perp$, $R\cdot dp$
ν_{10}	E_g	$R\cdot dp$	E''	$R\cdot dp$
ν_{11}	E_g	$R\cdot dp$	E''	$R\cdot dp$
ν_{12}	E_g	$R\cdot dp$	E''	$R\cdot dp$

TABLE III. Calculated values of fundamental frequencies of the hexafluoroethane molecule.

Notation	No F-F repulsions	F-F repulsion; $k_{F\text{-}C\text{-}C}=k_{F\text{-}C\text{-}F}$	F-F repulsion; $k_{F\text{-}C\text{-}C}>k_{F\text{-}C\text{-}F}$
ν_1	1734 cm^{-1}	1392 cm^{-1}	1510 cm^{-1}
ν_2	824	799	813
ν_3	346	209	301
ν_4	—	—	—
ν_5	1298	875	940
ν_6	722	505	742
ν_7	1710	1214	1223
ν_8	566	515	521
ν_9	316	134	316
ν_{10}	—	—	—
ν_{11}	—	—	—
ν_{12}	—	—	—

ing of the fundamentals is that used by Herzberg[11] for ethane. I means active in infra-red absorption, R active in the Raman effect, $\parallel$ denotes a parallel and $\perp$ a perpendicular infra-red band; p indicates a polarized and dp a depolarized Raman band.

As an aid in identifying the observed infra-red frequencies, we have computed eight of the fundamentals, following essentially Howard's procedure for ethane,[12] except that repulsive forces between F atoms within each CF_3 group were assumed in setting up two of the three potential functions used. The C−C stretching force constant was that given by Howard. The three remaining force constants were obtained by means of Urey and Bradley's equations[13] which give the CX_4 frequencies when X−X repulsion exist. The symmetry D_{3h} was assumed but the results would have been the same for D_{3d} or, more generally, for Howard's D_{3h}'. The results are given in Table III. In the first column are listed the frequencies obtained when no repulsive forces are assumed to act between the fluorine atoms, in the second column are given the frequencies obtained when such repulsion is assumed to exist and all angle constants are taken to be equal, and in the last column are listed the frequencies computed under the assumption that repulsion between the fluorine atoms exists and that the C-C-F angle constant is different from the constant for the F-C-F angles. Since these calculations were made we have solved the normal vibration problem more completely. The results will be published elsewhere.

In spite of the uncertainty as to which of three sets of computed frequencies is most nearly correct, comparison with the observed infra-red and Raman frequencies gives with certainty all but two of the twelve fundamentals. The interpretation of the Raman spectrum has already been given by Rank and Pace.[5] The infra-red spectrum of hexafluoroethane contains two very intense bands, at 714.0 and 1116.9 cm^{-1}, which clearly exhibit parallel structure. They must be ν_6 and ν_5, respectively. Another very intense band, at 1250.5 cm^{-1}, appears from the record obtained at the lowest pressure to be a perpendicular band. It must be interpreted as ν_7. The rather strong diffuse band at 522.5 cm^{-1} must be ν_8.

Great effort was spent in determining ν_9. The fact that no appreciable absorption is observed near the 25μ limit of the potassium bromide region shows that ν_9 must lie well below 400 cm^{-1}. The value of ν_9 which leads to the most satisfactory interpretation of the infra-red spectrum was obtained in the following manner. The observed spectrum was first interpreted as completely as possible in terms of the ten fundamental frequencies, ν_1, ν_2, ν_3, ν_5, ν_6, ν_7, ν_8, ν_{10}, ν_{11}, and ν_{12}. When that was done only four bands of medium intensity remained unassigned. If one of these, 1025 cm^{-1}, is assumed to be $\nu_2+\nu_9$, making $\nu_9=216$ cm^{-1}, each of the other bands finds either an entirely or a fairly satisfactory interpretation. Several other assumptions, lead-

[11] G. Herzberg, *Infrared and Raman Spectra of Polyatomic Molecules* (D. Van Nostrand Company, Inc., New York, 1945).
[12] J. B. Howard, J. Chem. Phys. **5**, 442 (1937).
[13] H. C. Urey and C. A. Bradley, Phys. Rev. **38**, 1969 (1931).

ing to different values for ν_9, have been considered and discarded as less plausible.

All attempts to identify combination bands involving ν_4, and thus to determine this frequency, failed. The values for the other fundamental frequencies are listed in Table IV. The spectrum from which the frequency is determined is listed in the third column. The fundamental frequencies obtained from the Raman spectrum of liquid hexafluoroethane are probably somewhat less accurate than the frequencies determined from the infra-red absorption spectrum of the gas. The value for ν_9 is considerably less certain than those found for the other fundamentals.

On the basis of the fundamental frequencies listed in Table IV it has been possible to give a satisfactory interpretation of all of the 51 observed infra-red absorption maxima with the exception of three very faint bands. The assignment of each band is given in the fifth column of Table I. The calculated frequency is given in the last column. The agreement between the observed and the calculated frequency is very close for practically all of the bands. Only for four bands is the difference greater than 5 cm^{-1} and only for one band does it exceed 10 cm^{-1}.

The designations $\parallel$, $\perp$, and $\parallel\perp$, for parallel, perpendicular, and parallel-perpendicular, bands given in Table I, assume the molecular equilibrium configuration to have the symmetry D_{3d}. If the molecular symmetry were D_{3h} some combination bands, such as $\nu_{7,8,9}\pm\nu_{10,11,12}$ and $\nu_{5,6}\pm2\nu_{7,8,9}$, would be $\parallel$ instead of $\parallel\perp$. Other bands, such as $\nu_{7,8,9}\pm2\nu_{8,9,7}$, would be $\perp$ instead of $\parallel\perp$.

TABLE IV. Fundamental vibration frequencies of hexafluoroethane.

Notation	Frequency	Spectrum in which observed
ν_1	1420 cm^{-1}	R (liq)
ν_2	809	R (liq)
ν_3	349	R (liq)
ν_4	—	—
ν_5	1116.9	I (g)
ν_6	714.0	I (g)
ν_7	1250.5	I (g)
ν_8	522.5	I (g)
ν_9	216	I (g)
ν_{10}	1237	R (liq)
ν_{11}	620	R (liq)
ν_{12}	380	R (liq)

DISCUSSION

Rank and Pace[5] observed a faint Raman band at 655 cm^{-1} and suggested that it might be $2\nu_9$, making $\nu_9=328$ cm^{-1}. This assumption explains the very weak infra-red band at 947 cm^{-1} as $\nu_9+\nu_{11}$ and the extremely weak band at 2187 cm^{-1} as $\nu_9+\nu_{10}+\nu_{11}$. However, it leads to the not very plausible interpretation of the band 1025 cm^{-1} as $2\nu_3+\nu_9$ and leaves the bands 1147.6, 1205.1, and 1453.1 cm^{-1} unassigned. For these reasons, Rank and Pace's interpretation of the faint Raman band at 655 cm^{-1} seems unacceptable. However, we have not been able to interpret this Raman band in any other plausible manner.

Four bands are interpreted as difference bands, $\nu_a-\nu_b$. In all but one case the corresponding band, $\nu_a+\nu_b$, has been observed with about the intensity to be expected from the intensity of $\nu_a-\nu_b$ and the Boltzmann factor for the excited initial state ν_b. The exception is 1205.1 cm^{-1} which is interpreted as $\nu_1-\nu_9$. The absorption maximum at 1639 cm^{-1} is probably $\nu_1+\nu_9$, but its intensity is abnormally low. It is possible that the intensity of the band 1205.1 cm^{-1} has been enhanced because of the proximity of ν_7.

The splitting of the bands at 1282–1284 and 1601–1603 cm^{-1} is interpreted by the assumption that the weaker component in either case is caused by a transition from an excited vibrational level to an upper level in which this vibration remains excited.[14] It is not possible to determine the initial excited levels ν_x and ν_y.

Two cases where the assigned band may be merged with a rotational branch of a stronger band are indicated in Table. I. A number of

TABLE V. Observed combinations $\nu_a+\nu_b$.

$A_{2u}\cdot A_{1g}=A_{2u}$		$A_{2u}\cdot E_g=E_u$		$E_u\cdot A_{1g}=E_u$		$E_u\cdot E_g=A_{1u}+A_{2u}+E_u$	
$\nu_5+\nu_2$	*vvw*	$\nu_5+\nu_{10}$	*m*	$\nu_7+\nu_1$	*m*	$\nu_7+\nu_{10}$	*m*
$\nu_5+\nu_3$	*vw*	$\nu_5+\nu_{11}$	*m*	$\nu_7+\nu_2$	*w*	$\nu_7+\nu_{11}$	*m*
$\nu_5-\nu_3$	*vvvw*	$\nu_5+\nu_{12}$	*vvw*	$\nu_7+\nu_3$	*m*	$\nu_7+\nu_{12}$	*m*
$\nu_6+\nu_1$	*vvw*	$\nu_6+\nu_{10}$	*vw*	$\nu_8+\nu_1$	*m*	$\nu_7-\nu_{12}$	*vvvw*
$\nu_6+\nu_2$	*vvw*	$\nu_6+\nu_{11}$		$\nu_1-\nu_8$	*vw*	$\nu_8+\nu_{10}$	*vvvw*
$\nu_6+\nu_3$	*vw*			$\nu_8+\nu_2$	*m*	$\nu_8+\nu_{11}$	*m*
				$\nu_8+\nu_3$	*vvvw*	$\nu_8+\nu_{12}$	*m*
				$\nu_1+\nu_9$	*vvw*	$\nu_9+\nu_{10}$	*m*
				$\nu_1-\nu_9$	*m*	$\nu_9+\nu_{11}$	*vvw*
				$\nu_9+\nu_2$	*m*	$\nu_9+\nu_{12}$	*vvw*

[14] Compare reference 11, p. 267.

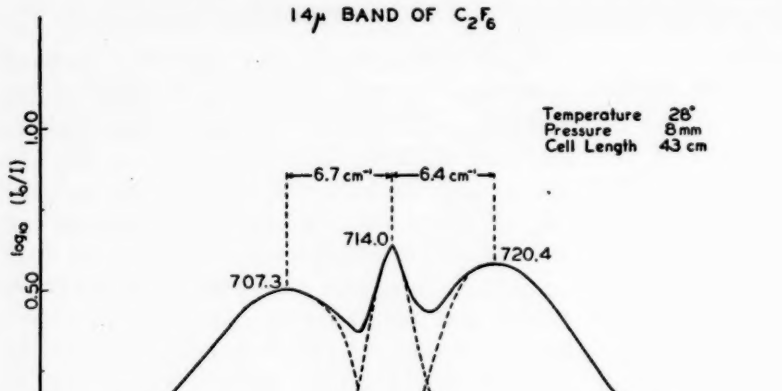

FIG. 2. Intensity distribution in the parallel band at 714.0 cm^{-1}. The extinction, $\log(I_0/I)$, obtained with hexafluoroethane at 6 mm and 30°C in the 43-cm cell is plotted against angular setting of Littrow mirror.

other bands, especially some of high wave numbers, can be interpreted in more than one way. Thus, the band at 902.5 cm^{-1} may also be interpreted as $\nu_7-\nu_3$; 1328.4 cm^{-1} may be interpreted as $\nu_6+\nu_{11}$, 1866.7 as $\nu_2+\nu_3+\nu_6$, and 2132 as $2\nu_2+\nu_8$. At least two alternative assignments, $\nu_5+2\nu_{11}$ and $\nu_5+\nu_6+\nu_8$, are possible for 2352 cm^{-1}. 2480 cm^{-1} may also be interpreted as $\nu_1+\nu_3+\nu_6$ and 2494 cm^{-1} as $\nu_3+3\nu_6$. In general, the interpretation chosen as the most plausible and given in Table I is that for which the total change in vibrational quantum numbers is least.

The combinations used in the assignment are all such which are active in infra-red absorption for both equilibrium configurations, D_{3d} and D_{3h}, of the hexafluoroethane molecule. The observed combination bands $\nu_a+\nu_b$, may be divided into four groups according to the symmetry species of ν_a and ν_b. This is shown in Table V which also gives the intensities of the observed bands, except in the case of $\nu_6+\nu_{11}$ which overlaps with $\nu_2+\nu_8$. It will be noticed that all of the combination bands of species A_{2u} (for D_{3d}) are very faint, whereas most of the other combination bands are of higher intensity.

It is a remarkable fact that only three combination bands of the types listed in Table V were not observed. The band $\nu_5+\nu_1$, which may be expected to be very faint, should lie in the short-wave region where identification is difficult. The band $\nu_9+\nu_3$, on the other hand, should lie in the potassium bromide region where the presence of a faint band may have escaped observation, since only one record was made. The third missing band, $\nu_6+\nu_{12}$, may be masked by ν_5. It is surprising also that it was not found necessary to assume the existence of Fermi coupling between any of the excited vibrational states.

The fact that no overtone band of the type $2\nu_a$ was observed may be taken as evidence in favor of the staggered model of symmetry D_{3d}; for, while all such overtones are forbidden for D_{3d}, overtones of type $2\nu_a$ belonging to the species E', i.e., $2\nu_7$, $2\nu_8$, and $2\nu_9$, can occur if the equilibrium configuration has the symmetry D_{3h}. There is no indication of a band in the long-wave region where $2\nu_9$ should occur. The absence of $2\nu_8$ cannot be claimed with certainty, since it would nearly coincide with the *P*-branch of the parallel band $\nu_3+\nu_6$. $2\nu_7$ would lie approximately at 2501 cm^{-1}. A band found at 2494 cm^{-1} is interpreted in Table I as $\nu_7+2\nu_{11}$. The possibility that this band is actually $2\nu_7$ cannot be entirely excluded; for, if the frequency ν_4, corresponding to a torsional oscillation of one CF_3 group relative to the other, is less than kT/h, a hindered rotation may occur and destroy the rigorous distinction between the molecular symmetries D_{3d} and D_{3h}. Six combination bands $\nu_{7,8,9}+\nu_{8,9,7}$ and $\nu_{10,11,12}+\nu_{11,12,10}$ are permitted if the symmetry of the molecule is D_{3h} but are forbidden for D_{3d}. The band $\nu_7+\nu_8$, if present, should lie at 1773 cm^{-1}. An extremely faint band found at this wave number has been interpreted in Table I as $\nu_8+\nu_{12}$, which should occur at 1760. $\nu_7+\nu_9$ should coincide with the parallel band $\nu_5+\nu_3$. The band $\nu_8+\nu_9$ should lie far

enough from the R-branch of ν_6 to be observable. However, there is no indication of its presence. Of the bands of the second type, $\nu_{10}+\nu_{11}$ should lie at 1857 cm^{-1}, which is close to $\nu_7+\nu_{11}$ at 1866.7 cm^{-1}. There is no indication of its presence. The bands $\nu_{10}+\nu_{12}$ and $\nu_{11}+\nu_{12}$ should both lie sufficiently far from other bands to be observable, but neither was found. Thus, the evidence favors the conclusion that the symmetry of the hexafluoroethane molecule is represented better by the staggered than by the eclipsed model.

The bands $\pm\nu_4+\nu_{10,11,12}$ and $\pm\nu_4+2\nu_{10,11,12}$ are active in infra-red absorption for both molecular symmetries. The bands $\pm\nu_4+2\nu_{7,8,9}$ are permitted for the staggered form but forbidden for D_{3h}. For either symmetry of the equilibrium configuration, $\pm 2\nu_4$ added to any active fundamental or combination band will give a pair of permitted bands. A thorough search was made for bands of the types mentioned, but no band involving ν_4 could be identified with any degree of certainty. Evidently, transitions in which the quantum number V_4 changes have a very low probability. It may be of interest to recall that a few bands involving ν_4 are believed to occur in the infra-red spectrum of ethane.[11] However, in no case have both bands of a pair, corresponding to both signs for ν_4, been found. Hence, the assignment of these ethane bands seems open to doubt.

MOMENTS OF INERTIA

According to Gerhard and Dennison[15] it is possible to determine the moments of inertia of fairly heavy symmetrical top molecules from measurements of the ratio of the intensity of the Q-branch to the total band intensity and the PR separation in a parallel band. We have tried to apply their theory to the 714 cm^{-1} hexafluoroethane band. The extinction, $\log I_0/I$, as obtained with hexafluoroethane at a pressure of 6 mm and a temperature of 30°C in the 43-cm cell, is plotted against the angular setting of the Littrow mirror in Fig. 2. No correction was made for stray radiation. The ratio between the intensity of the Q-branch and the total intensity of the band was estimated to be 0.17 by measuring with a planimeter the areas under the envelopes shown. The separation between the extinction maxima in the P- and R-branches is 13.1 cm^{-1}. From Gerhard and Dennison's curves $\beta=A/C-1$ is found to be 3.1 and $S=\pi\Delta\nu/(kT/A)^{\frac{1}{2}}$ is found to be 1.2. Solving for the molecular moment of inertia, A, about an axis perpendicular to the threefold symmetry axis and the moment of inertia, C, about the axis, we find $A=401\times10^{-40}$ and $C=98\times10^{-40}$.

These results, especially the low value for C, are not very reasonable. If the distance between the carbon atoms is taken to be 1.54A, as in ethane, if the distance C−F is 1.36A as in tetrafluoromethane, and if tetrahedral angles are assumed, the values $A=462.4\times10^{-40}$, $C=311.2\times10^{-40}$, and $\beta=0.486$ are obtained. If the C−C distance is smaller in hexafluoroethane than in ethane, as claimed by Brockway,[16] A and β would be somewhat smaller. Although no great accuracy can be claimed for the extinction curve given in Fig. 2, nor perhaps for Gerhard and Dennison's procedure, the high value found for β is nevertheless surprising. On the other hand, the perpendicular hexafluoroethane bands appear more different from the parallel bands than one would expect on the basis of Gerhard and Dennison's theory if β is as small as 0.486.

ACKNOWLEDGMENTS

The writers wish to acknowledge their great indebtedness to Professor J. H. Simons, Director of the Fluorine Laboratory of the Pennsylvania State College, for the loan of the hexafluoroethane and to Professor J. G. Aston, Pennsylvania State College, for suggesting the work and for helpful discussion. It is a pleasure also to acknowledge the valuable help rendered by Mr. D. C. Smith, Naval Research Laboratory, in obtaining the infra-red spectrum.

[15] S. L. Gerhard and D. M. Dennison, Phys. Rev. **43**, 197 (1933).

[16] Private communication.

THE JOURNAL OF CHEMICAL PHYSICS VOLUME 16, NUMBER 1 JANUARY, 1948

The Force Constants for CF_4 and C_2F_6

E. L. PACE
Morley Chemical Laboratory, Western Reserve University, Cleveland, Ohio
(Received July 30, 1947)

Vibrational potential functions of the quadratic type for CF_4 and C_2F_6, which assume no interaction between the CF_3 groups in C_2F_6 and include only the interaction terms involving bond-bending with bond-stretching motions, are used with the observed normal frequencies to evaluate a set of force constants for the molecules. The force constants associated with the CF_3 group are used interchangeably between the two molecules. The reproduction of the observed values of the normal frequencies resulting from the use of the force constants is of the order of five percent or better except for three of the frequencies. The omission of terms in the potential function for the interaction of the CF_3 groups is largely responsible for the relatively poor reproduction of the type E_u frequencies of C_2F_6. Additional interaction terms, e.g., between bond-bending motions, are necessary for the improvement of the agreement in the case of the type F_2 frequencies of CF_4.

INTRODUCTION

THE nature of the forces holding atoms together in molecules can be determined from a consideration of the force constants in a given molecule or in molecules with structurally similar groups. The force constants are calculated from the observed normal frequencies and the assumed model for each molecule. The calculation depends fundamentally on the proper choice of a vibrational potential function. At present, the most promising potential function is the general quadratic type, limited to small vibrational amplitudes, which contains the bond-stretching and the bond-bending force constants together with the interaction force constants that are considered important for the particular molecule. In general, the validity and usefulness of the potential function rests on the reproduction of observed normal frequencies in a greater number than the potential constants involved in it as well as in the agreement obtained between observed and calculated frequencies when the force constants for a given group in one molecule are used for the same group in a different molecule. For several molecules composed of carbon, hydrogen, deuterium, oxygen, and other atoms, excellent reproduction or prediction of observed frequencies has resulted from the transference between molecules of stretching, bending, and interaction force constants for the same group.[1-3]

The assignment of the normal frequencies of C_2F_6 from the infra-red[4] and Raman spectra,[5] when combined with that for CF_4,[6] now makes possible the consideration of the force field for molecules consisting solely of carbon and fluorine atoms. Because of the more complicated force field associated with the fluorine atom, the vibrational potential functions cannot be expected to be as simple as for the corresponding hydrogen or deuterium analog. Therefore, whereas a simple valence-force field is found to be adequate for CH_4 and CD_4, it is unsatisfactory for CF_4.[7] Likewise, the potential functions employed by Howard[8] and Stitt[9] for C_2H_6 and C_2D_6 do not give real force constants when used with the observed normal frequencies for C_2F_6.

Some information concerning the significant interaction terms in the potential function for molecules containing fluorine can be derived from a consideration of the structurally analogous hydrocarbons. Hence, in C_2H_6 and C_2D_6, the fact that the frequencies for either the two degenerate or the two non-degenerate types are essentially the same indicates that the C−H and C−D stretching motions are not coupled with any other motion.[9] Furthermore, the comparison of the corresponding symmetrical frequencies in

[1] H. W. Thompson and J. W. Linnett, J. Chem. Soc. 1376 (1937).
[2] B. L. Crawford, Jr. and S. R. Brinkley, Jr., J. Chem. Phys. **9**, 69 (1941).
[3] J. E. Kilpatrick and K. S. Pitzer, J. Research Nat. Bur. Stand. **38**, 191 (1947).
[4] From the paper by J. R. Nielsen, C. M. Richards, and H. L. McMurry, presented at the Symposium on Molecular Structure and Spectroscopy, Columbus, Ohio, June, 1947.
[5] D. H. Rank and E. L. Pace, J. Chem. Phys. **15**, 39 (1947).
[6] G. Herzberg, *Infrared and Raman Spectra of Polyatomic Molecules* (D. Van Nostrand Company, Inc., New York, 1945), p. 167.
[7] See reference 6, p. 181.
[8] J. B. Howard, J. Chem. Phys. **5**, 442 (1937).
[9] F. Stitt, J. Chem. Phys. **7**, 297 (1939).

C_2H_6 and C_2D_6 points to the absence of coupling between the H−C−H bending and the C−C stretching motions in C_2H_6 but to the presence of considerable interaction between the D−C−D bending and the C−C stretching motions in C_2D_6.

Stitt[9] also suggests that the weak intensity or entire absence of the line for the symmetrical hydrogen bending frequency in the Raman spectra of several molecules, e.g., C_2H_6, CH_3Cl, and CH_3OH, may be caused by the polarizability of the molecule undergoing little or no change in the uncoupled hydrogen bending vibration. Consequently, the appearance of the line for this vibration with considerable intensity in the Raman spectra of molecules such as C_2D_6 and C_2H_4 may be attributed to the interaction of the symmetrical bending motion with another having a pronounced change in polarizability such as the C−C stretching motion.

An examination of the data from the Raman and infra-red spectra of C_2F_6 in the light of that for C_2H_6 and C_2D_6 reveals two pertinent facts. First, the frequencies for both the C−F stretching and F−C−F bending vibrations are quite different for the two non-degenerate types. Secondly, the line in the Raman spectrum associated with the symmetrical bending frequency, ν_2, has a higher intensity than any other line.[5] Therefore, strong coupling probably exists between the F−C−F bending and both the C−F and C−C stretching motions.

In order to test the validity of the preceding conclusion, the succeeding calculation of force constants for CF_4 and C_2F_6 from observed normal frequencies is performed with potential functions containing bond-stretching and bond-bending force constants, and all interaction force constants involving bond-bending with bond-stretching motions exclusive of those for the interaction of the two CF_3 groups in C_2F_6. The development and solution of the secular equation from the potential function and geometry of the molecule follows the method devised by Wilson.[10]

CALCULATIONS FOR CF_4

The form of the potential function for CF_4, obtained from the preceding considerations, is

$$2V=f_d\sum_{i=1}^{i=4}(\Delta d_i)^2+f_\alpha\sum_{i>j=1}^{i=4}(d\Delta\alpha_{ij})^2+2f_{d\alpha}\sum_{i=1}^{i=4}(\Delta d_i)(d\Delta\alpha_{ij}),$$

in which V is the vibrational potential energy, d, the $C-F_i$ equilibrium distance, α_{ij}, the F_i-C-F_j equilibrium bond angle, and f_d, f_α, $f_{d\alpha}$ are, respectively, the C−F stretching constant, the F−C−F bending constant, and the constant for the interaction of these two motions.

The derivation of the secular equation for the vibrations of a molecule of this type has been done by Meister and Cleveland.[11] If their solution is modified by setting $f_{\alpha\alpha}=0$, the resulting equations become applicable to CF_4 with the preceding potential function.

The CF_4 molecule has the symmetry T_d. Therefore, the secular equation factors into one equation for the non-degenerate type A_1 vibration, a second equation for the doubly degenerate type E vibration, and a third equation for the two triply degenerate type F_2 vibrations. The two equations for the type A_1 and type E vibrations give values for f_d and f_α of 9.15×10^5 and 0.71×10^5 dynes per centimeter, respectively, if the frequency assignment given by Herzberg[6] is used. However, in the equation for the F_2 frequencies, it is impossible to evaluate a real force constant, $f_{d\alpha}$, which is consistent with the observed frequencies and the values of f_d and f_α calculated from the other type frequencies.

CALCULATIONS FOR C_2F_6

Following the procedure for CF_4, the potential function of the quadratic type containing all interaction terms involving bond-stretching with bond-bending motions excepting those for the opposing CF_3 groups for an assumed D_{3d} configuration is

$$2V=f_D(\Delta D)^2+f_d\sum_{i=1}^{i=3}[(\Delta d_i')^2+(\Delta d_i'')^2]+f_\alpha\sum_{i>j=1}^{i=3}[(d\Delta\alpha_{ij}')^2+(d\Delta\alpha_{ij}'')^2]+f_\beta\sum_{i=1}^{i=3}[(d\Delta\beta_i')^2+(d\Delta\beta_i'')^2]$$

(*continued on next page*)

[9] E. B. Wilson, Jr., J. Chem. Phys. **7**, 1047 (1939); *ibid.* **9**, 76 (1941).

[11] A. G. Meister and F. F. Cleveland, Am. J. Phys. **14** 13 (1946).

$$+2f_{D\alpha}\sum_{i>j=1}^{i=3}(\Delta D)(d\Delta\alpha_{ij}'+d\Delta\alpha_{ij}'')$$

$$+2f_{D\beta}\sum_{i=1}^{i=3}(\Delta D)(d\Delta\beta_i'+d\Delta\beta_i'')$$

$$+2f_{d\alpha}\sum_{i=1}^{i=3}[(\Delta d_i')(d\Delta\alpha_{i,i+1}'+d\Delta\alpha_{i,i-1}')+(\Delta d_i'')(d\Delta\alpha_{i,i+1}''+d\Delta\alpha_{i,i-1}'')]$$

$$+2f_{d\beta}\sum_{i=1}^{i=3}[(\Delta d_i')(d\Delta\beta_i')+(\Delta d_i'')(d\Delta\beta_i'')],$$

in which V is the vibrational potential energy; D and d_i, the equilibrium C−C and C−F$_i$ bond distances; α_{ij} and β_i, the equilibrium F$_i$−C−F$_j$ and F$_i$−C−C bond angles. The single and double primes refer to different CF_3 groups. The force constants f_D, f_d, f_α, f_β, $f_{D\alpha}$, $f_{D\beta}$, $f_{d\alpha}$, and $f_{d\beta}$ are defined by the bond and angle displacements associated with them in the above expression.

By making use of the symmetry of the molecule, the secular equation for the normal vibrations can be factored into equations for the E_g, E_u, A_{1g}, and A_{2u} symmetry types. Since these can be derived simply by the Wilson method[10] from the corresponding F and G matrices, the matrices will be presented in the following treatment rather than the expanded equations. The matrices are symmetrical with respect to the main diagonal. Hence, only the off-diagonal elements on the upper side of the main diagonal are shown.

The G matrices, assuming a tetrahedral CF_3 group, are, for the type A_{1g} and type A_{2u} vibrations

$$\begin{bmatrix} 2\mu_C & -(6^{\frac{1}{2}}/3)\mu_C & (4/3)(6^{\frac{1}{2}})\mu_C\epsilon \\ & \mu_F+\mu_C/3 & -(4/3)\mu_C\epsilon \\ & & [2\mu_F+(16/3)\mu_C]\epsilon^2 \end{bmatrix},$$

and for the E_g and E_u type vibrations

$$\begin{bmatrix} \mu_F+(4/3)\mu_C & -(2^{\frac{1}{2}}/3)\mu_C S\epsilon & (4/3)(2^{\frac{1}{2}})\mu_C\epsilon \\ & [\mu_F+(\mu_C/6)S^2]\epsilon^2 & [\mu_F/2-(2/3)\mu_C S]\epsilon^2 \\ & & [(5/2)\mu_F+(8/3)\mu_C]\epsilon^2 \end{bmatrix},$$

in which μ_F and μ_C are, respectively, the reciprocal masses of the fluorine and carbon atom; ϵ, the reciprocal C−F equilibrium bond distance and $S=1$ for type E_u vibrations and $S=6(\tau/\epsilon)+1$ for the type E_g vibrations, τ being the reciprocal of the C−C bond distance.

The F matrix for the type A_{1g} vibrations is

$$\begin{bmatrix} f_D & 0 & 3^{\frac{1}{2}}d(f_{D\alpha}-f_{D\beta}) \\ & f_d & 2^{\frac{1}{2}}d(f_{d\alpha}-f_{d\beta}/2) \\ & & (d^2/2)(f_\alpha+f_\beta) \end{bmatrix},$$

while that for the A_{2u} vibrations is obtained from the preceding by setting $f_D=f_{D\alpha}-f_{D\beta}=0$.

The F matrix for both the type E_g and type E_u frequencies is

$$\begin{bmatrix} f_d & df_{d\beta} & -df_{d\alpha} \\ & d^2f_\beta & 0 \\ & & d^2f_\alpha \end{bmatrix}.$$

The potential function and, hence, the secular equation make use of a total of eight different force constants, of which seven are independent since $f_{D\alpha}$ and $f_{D\beta}$ appear only in the combination $f_{D\alpha}-f_{D\beta}$.

In evaluating the most consistent set of force constants for C_2F_6, the values of two of the force constants, $f_d=9.15\times10^5$ dynes per centimeter and $f_\alpha=0.71\times10^5$ dynes per centimeter, are taken from the type A_1 and the type E frequencies for CF_4. The remaining force constants are derived by a process of adjustment to the best fit between observed and calculated values for the type A_{1g} and type E_g frequencies for C_2F_6. The values obtained, in units of 10^5 dyne per centimeter, are: $f_{d\alpha}=1.13$, $f_{d\beta}=1.35$, $f_\beta=0.80$, $f_{D\alpha}-f_{D\beta}=-0.28$, and $f_D=5.45$.

A C−F distance of 1.35A and the observed value of 1.45A for the C−C distance[12] were used in all calculations. The CF_3 group was assumed tetrahedral.

The order of the precision maintained in the calculations was such that the frequencies calculated from the force constants were correct to within ±2 cm^{-1}. In view of the approximate nature of the potential function and the tediousness of the calculations, it was felt that greater precision was not warranted.

[12] L. O. Brockway, J. H. Secrist, and C. M. Lucht, Abstracts, Buffalo Meeting of American Chemical Society, September, 1942.

DISCUSSION

A comparison of the observed normal frequencies with those calculated from the set of force constants is summarized in Table I for CF_4 and in Table II for C_2F_6.

In the case of CF_4, the test of the accuracy of the potential function is found in the results for the type F_2 vibrations. The agreement between the observed and calculated normal frequencies, although poor, represents a considerable improvement over the simple valence-force field. The addition of at least another interaction term, e.g., angle-angle, to the potential function is necessary.

The observed frequencies for C_2F_6, except for the type E_u frequencies, are reproduced to the order of five percent or better. The relatively larger discrepancies noted for the E_u frequencies stem largely from the assumption of no interaction between the CF_3 groups. From the nature of the equations for the type E_u frequencies, it is this particular interaction which would be effective in reducing the discrepancies between the observed and calculated values. The existence of this interaction is supported by heat capacity measurements which have assigned a barrier of the order of 4350 calories per mole, restricting the free rotation of the CF_3 groups.[13]

The value of 5.45×10^5 dynes per centimeter for the C−C stretching force constant in C_2F_6 is significantly greater than that observed for saturated hydrocarbon molecules. This is in apparent agreement with the observation by Brockway[12] that the presence of fluorine atoms, adjacent to a C−C bond, has a stabilizing influence on it. Hence, a C−C distance of 1.45A is observed as compared to the value of 1.54A for many saturated hydrocarbons. However, because of approximations introduced in the potential function, the interpretation that the high value of the force constant is the result of a shortening of the C−C bond is not altogether justifiable. A more rigorous treatment is required to resolve this point.

From the preceding results, it may be concluded that the potential functions assumed for CF_4 and C_2F_6 reproduce the observed normal frequencies to a good approximation. Moreover, an improvement in the agreement between calculated and observed values would result from the addition to the potential function of terms for the interaction between bond-bending motions, and between the CF_3 groups in C_2F_6. However, a normal coordinate treatment involving such a potential function would be so time consuming as to be impracticable.

TABLE I. Comparison of calculated and observed normal frequencies for CF_4.

Designation	Type	Obs. (cm^{-1})	Calc. (cm^{-1})
ν_1	A_1	904	904*
ν_2	E	437	436*
ν_3	F_2	1265	1316
ν_4	F_2	630	516

Force constants in 10^5 dynes per centimeter: $f_d=9.15$, $f_\alpha=0.71$, $f_{d\alpha}=1.13$.

* Frequencies used to evaluate f_d and f_α.

TABLE II. Comparison of calculated and observed normal frequencies for C_2F_6.

Designation	Type	Obs. (cm^{-1})	Calc. (cm^{-1})
ν_1	A_{1g}	1420	1417
ν_2	A_{1g}	809	828
ν_3	A_{1g}	349	330
ν_5	A_{2u}	1117	1107
ν_6	A_{2u}	714	697
ν_7	E_u	1251	1406
ν_8	E_u	523	488
ν_9	E_u	216	238
ν_{10}	E_g	1237	1230
ν_{11}	E_g	620	631
ν_{12}	E_g	380	399

Force constants in 10^5 dynes per centimeter: $f_d=9.15$, $f_\alpha=0.71$, $f_{d\alpha}=1.13$, $f_{d\beta}=1.35$, $f_\beta=0.80$, $f_D=5.45$, $f_{D\alpha}-f_{D\beta}=-0.28$.

[13] E. L. Pace and J. G. Aston, to be published.

THE JOURNAL OF CHEMICAL PHYSICS VOLUME 16, NUMBER 1 JANUARY, 1948

An Asymptotic Expression for the Energy Levels of the Rigid Asymmetric Rotor*

S. GOLDEN**
Mallinckrodt Chemical Laboratory, Harvard University, Cambridge, Massachusetts
(Received October 28, 1947)

The energy matrix of the rigid asymmetric rotor, evaluated in terms of symmetric rotor wave functions, has been examined under conditions where J is increased indefinitely. Asymptotically, the energy matrix assumes a form that is very much like the matrix that may be obtained from the characteristic value problem of Mathieu's differential equation. The characteristic values of Mathieu's equation serve as the basis for a good approximation to the energy values of those asymmetric rotor levels which, for a given, large value of J, correspond to a small value of K in the limiting symmetric cases. The differences which exist between the two matrices are accounted for by a perturbation technique which permits an accurate determination of the energy values.

When the characteristic values of Mathieu's equation lead to a successful approximation to the energy values of the asymmetric rotor, an estimate may be made of the asymmetric rotor wave functions.

INTRODUCTION

ALTHOUGH the equations defining the energy levels of the rigid asymmetric rotor have been derived by various authors,[1] the numerical solution of the equations is not available for all values of the rotational quantum numbers. Recently, however, King, Hainer, and Cross[2] have published tables of solutions for $J \leq 10$. There have been three methods for extension of the solutions to higher J values. Numerical solution of the equations becomes increasingly laborious for large J's. The approximations resulting from the usual perturbation theory yield rather slowly convergent series. Finally, there is the application of the correspondence principle.[3]

The result of the correspondence principle arguments is to give an asymptotic expression for the energy levels which fails to reveal one of the most important properties of the asymmetric rotor spectrum; *viz.*, the removal with increasing asymmetry of the twofold degeneracy in K ($K \neq 0$) which exists in the limiting case of the symmetric rotor. It would appear that the applicability of the correspondence principle result is restricted to those asymmetric rotor energy levels which are essentially twofold degenerate, i.e., under conditions of slight asymmetry and large J and K (for the limiting symmetric case).

In order to avoid this restriction, the energy matrix of the rigid asymmetric rotor, evaluated in terms of a basis of symmetric rotor wave functions, has been examined, and the limiting form that it assumes when J is increased indefinitely has been determined. This limiting form differs but slightly from that arising in the characteristic value problem involving Mathieu's differential equation. As a consequence of this asymptotic similarity, the characteristic values of Mathieu's equation have been utilized for a first approximation to the energy levels of the asymmetric rotor. It has been found possible to modify the Mathieu equation by the addition of a suitable perturbation operator that permits a better approximation to the energy values. In principle, a series of suitable perturbation operators may be developed which, together with the matrix equations derived below, will permit the energy values to be determined to as great a degree of accuracy as may be desired.

* The support given by the Navy Department is gratefully acknowledged for some of the computational work herein reported. It was carried out under Task Order V of Contract N5ori-76, Office of Naval Research, by Mrs. Dorothy A. H. Brown and Mr. F. C. Merriam.

** National Research Council Predoctoral Fellow.

[1] E. E. Witmer, Proc. Nat. Acad. Sci. **13**, 60 (1927); S. C. Wang, Phys. Rev. **34**, 243 (1929); H. A. Kramer and G. P. Ittman, Zeits. f. Physik **53**, 533 (1929); **58**, 217 (1929); **60**, 633 (1930); O. Klein, Zeits. f. Physik **58**, 730 (1929); H. B. Casimir, *Rotation of a Rigid Body in Quantum Mechanics* (J. B. Wolter's, The Hague, 1931).

[2] G. W. King, R. M. Hainer, and P. C. Cross, J. Chem. Phys. **11**, 27 (1943). These tables recently have been extended to $J=11$ and 12, R. M. Hainer, Thesis, Brown University, 1947.

[3] G. W. King, Phys. Rev. **70**, 108 (1946); J. Chem. Phys. **15**, 820 (1947); E.E. Witmer, Monthly Progress Reports of the University of Pennsylvania, Thermodynamics Research Laboratory, Contract NObs-2477, Navy Department Bureau of Ships.

ASYMPTOTIC FORM OF THE ENERGY MATRIX[4]

The energy levels of any rigid asymmetric rotor have the form

$$E_\tau^J(a, b, c)=\frac{a+c}{2}J(J+1)+\frac{a-c}{2}E_\tau^J(\kappa), \quad (1)$$

where J is the quantum number associated with the squared total angular momentum of the rotor, $\hbar^2J(J+1)$; $J=0, 1, 2, \cdots$; τ is a *pseudo* quantum number which indicates the order of the $2J+1$ energy levels having a given value of J; τ takes on integral values between $-J$ for the lowest energy level, and $+J$ for the highest; $a=\hbar^2/2I_a$, $b=\hbar^2/2I_b$, $c=\hbar^2/2I_c$, and $I_a\leq I_b\leq I_c$, the principal moments of inertia; $\kappa=[(2b-a-c)/(a-c)]$, an asymmetry parameter;[5] $E_\tau^J(\kappa)$ is a characteristic value of the energy matrix $\mathbf{E}(\kappa)$ discussed below.

The energy matrix $\mathbf{E}(\kappa)$, when evaluated in terms of symmetric rotor wave functions $\psi(J, K, M)$ as basis functions, does not depend upon M in the absence of an external field. Furthermore, it is diagonal in J, each J; J block being of order $2J+1$. In any J; J block it has the following non-vanishing elements:

$$E_{K;\,K}=FJ(J+1)+(G-F)K^2, \quad (2)$$

and

$$E_{K;\,K+2}=E_{K+2;\,K}=H[f(J, K+1)]^{\frac{1}{2}}. \quad (3)$$

F, G, and H depend upon the manner in which a set of Cartesian axes within the rotor is identified with the principal axes,[6] and upon the asymmetry parameter κ.

$$f(J, n)=f(J, -n)=\tfrac{1}{4}[J(J+1)-n(n+1)]\times[J(J+1)-n(n-1)]. \quad (4)$$

The energy matrix may be written as

$$\mathbf{E}(\kappa)=FJ(J+1)\mathbf{I}+(G-F)\mathbf{E}'(\kappa), \quad (5)$$

where $\mathbf{I}$ is the unit matrix of appropriate order $(2J+1)$, and $\mathbf{E}'(\kappa)$ now has the following non-vanishing elements in each J; J block:

$$E'_{K;\,K}=K^2, \quad (6)$$

and

$$E'_{K;\,K+2}=E'_{K+2;\,K}=\frac{H}{G-F}[f(J, K+1)]^{\frac{1}{2}}, \quad (7)$$

provided $G-F\neq 0$.

Now for finite n, the following asymptotic relationship $(J\to\infty)$ may be obtained:

$$[f(J, n)]^{\frac{1}{2}}\sim\frac{J(J+1)}{2}\left[1+O\left(\frac{n^2}{2J(J+1)}\right)\right]. \quad (8)$$

Thus, if the symmetric rotor wave functions are ordered: $\psi(J, -J, M)$, $\cdots$ $\psi(J, K, M)$, $\cdots$ $\psi(J, J, M)$, the energy matrix $\mathbf{E}'(\kappa)$ assumes the following limiting form.

$$\mathbf{E}'(\kappa)\sim\begin{pmatrix}
\vdots & \vdots & & \vdots & \vdots & \\
\cdots\ 2^2 & 0 & \frac{H}{G-F}\frac{J(J+1)}{2} & 0 & 0 & \cdots \\
\cdots\ 0 & 1^2 & 0 & \frac{H}{G-F}\frac{J(J+1)}{2} & 0 & \cdots \\
\cdots\ \frac{H}{G-F}\frac{J(J+1)}{2} & 0 & 0 & 0 & \frac{H}{G-F}\frac{J(J+1)}{2} & \cdots \\
\cdots\ 0 & \frac{H}{G-F}\frac{J(J+1)}{2} & 0 & 1^2 & 0 & \cdots \\
\cdots\ 0 & 0 & \frac{H}{G-F}\frac{J(J+1)}{2} & 0 & 2^2 & \cdots \\
\vdots & \vdots & \vdots & \vdots & \vdots &
\end{pmatrix}, \quad (9)$$

[4] The notation used by King, Hainer, and Cross, reference 2, will be adopted here.

[5] The use of κ as an asymmetry parameter is due to B. S. Ray, Zeits. f. Physik **78**, 74 (1932), and results from his choice of diagonalizing the angular momentum about the intermediate axis of inertia.

[6] Reference 2, Table III.

neglecting terms $O([n^2/J(J+1)])$ compared to unity for very large values of J. Equation (9) is similar in structure to the corresponding matrix that arises in the characteristic value problem that involves Mathieu's equation. It differs from the latter in that the former is of order $(2J+1)$, while the latter is of infinite order; also, the latter gives rise to off-diagonal elements which are truly constant, while the off-diagonal elements of the former are only asymptotically and approximately constant for $J \gg K$.

THE MATHIEU EQUATION MATRIX

To obtain the matrix arising from the characteristic value problem of Mathieu's equation, consider the equation itself.[7]

$$\frac{d^2y}{dx^2}+(\alpha-2\theta\cos 2x)y=0, \tag{10}$$

α and θ are parameters which are independent of x.

This equation has both periodic and nonperiodic solutions, depending upon the values of α and θ. However, for those solutions which are periodic in π or 2π it is found that α may assume only special values, which depend upon θ. The characteristic value problem, then, is to determine those values of α, for each value of θ, which permit solutions periodic in π or 2π. This may be accomplished as follows. Let $\theta=0$, obtaining

$$\frac{d^2y_0}{dx^2}+\alpha_0 y_0=0. \tag{11}$$

This equation will have solutions periodic in π or 2π if and only if $\alpha_0=K^2$ so that

$$y_0=\frac{1}{(2\pi)^{\frac{1}{2}}}e^{iKx}, \quad K=0, \pm 1, \pm 2\cdots, \tag{12}$$

which form a complete orthogonal and normalized set of functions in the interval $0\leq x\leq 2\pi$. The quantity $(-2\theta\cos 2x)y$ in Eq. (10) may be regarded as a perturbation term that is added to Eq. (11). This perturbation term, as well as those solutions y which are periodic in π or 2π, may now be expressed in terms of a linear combination of the unperturbed functions y_0. If the unperturbed functions, y_0, are ordered:

$$\cdots\frac{1}{(2\pi)^{\frac{1}{2}}}e^{-iKx}, \quad \frac{1}{(2\pi)^{\frac{1}{2}}}e^{-i(K-1)x}, \quad \cdots\frac{1}{(2\pi)^{\frac{1}{2}}}\cdots,$$

$$\frac{1}{(2\pi)^{\frac{1}{2}}}e^{i(K-1)x}, \quad \frac{1}{(2\pi)^{\frac{1}{2}}}e^{iKx}\cdots,$$

application of the usual perturbation procedure leads to the matrix

$$\mathbf{M}=\begin{pmatrix}
\cdot & \cdot & \cdot & \cdot & \cdot & & \\
\cdot & \cdot & \cdot & \cdot & \cdot & & \\
\cdot & \cdot & \cdot & \cdot & \cdot & & \\
\cdots & 2^2 & 0 & \theta & 0 & 0 & \cdots \\
\cdots & 0 & 1^2 & 0 & \theta & 0 & \cdots \\
\cdots & \theta & 0 & 0 & 0 & \theta & \cdots \\
\cdots & 0 & \theta & 0 & 1^2 & 0 & \cdots \\
\cdots & 0 & 0 & \theta & 0 & 2^2 & \cdots \\
 & \cdot & \cdot & \cdot & \cdot & \cdot & \\
 & \cdot & \cdot & \cdot & \cdot & \cdot & \\
 & \cdot & \cdot & \cdot & \cdot & \cdot &
\end{pmatrix}, \tag{13}$$

the characteristic values of which determine those values of α for which solutions of Eq. (10) having the required periodicity are obtained. Except for being of infinite order, Eq. (13) is clearly identical with Eq. (9), if

$$\frac{H}{G-F}\frac{J(J+1)}{2}\equiv\theta. \tag{14}$$

With the aid of Eq. (14) and tables of the characteristic values of Mathieu's equation, an estimate may be made of the energy levels of the asymmetric rotor. How this may be done will be considered in greater detail in a later section.

THE ELLIPTIC CYLINDER FUNCTIONS

The elliptic cylinder functions are those solutions of Mathieu's equation which are periodic in π or 2π. Although their properties are well known,[8] a summary will be given of those properties which pertain to the present treatment.

[7] Other forms of Mathieu's equation are frequently used, *viz.*, Eq. (29) below. The particular form here is that used by E. L. Ince, Proc. Roy. Soc. Edin. **52**, 355 (1931). An extensive bibliography relating to Mathieu's equation, with summaries of the contents of the most important papers, is given by W. G. Bickley, Mathematical Tables and Other Aids to Computation **I**, No. 11 (1945); **II**, No. 13 (1946).

[8] See W. G. Bickley, reference 7, for numerous references.

If Mathieu's equation is written as

$$\left(-\frac{d^2}{dx^2}+2\theta\cos 2x\right)y=\alpha y, \tag{15}$$

or

$$\mathfrak{L}y=\alpha y,$$

then it is readily verified that the operator $\mathfrak{L}$ is left invariant by the transformations

$$\begin{cases} E\colon\ x\to 2\pi+x, \\ \mathfrak{R}_1\colon\ x\to 2\pi-x, \\ \mathfrak{R}_2\colon\ x\to \pi-x, \\ \mathfrak{R}_3\colon\ x\to \pi+x. \end{cases} \tag{16}$$

The complete set of orthonormal functions generated by Eq. (15) can, at most, experience a change in sign when subjected to each of the transformations of Eq. (16). Since the set of transformations (16) form a group isomorphic with the point group $\mathbf{D}_2$, the functions generated by Eq. (15) must belong to each of the four irreducible representations of $\mathbf{D}_2$. In this respect the elliptic cylinder functions manifest a close analogy to the asymmetric rotor wave functions, which also belong to the irreducible representations of $\mathbf{D}_2$.

The elliptic cylinder functions have been defined[9] as

$$\begin{cases} ce_{2n}(x,\theta)=\sum_{r=0}^{\infty} A_{2r}^{(2n)}(\theta)\cos 2rx, \\ se_{2n+1}(x,\theta)=\sum_{r=0}^{\infty} B_{2r+1}^{(2n+1)}(\theta)\sin(2r+1)x, \\ ce_{2n+1}(x,\theta)=\sum_{r=0}^{\infty} A_{2r+1}^{(2n+1)}(\theta)\cos(2r+1)x, \\ se_{2n+2}(x,\theta)=\sum_{r=0}^{\infty} B_{2r}^{(2n+2)}(\theta)\sin 2rx, \end{cases} \tag{17}$$

where n takes on all non-negative integral values. The characteristic values corresponding to each of these species of functions are, respectively, $a_{2n}(\theta)$, $b_{2n+1}(\theta)$, $a_{2n+1}(\theta)$, $b_{2n+2}(\theta)$. The limiting values for θ equal to zero are

$$\begin{cases} a_{2n}(0)=(2n)^2, \\ b_{2n+1}(0)=(2n+1)^2, \\ a_{2n+1}(0)=(2n+1)^2, \\ b_{2n+2}(0)=(2n+2)^2. \end{cases} \tag{18}$$

Moreover, from the tabulated values it is found that for any n

$$\cdots\le a_{2n}(\theta)\le b_{2n+1}(\theta)\le a_{2n+1}(\theta)\le b_{2n+2}(\theta)\le a_{2(n+1)}(\theta)\cdots, \tag{19}$$

so that a distinct ordering of the characteristic values is possible that is independent of θ.

In view of the isomorphism existing between the elliptic cylinder functions and the asymmetric rotor functions it would seem desirable to find a one-one correspondence between them, based upon symmetry considerations. This would allow the unique identification of each characteristic value approximated by solution of the Mathieu equation with an energy value of the asymmetric rotor. This, unfortunately, is impossible because the transformations in Eq. (16) may not be identified in a unique fashion with the rotations forming the elements of the point group $\mathbf{D}_2$ to which the asymmetric rotor wave functions belong. Depending upon the evenness or oddness of J, a representation may be found which permits of the appropriate identification of elliptic cylinder functions with the wave functions of the rotor.

It is possible, however, to identify the two kinds of functions through their corresponding characteristic values. In the notation of reference 2, an asymmetric rotor energy level is denoted by the two numbers $J_\tau=J_{K_{-1},K_{+1}}$ with $\tau=K_{-1}-K_{+1}$; K_{-1} is the $|K|$ corresponding to the limiting prolate symmetric rotor and K_{+1} is the $|K|$ corresponding to the limiting oblate symmetric rotor.

Observe that either

$$\begin{aligned} K_{-1}+K_{+1}&=J+1 \quad \text{case (a), or} \\ &=J \quad \text{case (b),} \end{aligned} \tag{20}$$

so that

$$\begin{aligned} K_{+1}&=J+1-K_{-1} \quad \text{case (a),} \\ &=J-K_{-1} \quad \text{case (b).} \end{aligned}$$

Hence

$$\begin{aligned} \tau&=2K_{-1}-J-1 \quad \text{case (a),} \\ &=2K_{-1}-J \quad \text{case (b).} \end{aligned}$$

For the same value of K_{-1} (corresponding to the limiting case of K_{-1} degeneracy)

$$2K_{-1}-J>2K_{-1}-J-1.$$

Therefore, levels corresponding to *case* (a) are lower than those corresponding to *case* (b), for the same value of K_{-1}.

[9] Ince, see reference 7.

If J is added to both sides of Eq. (20),

$$J+K_{-1}+K_{+1}=(2J+1) \quad \text{case (a)},$$
$$=2J \quad \text{case (b)},$$

so that

case (a) corresponds to *odd* $(J+K_{-1}+K_{+1})$
case (b) corresponds to *even* $(J+K_{-1}+K_{+1})$.

Equation (19) may now be applied, permitting the following correspondences

$$\begin{cases} b_{K-1} \leftrightarrow J_{K-1,K+1} \text{ for } odd\ (J+K_{-1}+K_{+1}), \\ a_{K-1} \leftrightarrow J_{K-1,K+1} \text{ for } even\ (J+K_{-1}+K_{+1}). \end{cases} \quad (21)$$

Insofar as the characteristic values of Mathieu's equation approximate the asymmetric rotor energy levels, it should be possible by Eq. (21) to arrive at an estimate of the asymmetric rotor wave functions for J large and $|K|$ small (for the limiting symmetric case).

The asymmetric rotor wave functions are commonly expressed as a linear combination of a basis of the Wang[1] functions, which consist of the sums and differences of those pairs of symmetric rotor wave functions which have the same J and M but have K's of opposite sign. All these basis functions are normalized to unity, and the Wang function for which K is zero is identical with the symmetric rotor wave function for which K is zero.

This combination of the symmetric rotor wave functions corresponds precisely to the combination of the exponential functions generated by Eq. (11) to form either *sines* or *cosines*. It is in terms of these latter functions that the elliptic cylinder functions are commonly expressed. As a consequence, the coefficients employed in expressing the asymmetric rotor wave functions in terms of the Wang functions are simply related to the Fourier coefficients of the corresponding elliptic cylinder function.

In order to employ the tabulated Fourier coefficients of Ince, a slight modification is necessary. This modification arises because of Ince's choice of the basis function for which K is zero. When allowances are made for this, it turns out that all that is needed is to multiply the quantities A_0 by the quantity $\sqrt{2}$. With this modification the transformation coefficients from Wang functions to asymmetric rotor wave functions may be taken directly from the tabulated values, or interpolated when necessary. Some care must be exercised to maintain the proper sign of θ (i.e., as it appears in the energy matrix) if the correct characteristic vectors are to be obtained.

Since the characteristic vectors obtained for the elliptic cylinder functions are of infinite dimensionality, while those for the asymmetric rotor are finite (for finite J), it is necessary to adjust for this disparity. It is suggested that the first m Fourier coefficients of the appropriate elliptic cylinder function be taken as the approximation to the corresponding asymmetric rotor characteristic vector of dimensionality m. Consistency may be attained by normalizing the resulting vector to unity.

MODIFICATION OF MATHIEU'S EQUATION

To obtain a better approximation for the energy levels than that given simply by the characteristic value of Mathieu's equation the higher order terms of Eq. (8) must be considered. The following expansion may be obtained

$$[f(J,n)]^{\frac{1}{2}} \sim \frac{J(J+1)}{2} - \frac{n^2}{2}\left(1+\frac{1}{2J(J+1)}\right)+O\left(\frac{n^2}{J(J+1)}\right)^2. \quad (22)$$

For those cases where $n \ll J \gg 1$, the first two terms give an excellent approximation for the function. With this approximation, then, Eq. (7) becomes

$$E'_{K;\,K+2}=E'_{K+2;\,K}=\left(\frac{H}{G-F}\right)\left[\frac{J(J+1)}{2}-\frac{(K+1)^2}{2}\left(1+\frac{1}{2J(J+1)}\right)\right]$$
$$=\left(\frac{H}{G-F}\right)\left[\frac{J(J+1)}{2}-\frac{1}{2}\left(1+\frac{1}{2J(J+1)}\right)\right]$$
$$-\frac{1}{2}\left(\frac{H}{G-F}\right)\left[1+\frac{1}{2J(J+1)}\right](K^2+2K). \quad (23)$$

TABLE I. First-order corrections apart from factor θ'.

θ \ char. value	be_0	bo_1	be_1	bo_2	be_2	bo_3	be_3	bo_4	be_4	bo_5	be_5	bo_6
0	0.00000	−1.00000	1.00000	0.00000	0.00000	0.00000	0.00000	0.00000	0.00000	0.00000	0.00000	0.00000
1	0.09424	−0.32005	1.83468	1.32876	1.25074	1.19579	1.04153	1.07173	1.05792	1.04121	1.04073	1.02826
2	0.41579	0.25006	2.84494	2.63144	2.32442	2.50407	1.91671	2.17244	2.06401	2.08152	2.07401	2.05472
3	0.81976	0.74573	3.97885	3.88779	3.42380	3.88749	2.69191	3.32478	2.97109	3.12456	3.08712	3.07807
4	1.22537	1.18935	5.14014	5.08654	4.66321	5.31776	3.48317	4.38195	3.74826	4.17802	4.06222	4.09782
5	1.61321	1.59454	6.26512	6.22294	6.06460	6.77265	4.37809	5.82805	4.39930	5.25192	4.97741	5.11481
6	1.98021	1.97009	7.33437	7.29965	7.59044	8.23415	5.42184	7.18040	4.97322	6.35700	5.80951	6.13092
7	2.32744	2.32176	8.34847	8.31365	9.17178	9.68775	6.63650	8.59208	5.54855	7.50303	6.53867	7.15008
8	2.65694	2.65367	9.31301	9.29165	10.74443	11.12230	8.02937	10.05370	6.20048	8.69766	7.15560	8.17707
9	2.97075	2.96881	10.23381	10.21786	12.26998	12.52989	9.59010	11.55498	6.98025	9.81414	7.66933	9.21794
10	3.27069	3.26953	11.11594	11.10419	13.73425	13.93145	11.28789	13.08523	7.91630	10.08346	8.11090	10.27919

The first bracketed term is constant for a given J, and may be identified with the θ in Mathieu's equation. It can be verified that the second term in brackets may be obtained from the perturbation operator

$$\mathcal{P}(x) = -2\theta'\left[\cos 2x\frac{d^2}{dx^2} - 2\sin 2x\frac{d}{dx}\right], \quad (24)$$

so that Mathieu's equation, modified by the addition of this perturbation operator, is altered to

$$\frac{d^2y}{dx^2} + (\alpha - 2\theta\cos 2x)y - 2\theta'\left(\cos 2x\frac{d^2y}{dx^2} - 2\sin 2x\frac{dy}{dx}\right) = 0, \quad (25)$$

with

$$\theta = \left(\frac{H}{G-F}\right)\left[\frac{J(J+1)}{2} - \frac{1}{2}\left(1 + \frac{1}{2J(J+1)}\right)\right], \quad (26)$$

$$\theta' = \frac{1}{2}\left(\frac{H}{G-F}\right)\left(1 + \frac{1}{2J(J+1)}\right).$$

Equation (25) will be considered in the next section, where it will be solved by a perturbation procedure. In principle, additional perturbation operators may be found that will permit, with one exception, the construction of a secular equation that is identical with that arising in the asymmetric rotor problem. The exception is the disparity in the magnitudes of the order of the two secular equations. However, this may be handled by a perturbation procedure also.

PERTURBATION TECHNIQUE

To take into account the fact that for any finite J, the energy matrix of the asymmetric rotor is finite, while the matrix generated by Eq. (25) (in terms of the functions of Eq. (11)) is of infinite order, augment the former by rows and columns of zeros, so that $\mathbf{E}'(\kappa)$ remains symmetrical with respect to the main and anti-diagonals, i.e., equal numbers of rows and columns added to each side of $\mathbf{E}'(\kappa)$. Then, symbolically, the augmented matrix may be represented as

$$\mathbf{E}''(\kappa) = \mathbf{M} + \mathbf{P} + \mathbf{R}, \quad (27)$$

where $\mathbf{M}$ is the matrix in Eq. (13), $\mathbf{P}$ is the matrix arising from the perturbation operator in Eq. (24), and $\mathbf{R}$ is a remainder added to the sum of $\mathbf{M}$ and $\mathbf{P}$ to complete the equality; all matrix elements are evaluated in terms of the functions generated by Eq. (11).

The remainder matrix $\mathbf{R}$ will have elements that are small in magnitude and vanish asymptotically, connecting those diagonal terms which are of interest ($|K| \ll J$). Hence it will have but slight effect upon the characteristic values as determined from $\mathbf{M}+\mathbf{P}$ alone when J is only moderately large.

Formally, Eq. (27) may be diagonalized as follows. By its construction $\mathbf{M}$ will give characteristic roots of Mathieu's equation. These may be taken as known. $\mathbf{P}$ may be evaluated in terms of the periodic solutions of Mathieu's equation, the elliptic cylinder functions, and the perturbation operator in Eq. (24). Since a perturbation operator corresponding to R has not been obtained it is convenient to first determine R in terms of the basis of functions of Eq. (12). Transformation to a basis of elliptic cylinder functions is then carried out by matrix multi-

TABLE II.

Asymmetric rotor level	$(J+K_{-1}+K_{+1})$	Notation of ref. 7	Notation of ref. 12	Corresponding elliptic cylinder function
$JK_{-1}K_{+1}$	odd	$b_{K\pm1}$	$bo_{K\pm1}$	$se_{K\pm1}(x,\theta)$
$JK_{-1}K_{+1}$	even	$a_{K\pm1}$	$be_{K\pm1}$	$ce_{K\pm1}(x,\theta)$

TABLE III.

Quantity \ Representation	I	III
F	$\frac{\kappa-1}{2}$	$\frac{\kappa+1}{2}$
$G-F$	$\frac{3-\kappa}{2}$	$-\frac{3+\kappa}{2}$
$\left\lvert\frac{H}{G-F}\right\rvert$	$\frac{1+\kappa}{3-\kappa}$	$\frac{1-\kappa}{3+\kappa}$

plication. The required transformation matrices are readily obtained from the Fourier coefficients tabulated by Ince.[10]

In view of their construction both **P** and **R** may be expected to have elements which have absolute values considerably smaller than the differences in the characteristic values of the levels of **M** which they connect. Consequently, a rapid convergence of the usual perturbation series expansion may be expected.

Some comment is required concerning the sign of θ and θ' in Eq. (26). Since the characteristic values of Mathieu's equation are usually tabulated for positive θ, it would be convenient to have θ always positive. However, since the sign of θ (also θ') is determined by $[H/(G-F)]$, it may be either positive or negative,[6] depending upon the representation that is chosen in which to express the symmetric rotor wave functions. It is clearly possible to find an orthogonal transformation that will change the sign of the non-diagonal elements of $\mathbf{E}(\kappa)$, while the sign of the diagonal elements remains unchanged. Since the characteristic values are unaltered by orthogonal transformations, the quantity $[H/(G-F)]$ may be taken positive always. The same does not apply to the quantity $(G-F)$ however.

In evaluating the matrix elements of **P** in in terms of a basis of elliptic cylinder functions, a certain simplification is possible based upon the symmetry properties of these functions. Since the perturbation operator $\mathcal{P}$ has character $+1$ for all operations in Eq. (16), it is clear that **P** factors into four submatrices corresponding to the four species of elliptic cylinder functions. A similar factoring may be applied to **M**, but is unnecessary, since the characteristic values of **M** may be taken as known. This factoring is analogous to the factoring of the secular equation of the asymmetric rotor.

The necessary integrals have been evaluated by the use of Eq. (17). The general matrix element for each of the four species of functions follows:

$ce_{2n}(x,\theta)$:

$$P(2n,2n')=-4\theta\sum_{r=2}^{\infty}(r^2-r)\{A_{2r}^{(2n)}A_{2r-2}^{(2n')}+A_{2r}^{(2n')}A_{2r-2}^{(2n)}\}; \tag{28a}$$

$se_{2n+1}(x,\theta)$:

$$P(2n+1,2n'+1)=-\theta'\Big[B_1^{(2n+1)}B_1^{(2n'+1)}+\sum_{r=1}^{\infty}(4r^2-1)\times\{B_{2r+1}^{(2n+1)}B_{2r-1}^{(2n'+1)}+B_{2r+1}^{(2n'+1)}B_{2r-1}^{(2n+1)}\}\Big]; \tag{28b}$$

$ce_{2n+1}(x,\theta)$:

$$P(2n+1,2n'+1)=-\theta'\Big[-A_1^{(2n+1)}A_1^{(2n'+1)}+\sum_{r=1}^{\infty}(4r^2-1)\times\{A_{2r+1}^{(2n+1)}A_{2r-1}^{(2n'+1)}+A_{2r+1}^{(2n'+1)}A_{2r-1}^{(2n+1)}\}\Big]; \tag{28c}$$

$se_{2n+2}(x,\theta)$:

$$P(2n+2,2n'+2)=-4\theta'\sum_{r=2}^{\infty}(r^2-r)\{B_{2r}^{(2n+2)}B_{2r-2}^{(2n'+2)}+B_{2r}^{(2n'+2)}B_{2r-2}^{(2n+2)}\}. \tag{28d}$$

[10] Ince, see reference 7; J. A. Stratton, P. M. Morse, L. J. Chu, and R. A. Hunter, *Elliptic Cylinder and Spheroidal Wave Functions* (John Wiley and Sons, Inc., New York, 1941); S. Goldstein, Camb. Phil. Soc. Trans. **23**, 303 (1927).

The diagonal elements of **P**, apart from the factor θ', have been determined from the coefficients given by Ince[11] for a number of the elliptic cylinder functions. These quantities are given in Table I.

COMPUTATIONAL PROCEDURE

The computation of the characteristic values of Mathieu's equation, which form the basis for the approximation considered here, is made particularly simple by the recently published Tables of Characteristic Values of Mathieu's Differential Equation.[12]

Certain differences occur between the notation employed in the latter work and that employed here. These differences will be summarized. Mathieu's differential equation may be written in the form

$$\frac{d^2y}{dx^2}+(b-s\cos^2x)y=0. \tag{29}$$

Comparison with Eq. (10) reveals that

$$\begin{cases}\alpha=b-\frac{1}{2}s,\\ \theta=\frac{1}{4}s.\end{cases} \tag{30}$$

The tables give the characteristic values b to eight decimal places for various values of s. Interpolation for intermediate values of s is made particularly simple by the simultaneous tabulation of modified second central differences. When Everett's interpolation formula[13] is used with these modified differences the error is less than one half-unit in the last tabulated place.

The notation used for the characteristic values differs from that used above. The following correspondences are obtained.

$$\begin{cases} a_{2n}\leftrightarrow be_{2n}\\ b_{2n+1}\leftrightarrow bo_{2n+1}\\ a_{2n+1}\leftrightarrow be_{2n+1}\\ b_{2n+2}\leftrightarrow bo_{2n+2}.\end{cases} \tag{31}$$

The characteristic value of Mathieu's equation corresponding to a particular asymmetric rotor energy level may be obtained from Table II.

Before carrying out a computation for an energy value approximation it is best to choose a representation that will make $|H/(G-F)|$ small. In general, that representation should be chosen for which the asymmetric rotor energy matrix is most nearly diagonal. Thus for asymmetries in the vicinity of the limiting prolate symmetric case ($\kappa=-1$) a type I representation of reference 2 should be used; in the case of nearly oblate symmetry ($\kappa=+1$) a type III representation should be used. Table III gives the quantities needed in these computations for both representations. It should be remembered that K_{-1} is used with a type I representation, while K_{+1} is used with a type III representation.

The quantities θ and θ' may now be determined with the aid of Eq. (26) and Table III. The appropriate characteristic value to be computed may be determined from Table II. With the aid of Eq. (30) the quantity s may be obtained; the value of the appropriate characteristic value b may then be obtained from the Tables by interpolation, if necessary. The characteristic

TABLE IV. Approximate second-order correction apart from factor $(\theta')^2$.

θ	be_0	bo_1	be_1	bo_2	be_2	bo_3	be_3	bo_4
0	−0.00000	−1.12500	−1.12500	−5.33333	−5.33333	−12.93750	−12.93750	−23.46667
1	−0.39178	−1.20178	−1.37094	−5.41561	−5.00017	−12.88162	−12.71756	−23.40270
2	−0.97928	−1.41298	−2.11591	−5.64637	−4.58435	−12.72354	−12.06048	−23.22154
3	−1.40973	−1.65907	−3.26382	−6.00745	−4.42034	−12.55062	−11.07556	−22.95080
4	−1.72170	−1.90163	−4.48031	−6.44982	−4.42417	−12.39361	−10.10610	−22.62205
5	−1.96944	−2.12919	−5.53756	−6.93442	−4.46974	−12.26193	−9.38104	−22.27251
6	−2.18254	−2.34026	−6.39651	−7.44045	−4.46752	−12.16077	−8.92747	−21.91700
7	−2.37602	−2.53642	−7.09759	−7.94698	−4.40606	−12.09629	−8.67357	−21.57118
8	−2.55769	−2.71991	−7.68968	−8.44328	−4.34503	−12.07602	−8.51668	−21.24234
9	−2.73176	−2.89281	−8.21038	−8.92404	−4.36265	−12.10735	−8.35227	−20.93472
10	−2.77796	−3.05685	−8.67038	−9.38738	−4.51675	−12.19631	−8.11453	−20.65218

[11] Different authors use somewhat different conventions relating to the "normalization" of the functions. Ince "normalizes" the function to π instead of unity. This fact was taken into account in preparing Table I.

[12] A report prepared for the Applied Mathematics Panel, NDRC, by the Mathematical Tables Project, National Bureau of Standards, AMP Report 165.1R.

[13] E. T. Whittaker and G. Robinson, *The Calculus of Observations* (Blackie and Son, Ltd., London, 1932).

TABLE V. Computation of characteristic values of asymmetric rotor.

Level	Tables of ref. 2	Mathieu function approximation	Third-order perturbation formula, ref. 2
		$\kappa=-0.9$	
$10_{0,10}$	−106.11121	−106.11116	−106.40266
$10_{1,10}$	−105.67708	−106.67708	−105.67431
$10_{1,9}$	−100.32958	−100.32955	−100.32513
$10_{2,9}$	−96.96993	−96.96996	−96.97205
$10_{2,8}$	−95.36420	−95.36418	−95.06940
$10_{3,8}$	−86.74965	−86.74966	−86.75226
$10_{3,7}$	−86.59725	−86.59730	−86.60144
$10_{4,7}$	−73.14548	−73.14556	−73.14326
		$\kappa=-0.8$	
$10_{0,10}$	−104.00141	−104.00146	−106.79625
$10_{1,10}$	−103.90124	−103.90131	−103.83947
$10_{1,9}$	−94.02065	−94.02079	−94.04603
$10_{2,9}$	−92.48017	−92.48039	−92.99250
$10_{2,8}$	−87.56942	−87.56856	−84.71850
$10_{3,8}$	−81.32404	−81.32363	−80.28408
$10_{3,7}$	−80.20810	−80.20768	−80.17775
$10_{4,7}$	−67.99406	−67.99363	−67.95775

value α is then determined by Eq. (30). The approximate characteristic value of Eq. (5) is then given by

$$E_\tau{}^J(\kappa)=FJ(J+1)+(G-F)\alpha. \qquad (32)$$

Corrections to Eq. (32) may be obtained as indicated above. The diagonal elements of **P**, except for the factor θ', are given in Table I, from which the appropriate first-order correction to Eq. (32) may be determined by interpolation. Higher order corrections may be determined by evaluation of the non-diagonal elements of **P**, using Eq. (28a)–(28d), followed by the usual perturbation treatment. However, more non-diagonal elements of **P** are required that can be determined from the few elliptic cylinder functions that have been tabulated. Nevertheless a good *approximate* second-order correction may be obtained from the finite submatrix of **M** and **P** which contains those levels for which coupling elements may be evaluated. The second-order corrections so obtained will be larger than the complete second-order correction. Because of the rapidly increasing difference between successive characteristic values of **M**, the neglect of the influence of higher levels will probably not prove to be serious.

The approximate second-order correction to be applied to α, except for the factor $(\theta')^2$, may be determined from Table IV by interpolation, if necessary.

As an illustration of the procedure outlined above, the eight lowest energy values for $J=10$, with asymmetries of $\kappa=-0.9$, -0.8, have been computed. In Table V they are compared with the accurate values obtained by King, Hainer, and Cross, as well as with the values obtained from the third-order perturbation formulas given by these authors. It is seen that the agreement between the results of the present computation and the accurate values is very good, while the results of the third-order perturbation calculations are quite inadequate for the values of κ considered.

ACKNOWLEDGMENT

It is a pleasure to acknowledge the constant encouragement and aid given the author by Professor E. Bright Wilson, Jr., at whose suggestion this work was carried out.